NTNU – Trondheim
Norwegian University of
Science and Technology

Diagenesis and Reservoir Quality of the Hugin Formation Sandstones in the North Sea

A Petrographical Approach

Bendik Lunde

Geology
Submission date: June 2013
Supervisor: Mai Britt E. Mørk, IGB
Co-supervisor: Olav Walderhaug, Statoil ASA

Norwegian University of Science and Technology
Department of Geology and Mineral Resources Engineering

Abstract

The Middle Jurassic Hugin Formation in the Sleipner area has been studied in five wells in the southern Viking Graben in the Norwegian sector of the North Sea. The main objective is to understand how the diagenetic development has influenced the reservoir quality by the use of petrographical methods, in combination with core plug measurements of porosities and permeabilities.

The Hugin Formation sandstones are characterized by textural and compositional maturity, and are classified as quartz arenites, subarkoses and sublitharenites. Mechanical compaction and diagenetic minerals (such as calcite cement and quartz overgrowths) contributed the most to the reduction of reservoir quality. Porosity measurements from the core plugs vary from 6 to 16%, which is somewhat below the average regional trend at similar depths. Calcite cement does not follow any specific trend related to depth, but the amount of quartz cement clearly increases with increasing depth.

The main source of quartz cement is dissolution of detrital quartz grains at stylolites. The stylolites are formed where thin laminae of clay and insoluble organic material occur between detrital quartz grains, and the dissolved silica precipitated close to the stylolites.

Authigenic clay minerals are also involved in the reduction of the reservoir quality. Kaolinite and illite are present in varying amounts throughout the wells, and their abundance is closely related to the presence of alkali feldspar. It is believed that the variation of alkali feldspar is responsible for the varying degree of illitization seen in the Hugin Formation. The illitization of feldspar is an additional source of the quartz cement.

Secondary dissolution of alkali feldspar has occasionally contributed to preserve the reservoir quality, and this process is most commonly seen in the subarkoses.

Sammendrag

Hugin formasjonen av midt jura alder er studert i fem brønner fra Sleipner området i Vikinggraben på norsk sektor i Nordsjøen. Målsetningen med studiet er å få en bedre forståelse av hvordan diagenetisk utvikling har påvirket reservoarkvalitet. Dette er gjort ved å benytte petrografiske metoder. Porøsitet og permeabilitet fra kjerneplugger og modal analyser er plottet mot dybde for å undersøke dybde-relaterte trender i forbindelse med diagenesen.

Sandsteinene i Huginformasjonen er karakterisert ved teksturell og mineralogisk modenhet og klassifiserer som kvartsarenitt, subarkose og sublitisk arenitt. Mekanisk kompaksjon og diagenetiske mineraler som kalsittsement og kvartsovervekster er de viktigste porøsitetsregulerende faktorene i sandsteinene. Porøsitetsmålinger fra kjerneplugger varierer mellom 6 og 16%. Disse porøsitetsverdiene er noe lavere enn den gjennomsnittlige regionale trenden.

Kalsittsement følger ikke noen bestemt dybdetrend, men mengden av kvartssement øker med dybden, noe som resulterer i redusert porøsitet. Den viktigste kilden til kvartssementen er tolket å være oppløsning av detritale kvarts korn i kontakt med stylolitter. Stylolitter dannes der tynne lamina av leire og uoppløselig organisk materiale forekommer mellom detritale kvartskorn, og oppløst silika felles ut som sement i nærheten av stylolittene.

Tilstedeværelse av autigene leirmineraler bidrar også til reduksjon av reservoarkvalitet. Kaolinitt og illitt finnes i varierende mengder i alle brønnene, og innholdet av disse mineralene er trolig knyttet til omdannelse av alkalifeltspat. Det er mulig at varierende grad av illitt dannelse har sammenheng med varierende innhold detrital feltspat. Illitt dannelse er også en mulig kilde til kvartssement.

I intervaller med sekundær oppløsning av alkalifeltspat er det bevart høyere porøsitet. Av de klassifiserte sandsteinene er det observert høyest innhold av sekundær porøsitet i subarkosene.

Acknowledgement

I would like to thank my supervisor Professor Mai Britt E. Mørk for all her help during the work with my thesis. All my questions were always answered, and her guidance throughout the whole process has been invaluable. I would also like to thank Statoil ASA and Olav Walderhaug for giving permission to use the thin sections and the provided well data. Last but not least I want to thank my supportive family, especially Line for her moral support during all my years at the university. Without her help and patience I would not have been able to finish. I would also like to thank my brother helping out with delicate software problems. This thesis is dedicated to my beloved children, Oskar and August.

Tables of contents

Appendix

A. Tables
B. Figures
C. Legend

1 Introduction

1.1 Background

This is a core study from the wells 15/3-7, 15/5-7, 15/6-11 A, 15/9-19 A and 15/9-21 S. The wells are located in the southern Viking Graben in the Norwegian sector of the North Sea, close to Utsira High (Fig. 1.1). Core data has been used to make a petrographic and diagenetic study of the Middle Jurassic Hugin Formation sandstones belonging to the Vestland Group.
Depths are given as either true vertical depth (TVD) relative from the sea floor (mRSF), or measured depth from the Rotary Kelly Bushing (mRKB), which follows the well path.

Well 15/3-7 is an exploration well drilled in 2001, approximately 50 km north of the Sleipner gas/condensate fields. It was drilled to appraise the Gudrun discovery on the east flank of the South Viking Graben. Oil and gas were discovered in Upper Jurassic and Middle Jurassic sandstones. Four conventional cores were sampled from the Hugin Formation in the interval 4609 to 4670 mRKB, with a total of 46.4 m core recovered. Additional sidewall cores were taken at 4755 to 4791 mRKB.

Well 15/5-7 was drilled in 2008 as an exploration well on the Dagny discovery in the southern Viking Graben area, 10 km north of the Sleipner gas fields. The well penetrated the Hugin Formation at 3821 mRKB and proved precence of oil down to base of the formation. Three cores were sampled from the well. The first core was cut in the Hugin Formation, the second in the transition zone between Hugin and Sleipner Formation, and the third core was cut in the Sleipner Formation. Total core sample length was 114 m. Only data from the Hugin Formation has been used in this study.

Well 15/6-11 A was drilled in 2011 in order to prove the precence of oil and test the production properties of the oil zone in the Hugin Formation between the Dagny and

Ermintrude fields. While drilling, the well encountered a 30 m gas column in the Hugin Formation. Several tests were performed before the well was permanently plugged and abandoned with a total vertical depth of 3830 mRSF.

Well 15/9-19 A in the Volve Field was drilled in 1997, as a sidetrack of the well 15/9-19 S drilled in 1993. The well is located on the Theta Vest Structure, north of the Sleipner East Field. Top of Hugin Formation was penetrated at 3796.5 mRKB and supported a 153 m thick oil bearing formation. Seven cores were cut from the Hugin and Skagerak Formations, a total core recovery of 177.6 m.

Well 15/9-21 S was drilled as an exploration well from the Sleipner Vest Field in 1998. The Hugin Formation was penetrated at 4767 mRKB. Only small amounts of oil shows were discovered in the formation, with the strongest shows seen in the interval 4784 to 4798 mRKB. Four cores were cut from 4747 to 4843 mRKB.

Thin sections and corresponding core plug measurements from wells 15/3-7, 15/5-7, 15/6-11, 15/9-19 S and 15/9-21 S are used with permission from Statoil ASA.

1.1.1 Objectives of study

The objective of this study is to gain a better understanding of the reservoir properties in the Hugin Formation located in the Sleipner Field area (Fig. 1.1) in the North Sea. Data from the core samples studied are taken from depths varying from 2.9 to 4.6 km in total vertical depth (TVD) or mRSF. At such depths the reservoir quality is critical, due to both compaction and diagenetic processes. Based on study of porosity and permeability measurements from core plugs, in combination with petrography from thin sections, it is possible to predict the reservoir quality of the Hugin Formation in relation to depth. The main focus will be quartz cementation, and the factors controlling the precipitation of quartz in the Hugin Formation sandstones. Generally there is a trend showing increase in quartz cementation with increasing depth, reducing the reservoir quality due to lower porosity and permeability. Although the quartz precipitation is critical, other diagenetic reactions are also contribute to

a change in the reservoir quality. Factors such as shale content, authigenic kaolinite/ illite and carbonate cement make prediction of the reservoir quality non-straightforward. The North Sea is still an important area for oil and gas recovery, with undiscovered resources to be found. Not far from the studied area, the big oil field Johan Sverdrup was discovered last year and more recently the Geitungen Prospect was also found to contain oil. This shows that the sandstones in the area, including the Hugin Formation sandstones, are promising reservoir rocks. To get a better understanding of these late stage diagenetic sandstones will be important to establish an economic basement in the deep and hot sedimentary basin of the South Viking Graben.

1.1.2 Previous work

Several scientists have previously studied the Hugin Formation, and their work has been applied as a supplement to this study. Most focus has been applied to data concerning quartz cementation and general diagenesis of quartzose sandstones from the South Viking Graben. Publications by e.g. Walderhaug (1994, 1996), Oelkers et al. (1996), and Maast et al. (2011) have contributed to a better understanding of the Middle Jurassic sandstones of the South Viking Graben. Their detailed descriptions regarding the diagenesis of the sandstones have greatly assisted this work.

1.1.3 North Sea area

The North Sea is located between Great Britain, Germany, Scandinavia, The Netherlands, Belgium and France, and is a marginal sea of the Atlantic Ocean. It connects with the Atlantic Ocean through the English Channel in the south and to the Norwegian Sea in the north. It is more than 970 km long and 580 km wide, with an area of 750 000 square kilometer (Wikipedia, 2012). The formation of the North Sea area originates from a major continental collision between Laurentia and Baltica followed by a separation of the same continents. During stretching of the crust, a complex of several basins, platforms and heights were formed in the North Sea, due to the tectonic events and several rifting phases (Devonian to

Late Cretaceous). This study focuses on the southern Viking Graben area close to the Utsira High (Fig. 1.1).

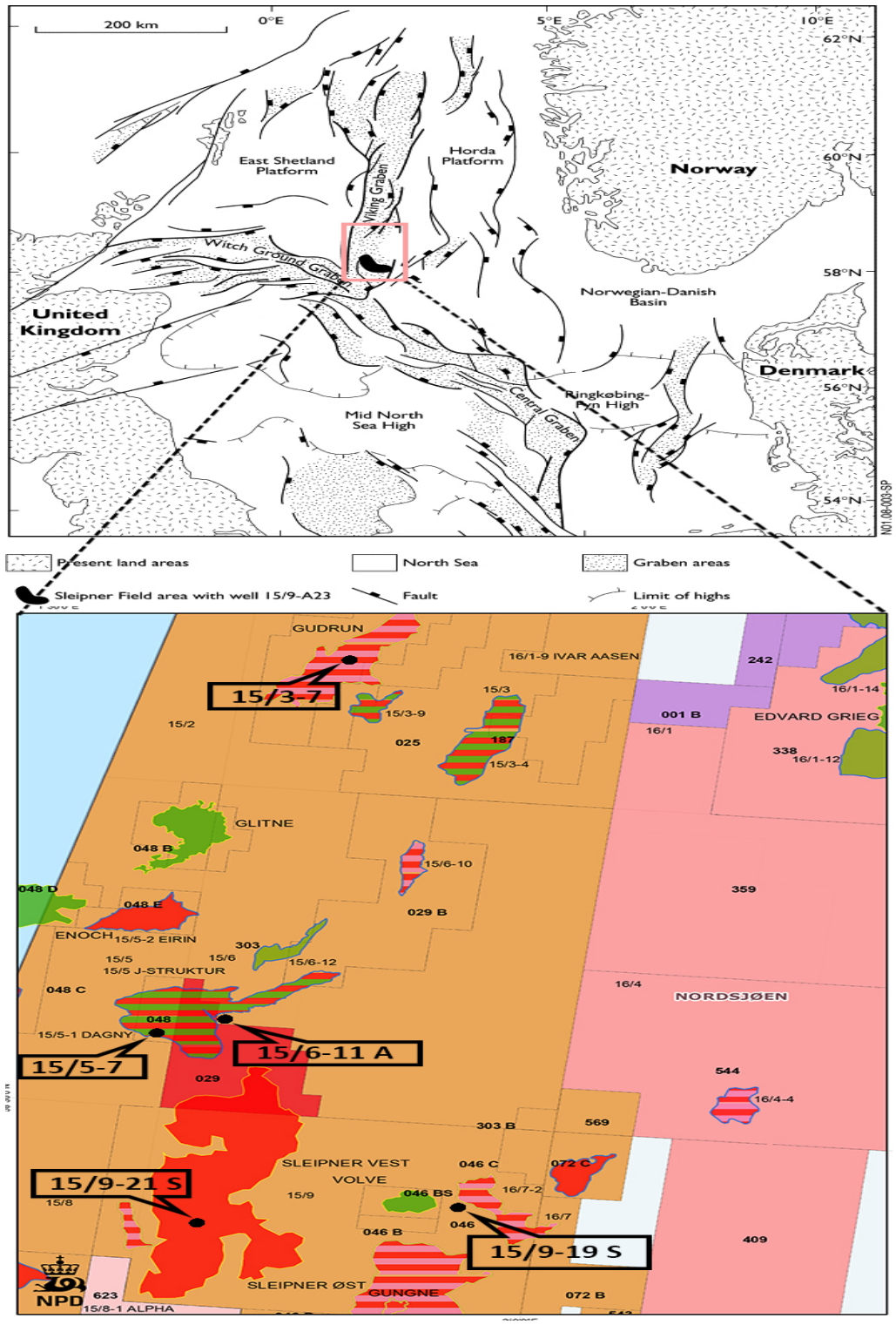

Figure 1.1: Illustrates the Sleipner Field area in the South Viking Graben, with the highlighted wells 15/3-7, 15/5-7, 15/6-11 A, 15/9-19 A and 15/9-21 S. The figure is modified from Norwegian Petroleum Directorate (NPD).

A regional stratigraphy of the southern Viking Graben with the Triassic and Jurassic formations in the Sleipner area is represented in Figure 1.2. The Hugin Formation studied is a part of the Vestland Group of Late Bathonian to Early Oxfordian age. Sandstones from the Hugin Formation in the Vestland Group have been studied and interpreted based on available core data from NPD and Statoil ASA. The core data provided by Statoil ASA include both core photos and thin sections, while the data from NPD is restricted to core photos. The Middle Jurassic Hugin Formation is a Brent derived sandstone with good reservoir quality, despite its deep burial (2.9 to 4.6 km).

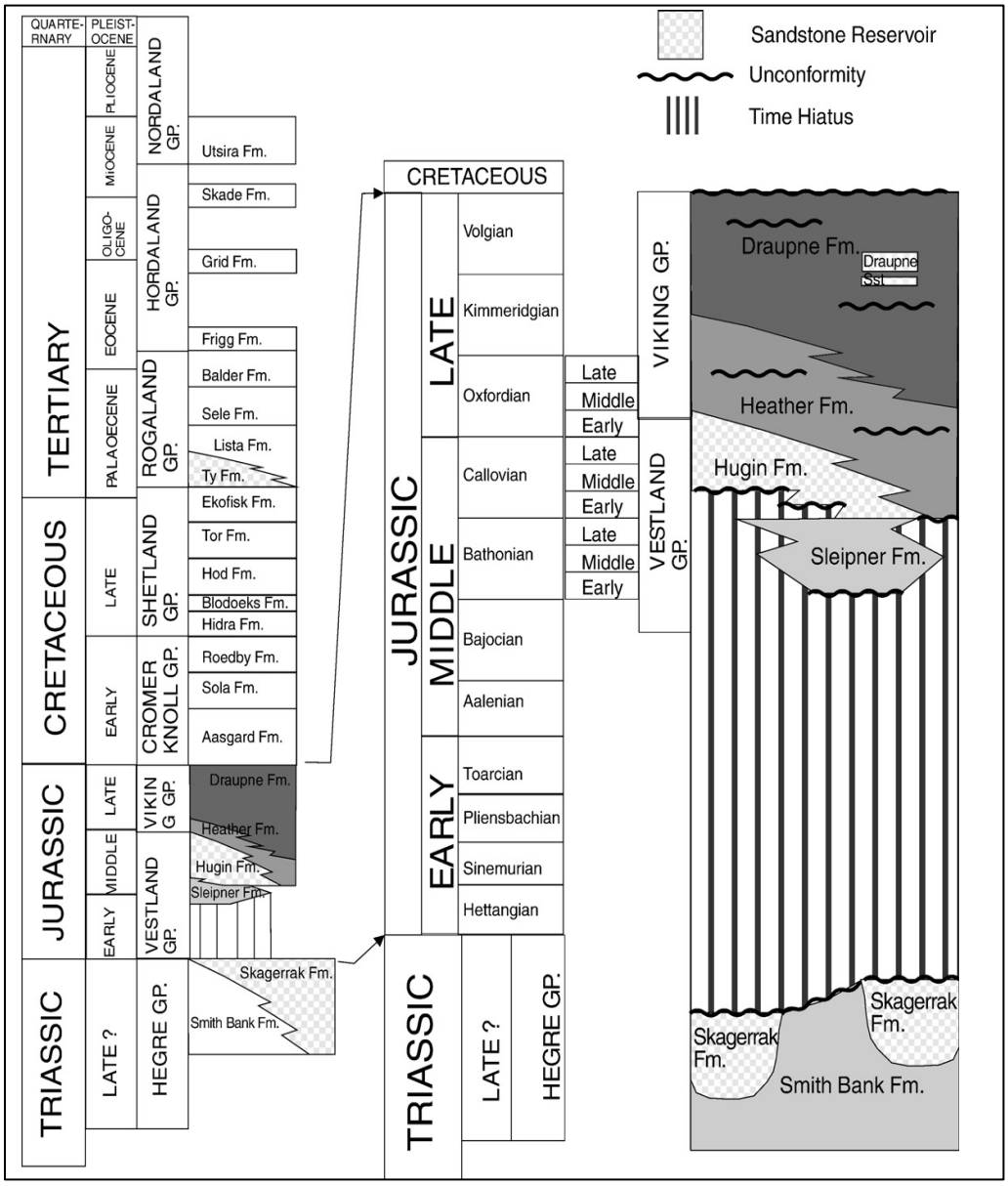

Figure 1.2: The regional stratigraphy of the southern Viking Graben with the Triassic and Jurassic formations in the Sleipner area (Folkestad and Satur, 2008).

1.1.4 Hugin Formation

The Hugin Formation consists of shallow marine sandstones, which encompasses coarsening–upward units of mouth bars and shorefacies, and fining-upward units with tidal channels, and tidal flats facies (Folkestad and Satur, 2008). The coarsening-upward units are a result of delta outbuilding during regression, while the fining-upward units are a result of an estuary environment during transgression. The Hugin Formation has been linked to the retreat and drowning of the older Brent Delta (Folkestad and Satur, 2008), and Figure 1.3 illustrates how the sedimentation was changed during the drowning event. Folkestad and Satur (2008) proposed two different depositional environments based on different facies associations of the Hugin Formation. These environments are: a) regressive or coarsening-upward facies, and b) transgressive or fining-upwards facies. Within these two environments, several facies associations have been accounted for, such as offshore mudstones, shoreface sandstones and mouthbars belonging to the regressive facies, and tidal channels, tidal dunes and tidal flats belonging to the transgressive facies.

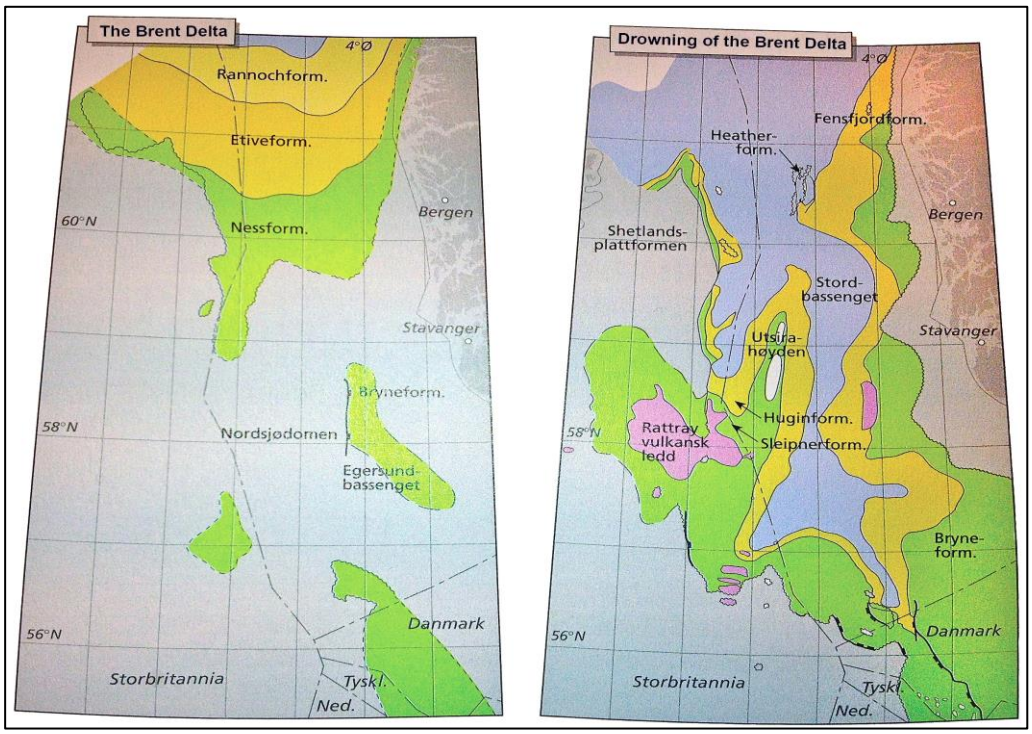

Figure 1.3: The figure displays two stages of the development of the Brent Delta during Middle Jurassic, the Bajocian and the Callovian stage (Fig. 1.2). During Bajocian the Brent Delta developed to the latitude of 62 degrees north (left illustration). In Cavollian age the Brent Delta drowned (right illustration). (Johannesen and Nøttvedt, 2006).

1.1.5 Development of the Hugin Formation

The Hugin Formation developed as a result of weathered products deposited during regressive and transgressive events (Fig. 1.3). The sediments belonged to a former provenance area, hence the North Sea Dome. The events showed progradational, aggradational and retrogradational stacking patterns, a trend representing the drowning of the Brent delta in Aalenian and Bajocian. The stacking pattern observed is also referred to as ”the back-stepping Brent Delta”. The Hugin Formation, which is equivalent to the Tarbert Formation in the Norwegian Sea, is interfingered, and overlain by the open marine mudstones of the Heather Formation. The thickness of the Hugin Formation in the studied area ranges from 80 to 263 m (Tab. 3.1), reflecting varying depositional thickness and erosion as a result of Late Jurassic and Early Cretaceous rift tectonics and block faulting.

1.2 Physical principles

In the following sections, the physical principles of porosity and permeability will be described. The reservoir quality is strongly dependent on these parameters, and insufficient values of either porosity or permeability will retard the possibility of producing from potential oil or gas fields.

1.2.1 Porosity

Porosity is an important property of the reservoir rock, and represents the storage capacity of the reservoir. Porosity can be expressed as a percentage or fraction, and is calculated using the relationship (Torsæter and Abtahi, 2003; Amyx et al., 1960):

Equation 1:

$$\phi = \frac{\text{pore volume}}{\text{bulk volume}} = \frac{\text{bulk volume} - \text{grain volume}}{\text{bulk volume}}$$

Two types of porosity can be measured, total and effective porosity. Total porosity (ϕ_t) is the total amount of voids in the rock compared to the bulk volume of the rock. Effective porosity (ϕ_e) is the ratio of interconnected voids to the bulk volume of the rock. In other words, it is the ϕ_e (among other parameters) that makes the fluids producible from a reservoir. A typical example of a rock with intergranular (interconnected) porosity, hence ϕ_e, is a texturally and mineralogically mature Middle Jurassic Brent sandstone.
Oil or gas "trapped" in intragranular porosity does not contribute to any specific fluid flow, and an example of such a rock can be a skeletal limestone.

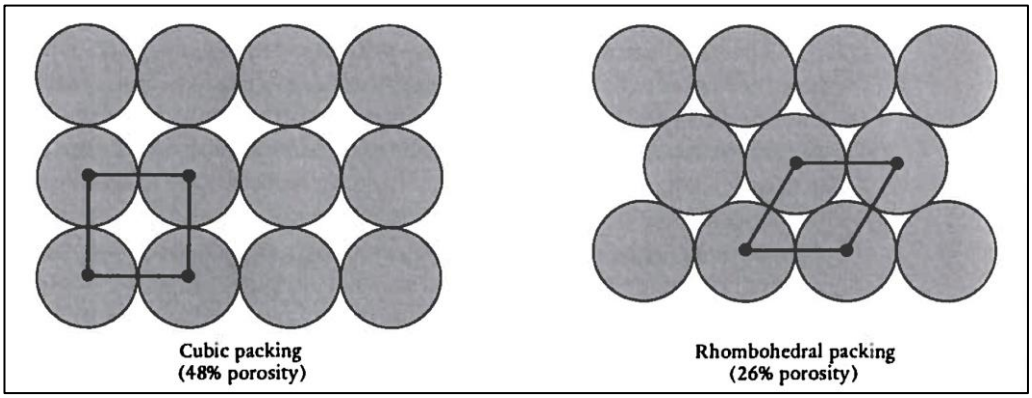

Figure 1.3: The loosest and tightest packing arrangements of uniformly-sized spherical grains give rise to a porosity of 48% for the cubic packing and 26% for the rhombohedral packing (Selley, 1998).

Porosity can be classified as primary or secondary. During deposition, the sediments will be laid down with a primary porosity or original porosity. There are several factors which influence the porosity in this process, such as packing of grains, sorting of grains and the grain shape. In an idealized rock, the maximum primary porosity can be as high as 48% (Fig. 1.3) (Torsæter and Abtahi, 2003). To obtain such a high theoretical value, the spherical grains have to be cubically packed. However, rhombohedral packing of the grains is more representative for sandstone reservoirs, where a porosity of 26 % is achieved (Torsæter and Abtahi, 2003). Depending on the sorting of the grains, a primary porosity can be less than the rhombohedral packing. Smaller grains will fill up available space between the grains, resulting in even lower porosity. Geological processes subsequent to formation of the deposits cause secondary, or post depositional, porosity. The alteration of the original pore spaces in the sediments is a result of both compaction and diagenetic processes. Reservoir properties can either be improved or worsened, depending on the composition of the

sediments when buried. Much of the porosity found in sandstone reservoirs is preserved intergranular porosity. Referring to Selley (1998), secondary porosity is more common in carbonate reservoirs. In these cases, secondary pores are often caused by dissolution, enhancing the reservoir properties compared to the primary porosity.
There are several methods to measure porosity. It can be done by core plug measurements, petrophysical methods or microscopic methods. In this study, data from core plugs and thin sections are used in order to examine the Hugin Formation reservoir properties. A more detailed description regarding the methods will be covered in Chapter 2.

1.2.2 Permeability

Permeability is a property of porous mediums, and reflects the medium's capacity to transmit fluids. A rock may be highly porous, but not possess sufficient permeability to serve as a reservoir rock (Selley, 1998; Bjørlykke, 2001). In order to transport fluids out of the pores, a certain amount of permeability has to be present. Figure 1.4 illustrates the permeability, where fluids can pass through different passages within the rock. These passages can be straight or tortuous, depending on the inner structure of the rock. Permeability can be measured using Darcy's law, which actually defines the parameter. Darcy (1856) performed a series of experiments by letting water flow downwards through sand, and observing factors which affected the flow. Darcy's law (Eq. 2) expresses fluid-flow through a media with respect to the hydraulic potential of the media. The fluid-flow (Q) is controlled by the permeability (k), difference in pressure (Δh), viscosity (μ) and distance (L).

Equation 2:

$$Q = \frac{k\,A\,(P_2 - P_1)}{L\,A}$$

Fluid-flow, Q = $\left[\frac{m^3}{s}\right]$*, Permeability, k =* $[m^2]$*, Difference in pressure, ΔP =* $P_2 - P_1 = [Pa]$*, Viscosity, in* $\left[\frac{Ns}{m^2}\right]$*, Length, L =* $[m]$.

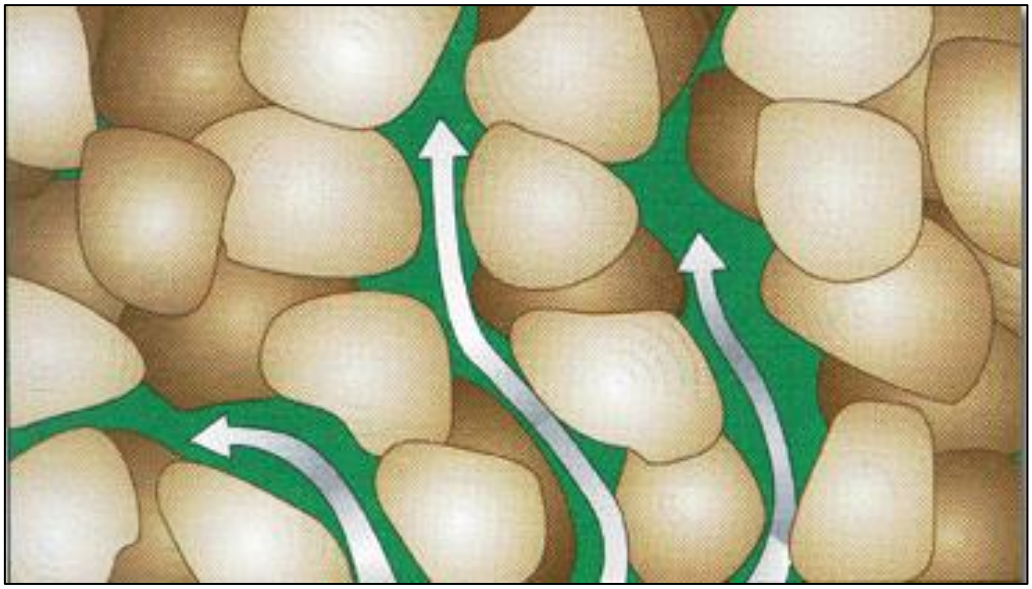

Figure 1.4: Permeability (k) is greater (flow is faster) through the wider passage on the right. Not all the pore spaces are interconnected, but they contribute to the total porosity thoughout (Wikipedia, 2003).

Figure 1.5 illustrates the permeability by using Darcy's law. The fluid-flow (Q), which runs through an area (A) with length (L), is controlled by the permeability (k), the difference in pressure (Δ), and the viscosity of the fluid (μ).

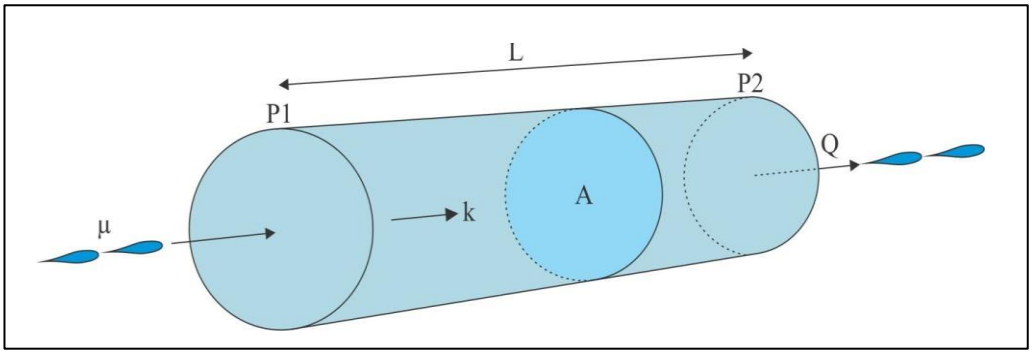

Figure 1.5: The fluid flows through a cylinder with a specific area and length, and is controlled by the permeability, the difference in pressure, and the viscosity of the fluid. Modified after Wikipedia (2011).

There are several methods to measure the permeability, for example, laboratorial experiments on core plugs, well testing, and petrophysical methods. Langeland (1992), claims that permeability by well testing will best reflect the reservoir properties. Allowing fluids to flow naturally into the wellbore will give the best result regarding the true permeability. Analyzing small and narrow core plugs in laboratorial experiments will only

measure the permeability in that specific area. In order to get reasonable measurements by this method, numerous samplings on core plugs must be performed to obtain an average and representative result (Langeland, 1992).

Various techniques are used for permeability measurements of cores, depending on sample dimension and shape, degree of consolidation, type of fluid used, ranges of confining and fluid pressure applied, and range of permeability of the core. The permeability tests are performed on cleaned and dried samples, and the Constant Head Permeameter is often used for this method (Torsæter and Abtahi, 2003).

It is possible to measure the permeability in different directions, both horizontally and vertically. The orientation of the grains may have small effect on porosity, but has a major effect on the permeability. Most of the grains in sandstones have a preferred orientation, and are elongated along with the former current (Fig. 1.6). Most of the sediments are also stratified in layers containing flaky grains, such as mica, shells and clay laminae. In combination, this makes the horizontal permeability higher than the vertical permeability. In general, the horizontal permeability is higher than the vertical permeability although there are exceptions. Overall, the horizontal permeability is considered the most important parameter when it comes to evaluating reservoir quality.

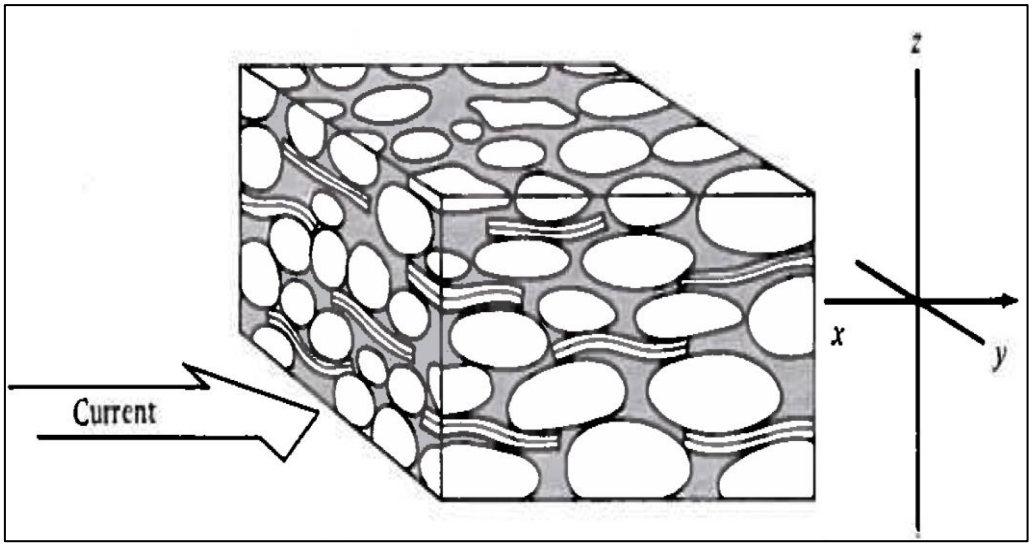

Figure 1.6: Block diagram showing the layered structure of sand, with a preferred direction of the grains parallel to the current. The grains are prolate spheroids, slightly elongated with the current, together with flaky clay minerals, making the horizontal permeability higher than the vertical permeability. Generally, $K_x > K_y > K_z$ (Selley, 1998).

There is often a connection between the porosity and permeability in reservoirs. Porosity-permeability trends for different lithologies can be plotted together, forming a map of porosity and permeability relationships (Fig. 1.7). The general trend is that an increase in porosity will give an increase of the permeability. But that is not always the case. For example, fractured rocks fall above the sandstones since the porosity is very low, but the fractures are often connected and follow a preferred direction, and hence the permeability is high. Clay cemented sandstones possess a high porosity, but the porosity is caused by microporosity due to clay-bound and capillary-bound water (Website, 2011). This water will not contribute to any fluid flow, so the permeability is low. For clean sandstones, there is a distinct positive correlation between porosity and permeability. With such a lithology there will be a linear increase of the porosity together with the permeability (Fig. 1.7).

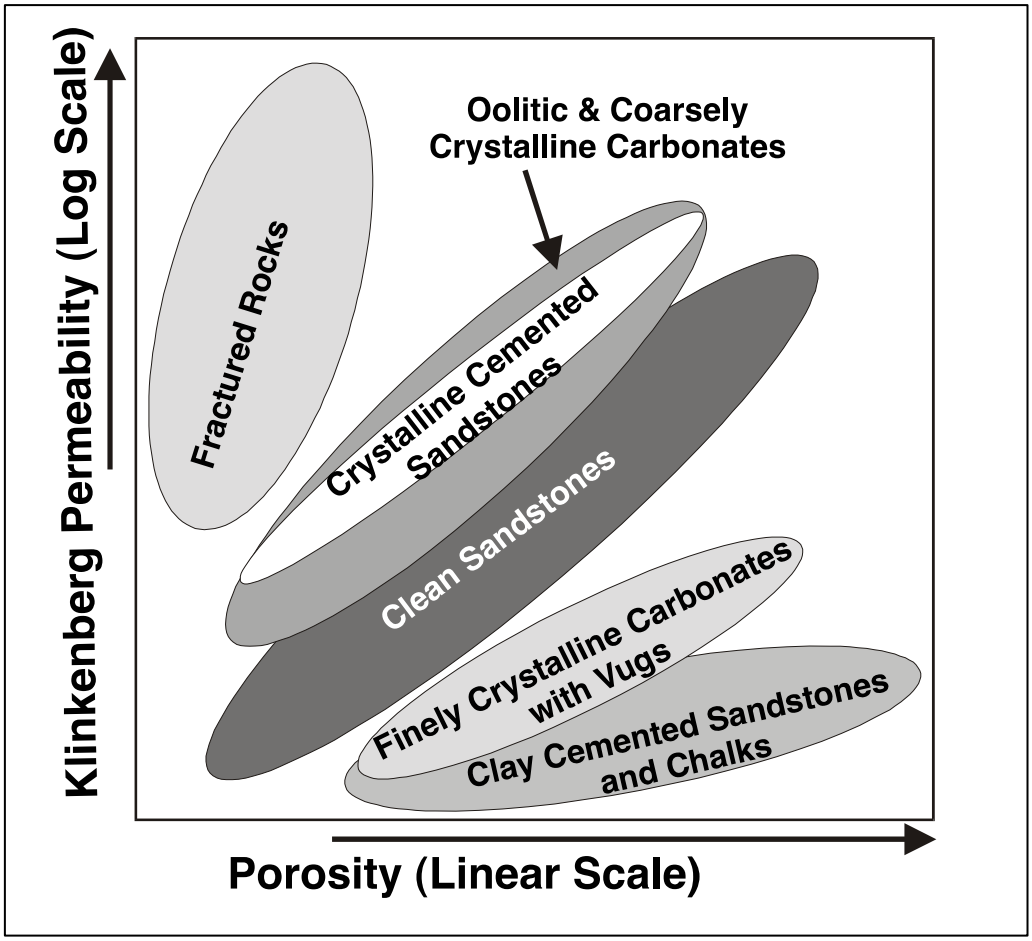

Figure 1.7: Porosity-permeability trends for different lithologies. Fractured rocks plot above the sandstones since the porosity is very low, but the fractures are often connected and follow a preferred direction, and hence the permeability is high. By comparison, clay cemented sandstones possess a high porosity, but the porosity is mainly due to microporosity because of the clay bound and capillary bound water. For clean sandstones there is a distinct positive correlation between porosity and permeability (Website, 2011).

1.3 Diagenetic processes

In order to predict the sandstone reservoir quality, it is crucial to understand the diagenetic processes which take place after the deposition of the sediments. This study focuses on diagenetic processes influencing porosity and permeability of Middle Jurassic sandstones of the Hugin Formation in the southern part of the Viking Graben. The diagenetic processes are interpreted by optical microscopy and modal analysis of thin sections, integrated with data from core plug measurements and study of core photos. In the broadest sense, diagenesis encompasses all changes or modifications to the sediment after deposition. The sediments

may experience several diagenetic stages and regimes. After Burley et al. (1985), the different regimes include eogenesis (diagenesis in the depositional environment), mesogenesis (the deep burial phase of diagenesis) and telogenesis (late-stage diagenesis followed by uplift). During burial, the sediments undergo sequential changes, depending on the regime, and may be influenced by biogenic activity, changed pore-water composition, and higher pressures and temperatures. The diagenetic changes in the sediments can involve:

- Rearrangement of grain packing and decreased porosity (Fig. 1.3) as a result of compaction;
- Loss of porosity due to cementation;
- Partial destruction of framework grain owing to pressure solution;
- Destruction of framework grains due to dissolution, causing secondary porosity;
- Replacement of some minerals by others, and;
- Clay-mineral authigenesis.

Many of these processes are discovered and well documented in this thesis in Chapter 3. In the following sections, physical and chemical diagenesis are briefly described.

1.3.1 Physical diagenesis

Mechanical compaction of sediments is mainly a result of an increase of the overburden or tectonic forces. The porosity will often decrease because of this, for example, by grain rearrangement. The compaction, besides grain rearrangement, involves bending of flexible grains such as micas, plastic and ductile deformation of grains, grain fractures, and pressure solution of quartz and other minerals (Boggs, 1992). Pressure solution is often referred to as chemical compaction since it involves dissolution at grain contacts.
Depending on sandstones lithologies, different patterns of mechanical compaction are seen, as illustrated in Figure 1.8. Quartz arenite is more rigid than sandstones containing higher degree of feldspar or lithic fragments, preserving porosity to greater depths (Worden and Burley, 2003).

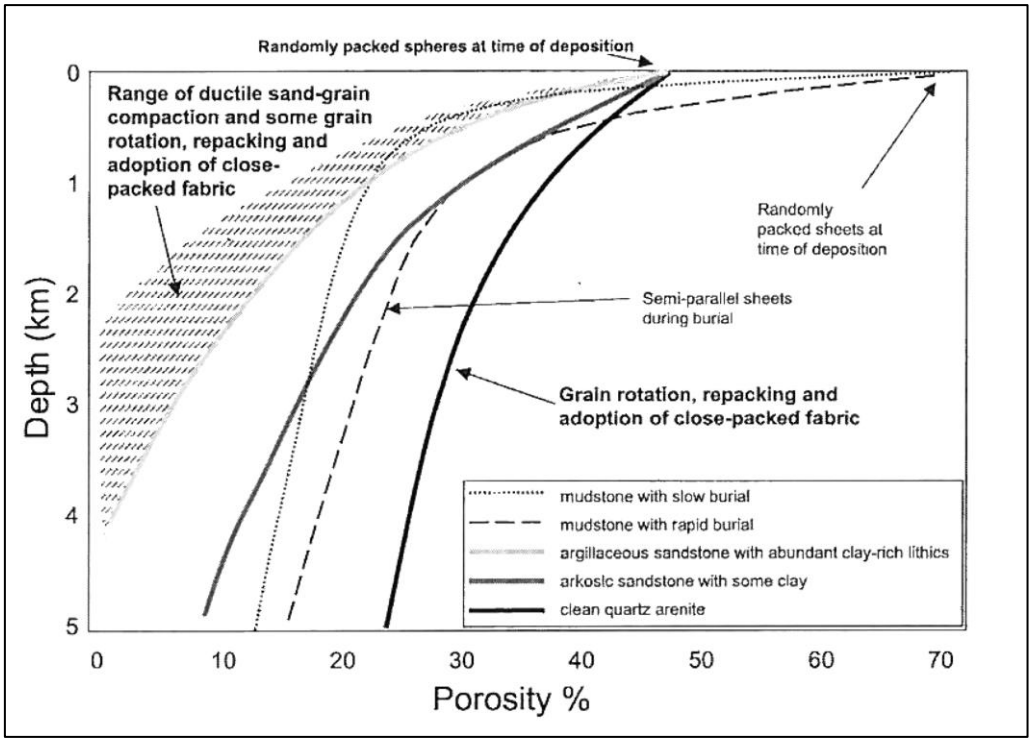

Figure 1.8: Porosity plot showing lithologies with different patterns of mechanical compaction. A quartz arenite will possess more rigidity than arkosic sandstone due to grain composition. Argillaceous sandstones possessing a high degree of fine material will rapidly loose porosity (Worden and Burley, 2003).

Mechanical compaction takes place in the shallower parts, extending to depths of 0.6 to 1.5 km (Boggs, 1992). Chemical compaction proceeds to depths reaching metamorphic regimes. Normally, the metamorphic regime will be encountered at depths of approximately 10 km, with a geothermal gradient of 30 °C per km of depth.

1.3.2 Chemical diagenesis

Generally, siliciclastic sandstones are deposited in subaqueous environments. The sediments experience different environments during burial, relative to pore water compositions. The different environments can range from fresh to hyper saline water, pH can range from acid to alkaline, and the redox conditions can vary from oxidized to reduced. Also, the abundance of different elements will differ between fresh and saline water.

The Hugin Formation consists of marine sandstones, and comprises offshore mudstones, shallow marine sandstones and coastal plain deposits (Folkestad et al., 2008). Common

authigenic minerals in marine sediments are chlorites, glauconite, illite/smectite clays, K-feldspar overgrowths, quartz overgrowths and carbonate cement (Boggs, 2006). The authigenic minerals will be presented in Chapter 3 and 4, and discussed further in Chapter 5.
Dissolution of framework grains, in particular feldspar, is common in environments where meteoric waters flushes through the sediments, hence in the eogenetic regime. The dissolution is a weathering reaction, mostly seen in fluvial and shallow marine sediments, where feldspar dissolves to form kaolinite and potassium ions. The reaction occurs mostly at depths shallower than 100 m, since the reaction requires a constant supply of protons and removal of cations (such as Na^+, K^+, and silica) by fluid flow. Clay mineral reactions also take place in the mesogenetic regime, where illitization of kaolinite, and the smectite replacement by illite, are the most common occurance.
Silica cement, such as quartz overgrowths, is common in both sandstones and shales. In sandstones, they are typically most common in quartz arenites but are also described from less mature rocks containing matrix, e.g. arkoses (Boggs, 1992). Dutton and Diggs (1990) showed that the content of quartz cement tended to decrease exponentially with increasing matrix content of sandstones. Pure quartz sandstones are most common in depositional environments of high kinetic energy, therefore quartz cement is most commonly associated with facies such as ancient beaches, marine bars, dessert dunes and fluvial sandbars (Wescott, 1983). The pore spaces available after mechanical compaction can be partially or completely filled with quartz. This secondary quartz will grow as a coating on the detrital grains, and in crystallographic continuity with them.
The source of silica cement could be from pressure solution at grain contacts, and feldspar alteration and dissolution (Tracy et al., 2006). Local quartz dissolution at mica/quartz boundaries, and adjoining stylolites, is another source of silica (Oelkers et al., 1996). The source of silica cement is problematic and debated amongst scientists today. Many petrographic studies have been done to try and predict the source, and many theories have been postulated. The sources of quartz cement will be further discussed in Chapter 5.

1.4 Sources of errors

There are several sources of errors in this analysis. In relation to the petrograpic work and the modal analysis, the point counted minerals may not be representative of the whole sample since the step lengths represent the average grain size. Some grains could therefore not have been counted due to different sizes. Regarding the framework grains, there are some pitfalls when the interpretation is being done. If plane-polarized and cross-polarized light are not used consistently, the polycrystalline quartz grain can be mistaken for monocrystalline, and quartz and feldspar grains can be mistaken. The quartz grains can also be mistaken for feldspar, which can result in an overestimation of the amount of feldspar grains in the samples. The thin sections studied clearly showed the feldspar, with both cleavage and dissolution features making it easy to distinguish from quartz. Despite this clear separation, in most of the samples there could have been some degree of misinterpretation. In addition, orthoclase can strongly resemble the quartz grain. However, orthoclase often possesses cleavage and displays a slight cloudiness. In well 15/5-7 and 15/6-11 A, the thin sections were stained to distinguish between alkali feldspar and plagioclase, as alkali feldspar is shown by yellow in color. In such case, there was little chance of misinterpretation concerning the quartz and alkali feldspar. However, in some samples, it was difficult to distinguish between the untwinned plagioclase and the detrital quartz grain. Viewing at higher magnification could reveal the cleavage, and the slightly alteration of the plagioclase, but minor misinterpretation could have been made.
The quartz cement was sometimes difficult to predict, since the dust ring surrounding the detrital quartz grain was missing in rare cases, and occasionally the grains were interlocking each other making it harder to predict the actual amount of cement. To better recognize the quartz cement from the detrital quartz grains, other methods could have been applied, such as cathodoluminescence (CL) (Smith and Stenstrom, 1965). In this work, the quartz cement was easily detected except from some minor samples, so any extended methods were not applied.
Regarding the appearance of other authigenic minerals, mistakes could have been made in determining the precise amount appearing in the samples. Pyrite could be mistaken for

organic material where thin sections were not sufficiently polished, and glauconite may have been mistaken for matrix in places.

2 Methods

Optical microscopy by thin sections and core plug measurements are used to examine the reservoir properties of the Hugin Formation. Thin sections and core plugs measurements are provided by Statoil ASA. Additional core photos from the Norwegian Petroleum Directorate (NPD) homepage are also applied, in order to assist the reservoir characterization.

2.1 Thin sections

All the thin sections were borrowed from Statoil ASA and analyzed in the microscopy laboratory at the Department of Geology and Mineral Resources Engineering at NTNU. The thin sections were analyzed by using an optical microscope (Leika DM 2500P), with both transmitted and reflected light. The reflected light was used to distinguish pyrite in the samples, since it tends to reflect a significant amount of light. In cases of limited reflection, the crystal shape of pyrite was used for interpretation.
Transmitted light was used for the identification of the remaining minerals. All the thin sections were polished and possessed good quality. The samples from the wells 15/5-7 and 15/6-11 A were also colored for easier identification of alkali feldspar and carbonate. Sodium cobaltinitrite staining was used to identify alkali feldspar, and potassium ferricyanide and Alizarin Red S were applied to identify carbonates.
The staining technique, with respect to calcite cement, makes the iron-rich cement appear blue under the polarized microscope. Since the iron-rich calcite precipitates at a later stage, the interpretation was easier concerning the paragenetic sequence presented in Table 5.1. The staining method also makes it possible to distinguish between ferrous dolomite and calcite, since both minerals react differently with the staining. Calcite will appear as pale to deep blue (depending on iron content), while dolomite will appear as very pale blue (Adams and MacKenzie, 2001). Since the dolomite has a minimal reaction with the potassium ferricyanide acid, the blue color is much weaker.

2.2 Modal analysis

Modal analysis was done using a Pelcon Point Counter program, and using 300 points counted in each sample. The step length varied from one sample to another, equal to the dominant size of the framework grains.
Modal analysis, based on point counting on thin sections, will measure closer to the effective porosity rather than total porosity if the samples include fine-grained, clay materials. The microporosity in such cases may be overlooked, and the estimates of porosity will be lower compared to core plug measurements. In cases with clay-supported sandstones, corrections can be made regarding the microporosity. Such corrections were not done in this study.

2.3 SEM analysis

Sample 3826.0 mRKB from well 15/5-7, and sample 3838.5 mRKB were analyzed by Scanning electron microscopy (SEM), in order to identify diagnostic features of authigenic clay, matrix and diagenetic cements, in particular for the identification of glauconite and illite. The SEM analysis included backscattered electron images (BEI), in combination with energy dispersive spectra (EDS). The different peak positions seen in EDS reflect energy, and the intensity of the peaks is proportional to the different elements concentrations. The SEM analysis was performed at the Department of Material Science and Technology, NTNU, and thin sections were prepared with a carbon coating before examination. SEM analysis had to be applied in order to detect the authigenic minerals illite and glauconite.

2.4 Permeability

The permeability on both horizontal and vertical core plugs was determined by allowing nitrogen gas to flow through the samples. Using Darcy's law (Eq. 2), the gas permeability was calculated and established. In addition, liquid permeability was also measured by letting brine flush through the samples and then performing the calculation using Darcy's law.

Regarding this thesis, the horizontal gas permeability (K_g) will be applied when the reservoir properties in the Hugin Formation are analyzed.

2.5 Porosity

Porosity examined in the thesis is provided from excising core plug measurements and modal analysis. The porosity from the modal analysis is presented in a subsection below. In core plug measurements, the grain volume is measured by helium injection using Boyle's law Porosimeter, and the bulk volume is determined by immersion of the sample in mercury. Porosity is then calculated using Equation 1. Helium has several advantages compared to other gases: Its small molecules rapidly penetrate pores, and the gas is inert and does not adsorb onto rock surfaces as air might do. In addition, helium possesses high diffusivity and therefore affords a useful means for determining porosity of low-permeability rocks. In immature textural sandstone, the helium porosity will measure closely to the total porosity, and give a higher value than porosity measured by point counting using a standard microscope. It is the horizontal porosity from the core plugs which is used in this thesis to examine the reservoir properties in the Hugin Formation.

3 Petrography

3.1 Introduction

This study of the Hugin Formation is a petrographical study, but since Statoil ASA also provided core photos, a short introduction of how this material has been used, in addition to the thin sections, is briefly described below.

The thickness of the Hugin Formation varies from 80 to 263 m in the studied wells (Tab. 3.1). Based on the core photos, the sandstones appear to be homogeneous with some intervals of finer materials, such as clay laminaes. The formation also contains cemented intervals with both quartz and calcite. It is important to emphasize that the interpretation is not based on visualization of actual cores, but by studying core photos together with provided data from core plugs. A short presentation of well 15/6-11 A will be given below, where core photos and data from core plugs have been used to interpret the Hugin Formation. Characterizations of the other wells studied are given in Tables A.1, A.2, A.4 and A.5 in the Appendix, which is based entirely on the study of thin sections.

Well 15/6-11 S is located north of the Sleipner Field (Fig 1.1). As Table 3.1 displays, the interval studied is 32 m of the total lithostratigraphy containing 80 m. Figure 3.1 shows core photos from the depth of 4148 to 4158 mRKB. The interval consists of a very well to well sorted fine sandstone which is subrounded, and it contains both calcite and quartz cement to a varying degree (Tab. A.3). Calcite cement is quite easy to detect just looking at the core photos, since the cement appears as white sections, quite distinct from the rest of the core which has darker color. Presence of calcite cement can be verified by checking porosity and permeability data from the core plugs. In the interval 4149.29 to 4149.50 mRKB, and 4150.85 to 4151.50 mRKB, calcite cement is clearly visible (Fig. 3.1). In between these two intervals, there are some thinner calcite cement intervals, also seen visually due to a more greyish color. From 4151.50 mRKB, some thin laminaes of finer material is present together with the calcite cement until cleaner sandstone appears from 4152.00 mRKB.

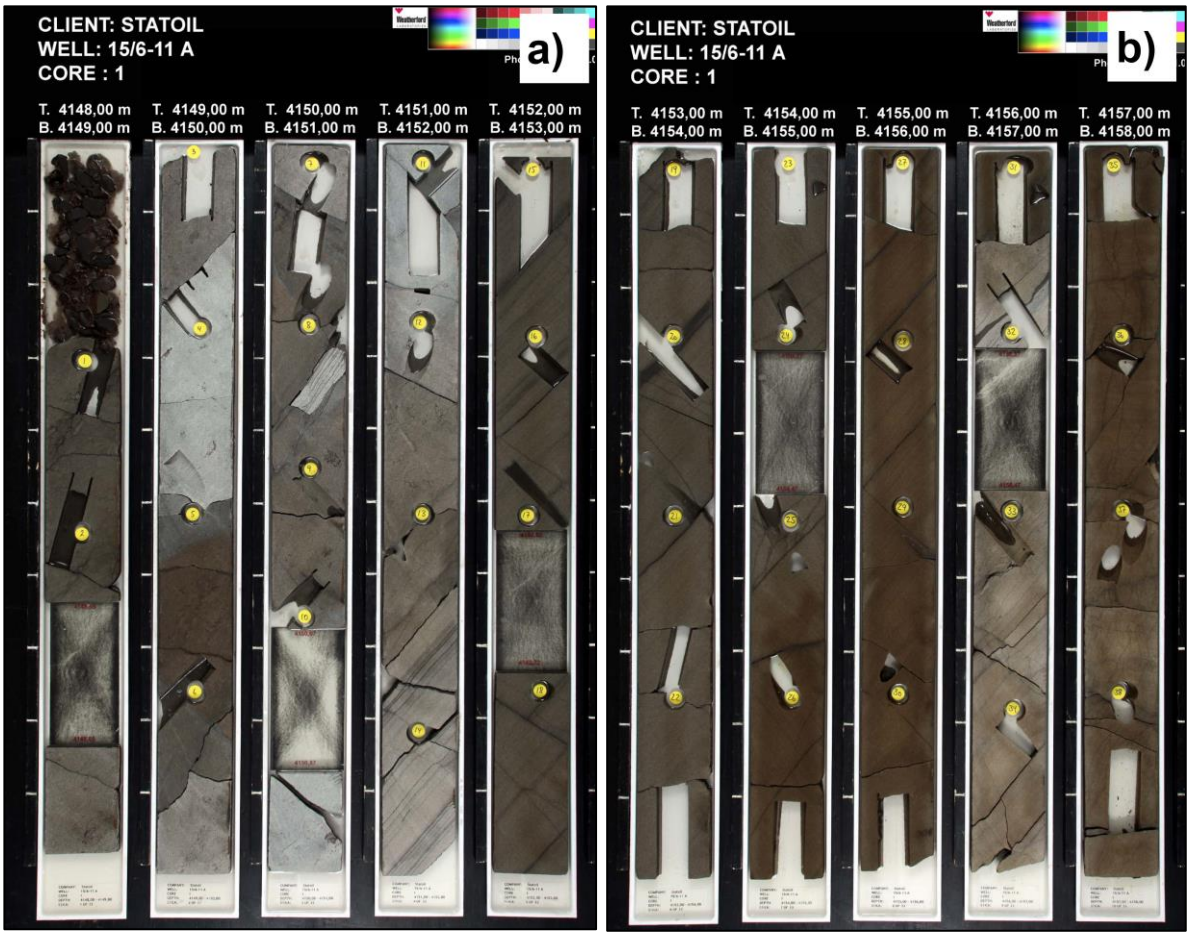

Figure 3.1: Core photos from well 15/6-11 A, showing the interval 4149 to 4158 mRKB. a) Interval 4149 to 4153 mRKB consists of a well-sorted sandstone with calcite cement present in varying amounts. At 4149.25 mRKB the intense white color is due to abundant calcite cementation, while darker color in the interval indicates lesser cementation. b) Interval 4153 to 4158 mRKB contains less calcite cement, but quartz cement is more abundant. In the section 4156.15 to 4157 mRKB the white color is due to quartz cement, which could be mistaken for calcite cement. This interval also consists of a well-sorted sandstone, but with hydrocarbons present, seen as a darker brown interval from 4154.50 to 4156.15 mRKB.

This clean sandstone is continuous to 4156.15 mRKB where it suddenly changes character to a brighter color which resembles the previous calcite cemented intervals. Although the color is similar, the origin is not the same. The brighter color in the interval is caused by an extensive quartz cementation (instead of calcite cement) and besides the quartz cement, stylolites are also present (Fig. 3.2b). The stylolites are visible with their characteristic zigzag pattern. The use of fluorescent light gives an indication of hydrocarbons present in the formation (Fig. 3.2a). The original colors of the formation might be hidden because of the hydrocarbons present, so it is not possible to accurately judge the color by looking at core

photos alone. The available data from the core plugs is a better indicator of composition, and shows the brighter color is due to quartz cement and not calcite.

Throughout the rest of the well, the trend is an on-and-off sequence of both quartz- and calcite cementation, and the sand is homogenous, varying from moderate to very-well sorted, very-fine to fine grained (except from a couple of coarse samples), and the roundness is subrounded to subangular. Since no direct visual contact with the cores has been established, no structures have been detected, and sedimentary facies have been difficult to predict. But some authigenic minerals, such as pyrite, may be helpful to draw conclusions about the sedimentary environment where the sediments were deposited.

For the remaining description of well 15/6-11 A, the reference is Table A.3 (Appx. A).

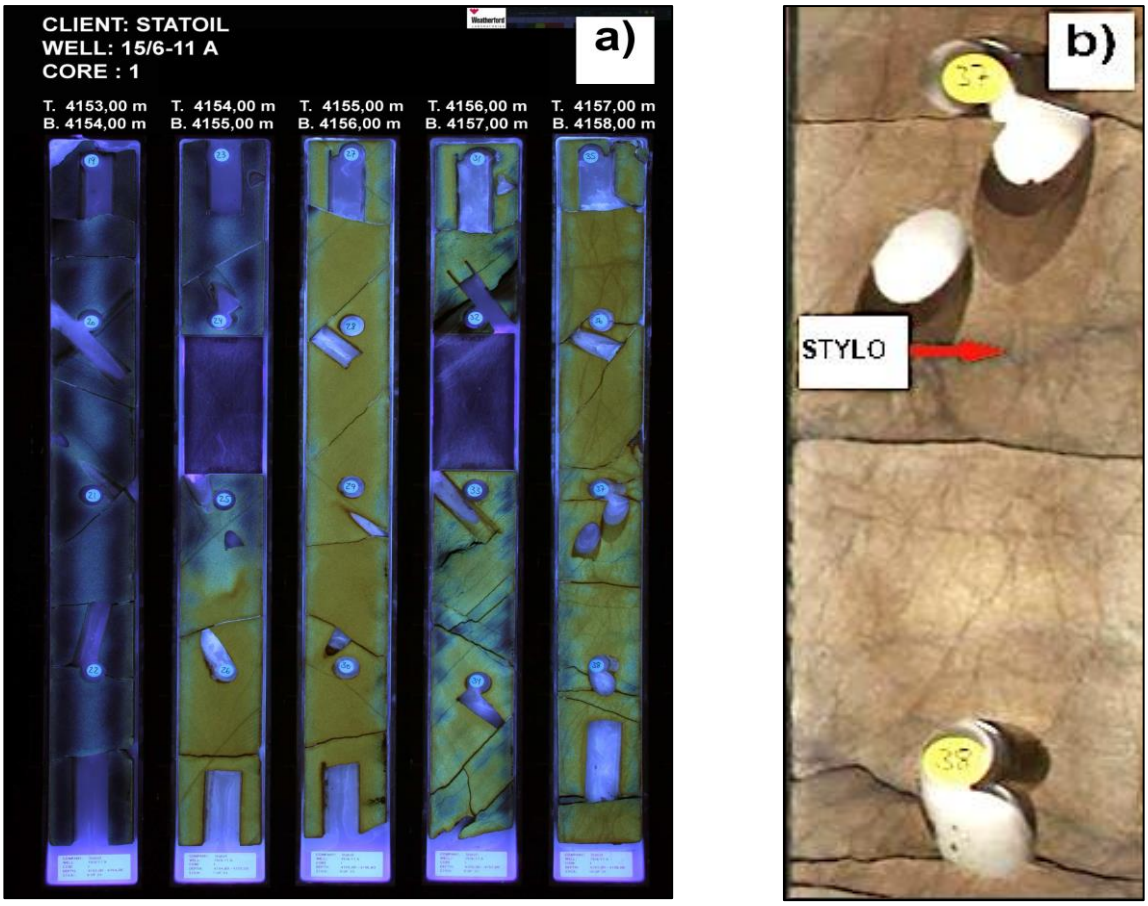

Figure 3.2: Core photos from well 15/6-11 A. a) Showing the interval from 4153 to 4158 mRKB with fluorescent light. The greenish/yellowish color is an indicator of hydrocarbons present in the formation. b) Stylolites (STYLO) appearing as dark lines showing a zigzag pattern in the core, taken from 4156.50 mRKB.

The wells 15/3-7, 15/5-7, 15/6-11 A, 15/9-19 A and 15/9-21 S were analyzed using an optical microscope. Based on the study of 262 thin sections, the petrography and the texture of the Hugin Formation was discovered, and is described in the sections below. All the information is available in Tables A.1, A.2, A.3, A.4 and A.5 in the Appendix. The modal analysis is performed on a selection of the thin sections, to compare properties from different depths, and to compare modal analyzes against core plug measurements. Well 15/3-7 represents the deepest well regarding the modal analysis, while 15/9-19 A represents the most shallow well. The main focus has been study of the distribution of porosity and permeability, and interpretation of diagenetic processes which influence the reservoir property of the formation. Optical micrographs taken are from samples which best illustrate phenomena as texture, mineralogy, and diagenetic features. Where there are special features or special footprints regarding textures, mineralogy, or diagenesis, it will be highlighted in the form of an extended description in this chapter.

Table 3.1 displays all the wells with information about the core photos, thin sections and the lithostratigraphy of the Hugin Formation. The core photos cover a greater depth interval compared to the thin sections, except from well 15/6-11 A. In this well, the depth interval for both core photos and thin sections is identical. The table gives a good overview of the wells, and the data available from each for examination.

Table 3.1: Overview of the available core photos and thin sections related to depth (mRKB). The litostratigraphy of the Hugin Formation is also provided.

Well	Core photos		Thin sections				Lithostratigraphy Hugin Formation (m)	
	Interval (mRKB)	Total (m)	Interval (mRKB)	Samples	Total samples	Total (m)	Interval (mRKB)	Total (m)
15/3-7	4609-4668	59	4609-4622	12	31	13	4607-4793	187
			4650-4652	3		2		
			4755-4779	10		24		
			4782-4791	6		9		
15/5-7	3826-3940	114	3826-3841	13	24	15	3821-3919	98
			3848-3853	3		5		
			3861-3865	2		4		
			3875-3885	3		10		
			3897	1		-		
			3912-3913	2		1		
15/6-11 A	4148-4180	32	4148-4180	57	57	32	4121-4201	80
15/9-19 A	3837-4017	180	3837-3918	78	78	81	3797-3919	122
15/9-21 S	4747-4841	94	4769-4841	72	72	72	4769-5032	263

3.2 Petrography of the Hugin Formation

The sample materials are provided from wells at depths between 3826 and 4841 mRKB. Depending on the mean sea level, kelly bushing elevation and degree of inclination of the deviated wells, the depth relative to the sea floor (mRSF), or true vertical depth (TVD) will vary from approximately 2900 to 4660 mRSF (Tab. A.1 to A.5).

In well 15/3-7, the entire Hugin Formation lithostratigraphy is not covered according to the available core photos and thin sections. The core photos only cover the interval of 4609 to 4668 mRKB, leaving the final 125 m uncovered. Regarding the thin sections, there is a gap of missing samples between the depths of 4652 to 4755 mRKB. Well 15/5-7 provides good data throughout the entire lithostratigraphy, for both the core photos and the thin sections. Almost half of the Hugin Formation in well 15/6-11 A is covered by both core photos and thin sections, and well 15/9-19 A is also sufficiently covered. For well 15/9-21 S, there is a missing section between 4841 and 5032 mRKB.

Despite the missing intervals, the data is adequate to analyze the Hugin Formation reservoir properties in relation to depth.

3.3 Detrital grains

The main content of detrital grains in the Hugin Formation is quartz, feldspar, muscovite, glauconite and rock fragments such as chert, quartzite, shistose quartzite, and in addition small amounts of heavy minerals as zircon, tourmaline and rutile. Some opaque minerals were also discovered, primarily pyrite. Pyrite and glauconite will be described in Section 3.6.

3.3.1 Quartz

The Hugin Formation consists mainly of detrital quartz grains, both polycrystalline and monocrystalline, but with a predominance of monocrystalline quartz grains. The monocrystalline grains show both uniform and undulose extinction (Fig. 3.3). The undulose extinction can be a result of strain, and is found in quartz grains from both metamorphic and igneous rocks. The polycrystalline grains are easily identified in cross-polarized light, (Fig. 3.4b). The boundaries appear both sutured and straight, and the texture can be helpful to predict the provenance. Sutured contacts between grains are characteristic of quartz from a metamorphic source, and straight contacts are found in quartz grains from an igneous source or in recrystallized metamorphic rocks (Adams et al., 1984). Sometimes the quartz grain can be mistaken for one individual grain when viewed in plane-polarized light, but in this case the polycrystalline quartz grain was clearly recognizably in both plane-polarized and cross-polarized light (Fig. 3.4).

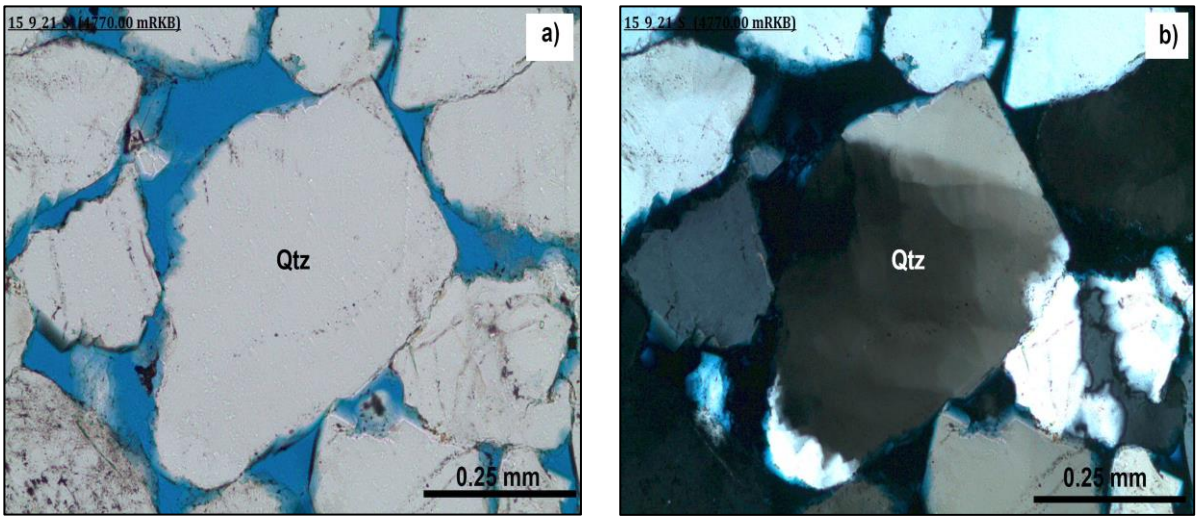

Figure 3.3: Optical micrographs of sample 4770.00 mRKB from well 15/9-21 S. a) Monocrystalline quartz grain is present in the middle of image taken with plane-polizared light. b) Identical to (a) only taken with cross-polarized light. The undulose extinction is clearly visible with cross-polarized light, which may be a result of deformation. (Qtz = quartz).

Some of the polycrystalline grains show preferred crystal orientations, which is typical for foliated metamorphic rocks. The collection and content of the polycrystalline grains can be used to establish the provenance area.

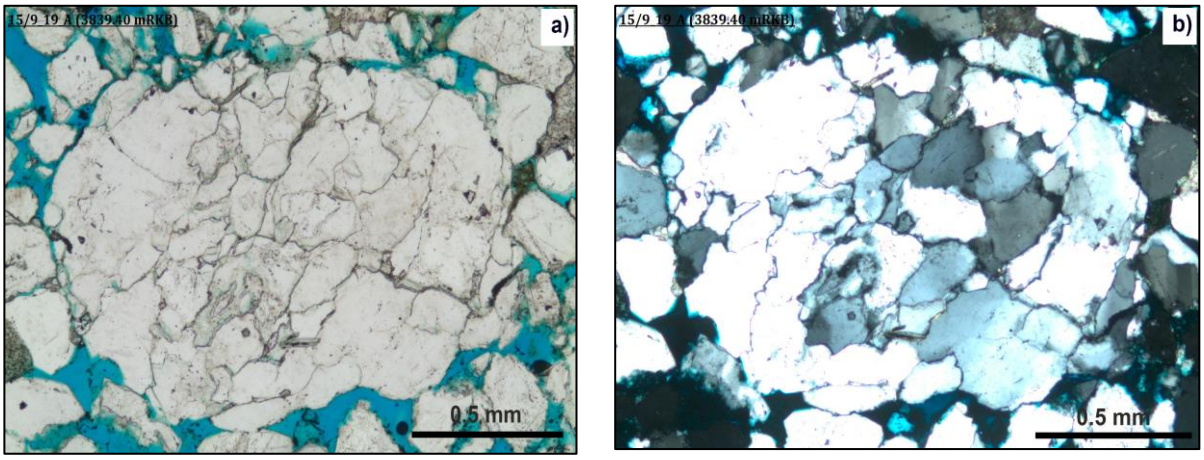

Figure 3.4: Optical micrographs of sample 3839.40 mRKB from well 15/9-19 A. Polycrystalline quartz grain in the middle of figure with sutured grain contacts with plane-polarized light in a), and cross-polarized light in b). Individual grains are clearly visible with cross-polarized light (b). The sutured grain contacts are well seen in both images.

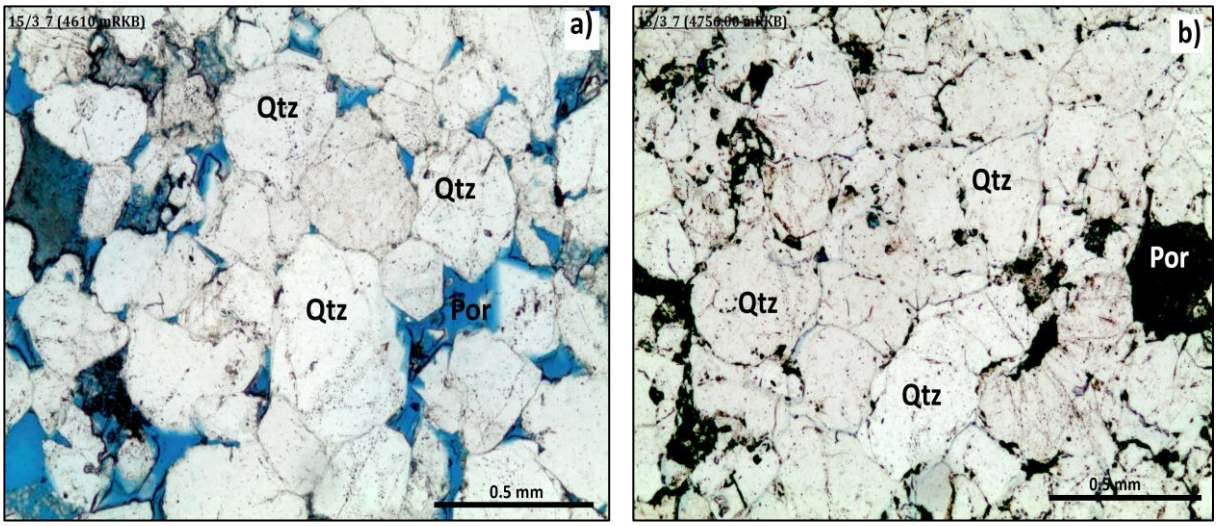

Figure 3.5: Optical micrograph of sample 4610.00 mRKB and 4756.00 mRKB from well 15/3-7. Interlocking texture of quartz grains as a result of mechanical compaction and quartz precipitation seen in both images. (Qtz = quartz, Por = Porosity).

In several samples, the quartz grains have inclusions and in some places the grains are fractured which can be evidence of mechanical deformation. In some intervals, the quartz grains are interlock (Fig. 3.5) as a result of either compaction and/or quartz precipitation.

3.3.2 Feldspar

Feldspar is common in most of the samples from the Hugin Formation. Both plagioclase and alkali feldspar are present in varying amounts. In well 15/5-7 and 15/6 11 A, the samples have been colored to distinguish between plagioclase and alkali feldspar, as the latter will appear yellow and is therefore easily recognizable. The samples have been stained with sodium cobaltinitrite.

Plagioclase is easy to identify where the Carlsbad and albite twins are present, but untwinned plagioclase resembles quartz and can be overlooked. However, quartz does have distinguishing features; it is uniaxial, has no cleavage and does not usually show signs of alteration. Plagioclase is often seen with alteration to sericite (fine-grained white mica) in several samples in the wells (Fig. 3.6).

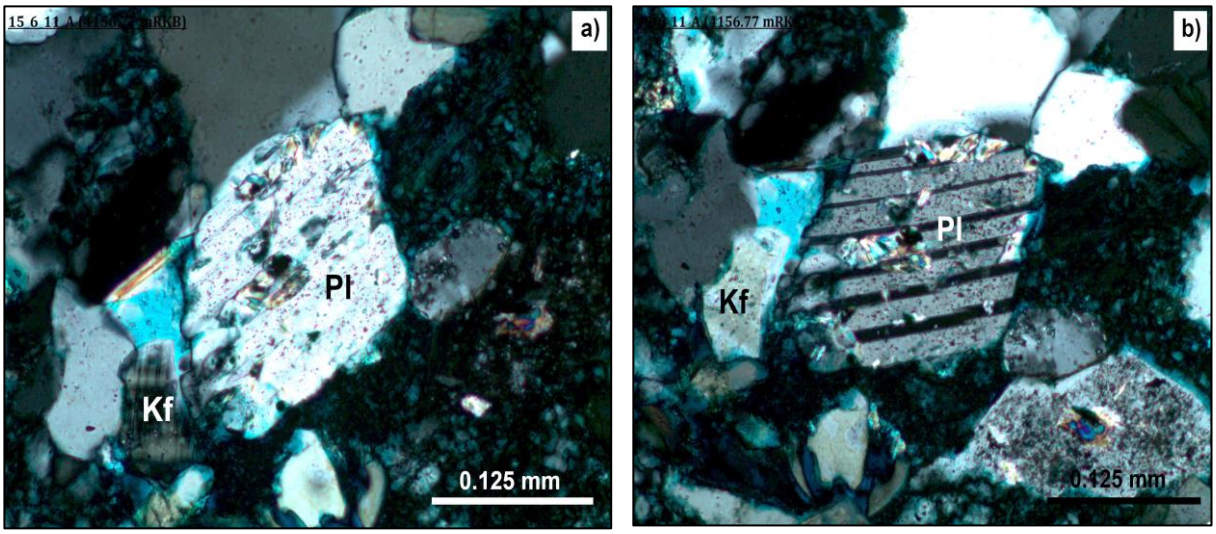

Figure 3.6: Optical micrographs of sample 4156.77 mRKB from well 15/6-11 A. Both images are taken with cross-polarized light. a) Detrital grain of plagioclase, which is partly altered to sericite. The sericite is distributed along the twin lamellae in the plagioclase grain. Alkali feldspar is present showing the characteristic tartan twin pattern for microcline. b) Twins in plagioclase is clearly visible in image. (Kf = Alkali feldspar, Pl = Plagioclase).

Microcline is recognized by the tartan twin pattern. This grid-twinning pattern is common for alkali feldspar, and the pattern has a tendency to pinch and swell. Orthoclase lacks the diagnostic tartan pattern and can be overlooked if it resembles quartz. However, orthoclase is often slightly clouded due to alteration so it can be distinguished from quartz. In Figure 3.7a, the alkali feldspar grain is present in the center of the figure, and has been identified by staining.

In many samples, the plagioclase is clouded due to partial alteration to sericite or clay, leaving the mineral pale reddish, brownish, and grey. In figure 3.7b, the typical tartan twin pattern is visible. In unstained samples, the pinching and swelling of the twins is a distinct criteria for identification. In some samples it was difficult to distinguish between quartz and feldspar. However, since feldspar possesses cleavage and contained evidence of dissolution, it was possible to identify both minerals in the samples.

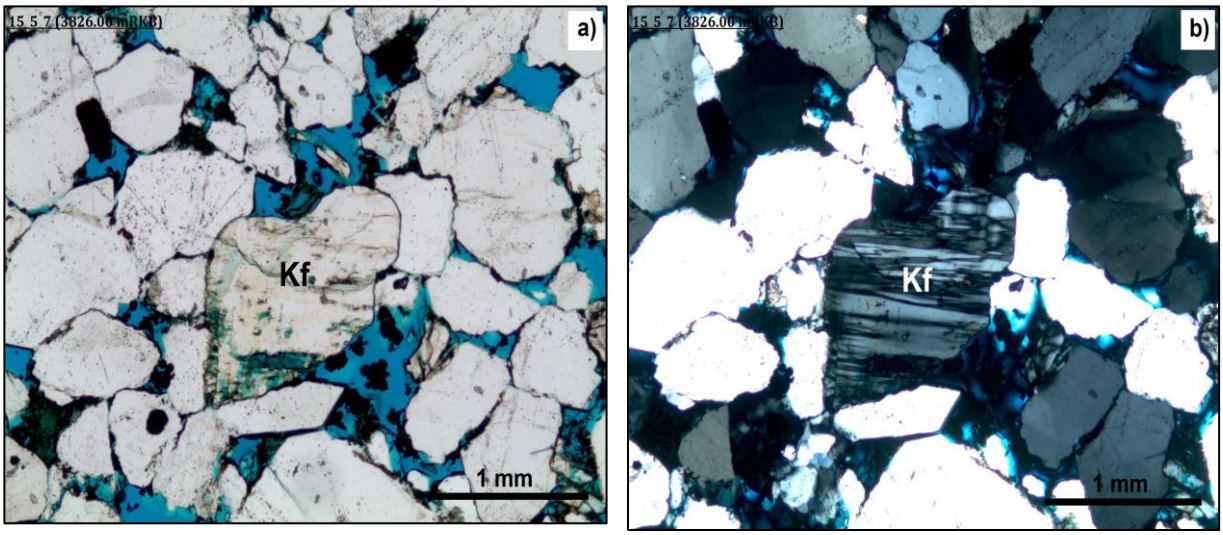

Figure 3.7: Optical micrographs of sample 3826.00 mRKB from well 15/5-7. a) Because of green/yellow color due to staining of sample, the detrital grain in middle of figure is identified as alkali feldspar in plane-polarized light. b) Alkali feldspar with characteristic ”tartan plaid” pattern and visible twin lamellaes viewed with cross-polarized light. (Kf = Alkali feldspar).

3.3.3 Micas

Micas do appear in samples from all the wells within the Hugin Formation. Some of them (Fig. 3.8) are bent while others are straight flakes of mineral crystals. Only a few biotite grains are present, characterized by brown color and pleochroism. The majority of mica grains found in the samples are muscovite. The muscovite seen in Figure 3.8a is colorless in plane-polarized light, and it forms interference colors up to third order in cross-polarized light (Fig. 3.8b).

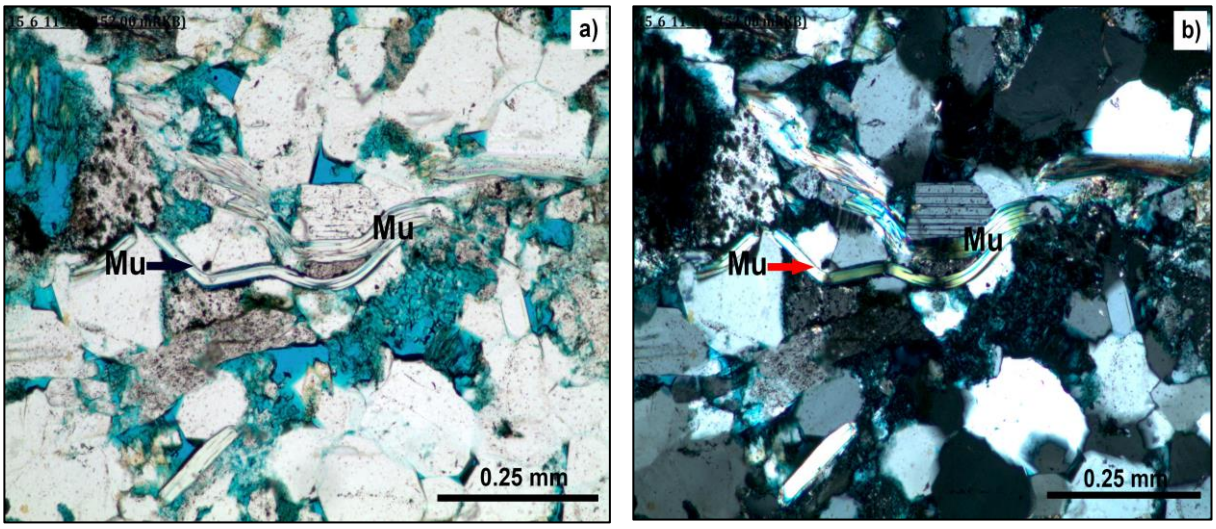

Figure 3.8: Optical micrograph of sample 4152.00 mRKB from well 15/6-11 A. a) Bent muscovite grains, which appear colorless in plane-polarized light. b) Muscovite with interference colors of third and forth order in cross-polarized light. (Mu = muscovite).

3.3.4 Accessory minerals

Accessory minerals identified are zircon, turmaline, and rutile in the samples. The zircon mineral in Figure 3.9a shows no color, or a pale brownish color, in plane-polarized and possesses a very high relief. With cross-polarized light (as in Figure 3.9b), the mineral has interference colors that range up to third and forth order.

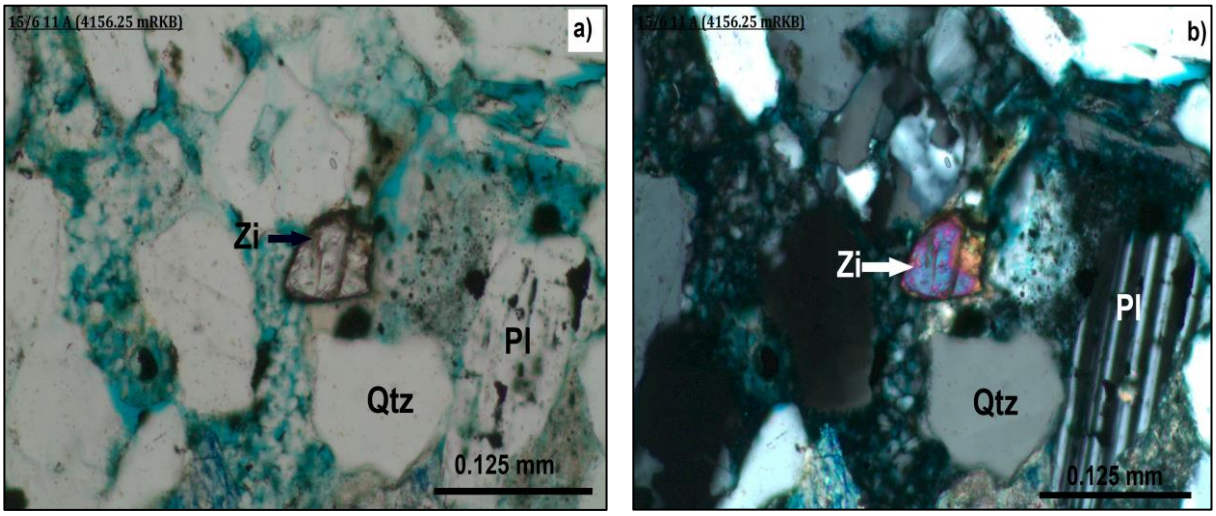

Figure 3.9: Optical micrographs of sample 4156.25 mRKB from well 15/6-11 A. a) Zircon in center of image showing pale brown color and a very high relief. Micrograph is taken with plane-polarized light. b) Zircon with reference colors of third and forth order in cross-polarized light. (Zi = zircon, Qtz = quartz, Pl = Plagiocl.).

3.4 Matrix

Varying amount of stylolites were observed in thin sections, and they are present in matrix throughout all the wells. The stylolites will be thoroughly discussed in Section 3.6.

In the samples there are clay mineral aggregates forming a matrix of random occurrence (Tab. A.1, A.2, A.3, A.4, and A.5). In places, a brownish-/greenish material is present as a partly void-filling substance (Fig. 3.10). The substance shows no specific crystal shape. This mineral is present in all the wells in varying amounts. In Figure 3.10a, the matrix is clearly recognizable, occupying most of the space in between the detrital grains. The greenish clay mineral is clearly occupying the voids in the formation, getting squeezed in between the framework grains.

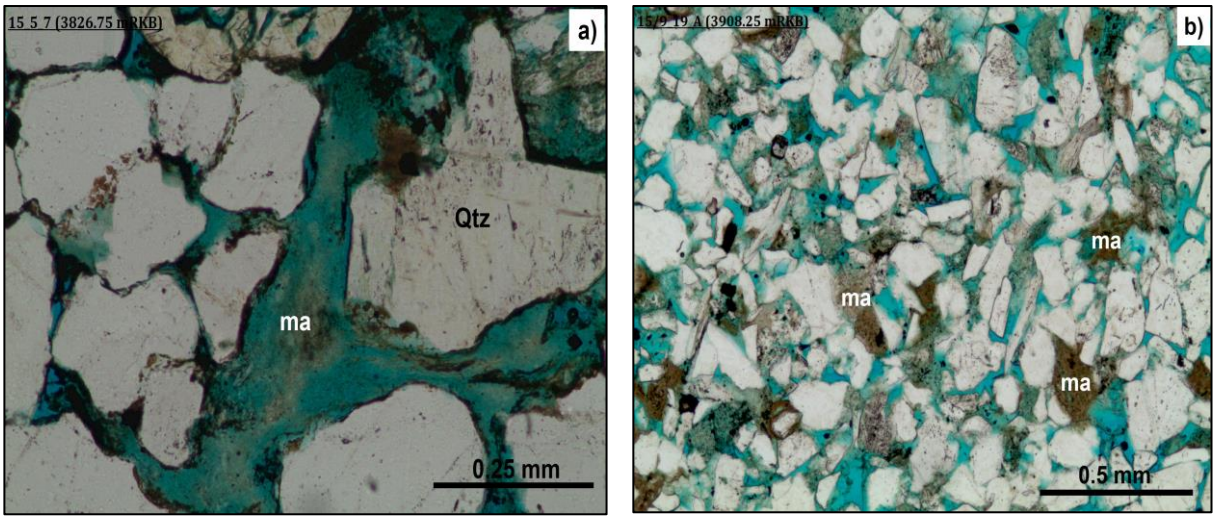

Figure 3.10: Optical micrographs of greenish/brownish matrix which fills the pores and pore throats in the formation in well 15/5-7 (a) sample 3826.75 mRKB, and well 15/9-19 A (b) sample 3908.25 mRKB. Both figures are taken with plane-polarized light. The pore-filling substance is present to a varying extent throughout the wells, and does not positively contribute to the reservoir properties. (ma = matrix, Qtz = quartz).

Matrix is also shown in Figure 3.11. The pores appear unfilled in the cross-polarized light view (Fig. 3.11b). However, when viewed in plane-polarized light the pores are actually filled with numerous small crystals with low relief and which show low order interference colors. Some crystals are large enough to be detected with cross-polarized light (Fig. 3.11b), and

these are most likely kaolinite. Because of their fine grain size, clay minerals can easily be overlooked using a petrographic microscope.

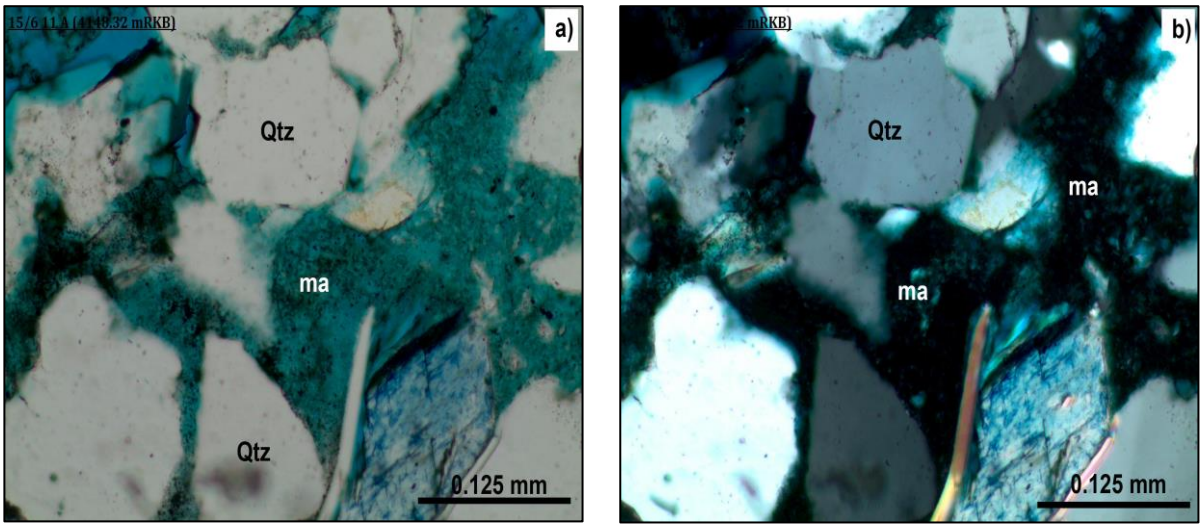

Figure 3.11: Optical micrograph of matrix filling the pores in sample 4148.32 from well 15/6-11 A. a) Picture taken with plane-polarized light showing matrix as a green and black pore filling substance. b) Matrix visible in cross-polarized light as small crystals, most probably kaolinite.

Earlier workers believed that matrix was mainly deposited together with the detrital grains. More recent studies suggest that most matrix in sandstones originates from post depositional infiltration of clay, or authigenic filling due to diagenetic alteration of e.g. feldspar (Boggs 1992).

The matrix described above represents the authigenic clay minerals illite and kaolinite. Both minerals are further described in Section 3.6.

3.5 Stylolites

There are stylolites present in all the wells studied (Tab. A.1, A.2, A.3, A.4, A.5). They appear clustered throughout the formation, interspersed by sections without any stylolites. In well 15/3-7 there are stylolites present at several depths, with a tendency of swarming in three intervals: 4650.00 to 4651.05 mRKB, 4755.30 to 4756.20 mRKB and 4775.50 to 4776.40 mRKB. Well 15/3-7 is the deepest well studied and it possesses both a high density and large

amount of stylolites. The appearance and abundance of the stylolites will be described further in Chapter 5.

The presence of stylolites in the samples contributes to a general increase of the matrix content in the formation. The stylolites form sutured seams, as a result of differential dissolution during compaction.

Many of the dark stylolite seams have a characteristic saw-tooth like appearances (Fig. 3.12). The seams result from the interlocking texture of rock on both sides of the stylolite, and they are normally only a few cm thick (Boggs, 1992). Stylolites can also occur on micro scale as grain-to-grain suturing (Fig. 3.13). Before the pores are filled with cement, stress is concentrated between adjoining grains (grain contacts), and the result may be dissolution. Dissolved minerals then migrate by diffusion, and precipitate on grain surfaces close to the stylolite. Stylolites occur in sedimentary rocks such as limestones and sandstones (quartz arenites). Normally they form parallel to bedding planes, but they can also form at an angle to the planes or sometimes perpendicular to the bedding. The stylolites consist of materials with low solubility, such as micas, iron oxide minerals and organic material. The mechanisms of stylolite formation will be covered in Chapter 4 and 5.

Figure 3.12 illustrates a stylolite with curvy shape, containing practically insoluble materials such as micas, clay minerals, iron oxides and fine organic matter in a well-sorted medium-grained sandstone. The mica grains are bent, following the curvy shape of the stylolite. Interlocking texture of the quartz grains on both sides of the dissolution seam is seen in both Figure 3.12a and 3.12b. Also present in the figure are different detrital minerals, together with some authigenic minerals adjacent to the porous area, identified by blue coloration in the image. Because of the low magnification, some of the framework minerals are hard to detect.

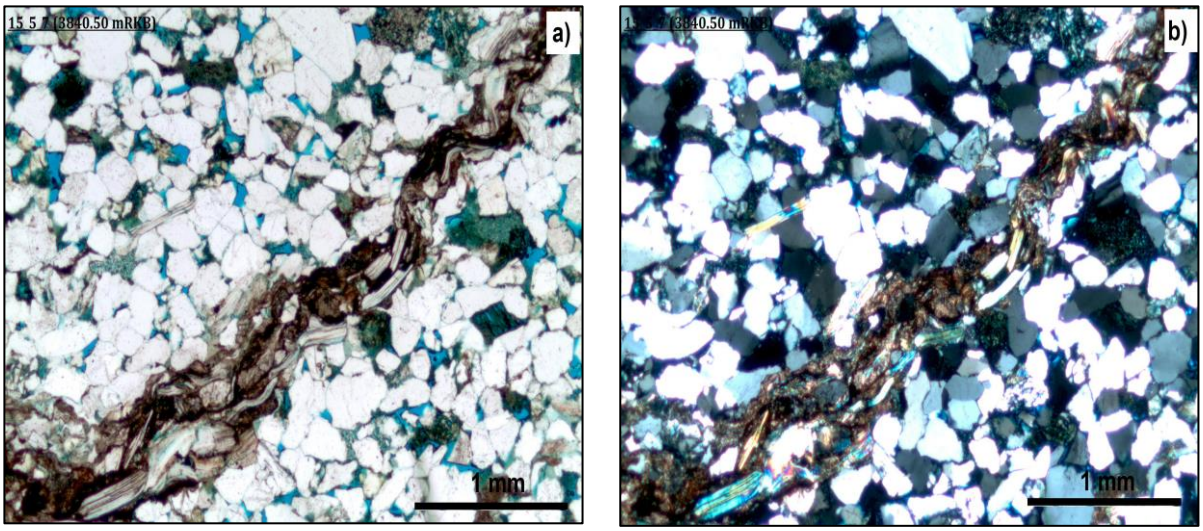

Figure 3.12: Optical micrographs from well 15/5-7 sample 3840.50 mRKB. a) Image of stylolite containing clay minerals, micas, iron oxides, and fine organic matter in plane-polarized light. The micas are bent, following the curvy path of the stylolite. Notice the interlocking texture of the quartz grains (white grains) on each side of the sutured seam solution. b) Same as (a) only taken with cross-polarized light. The interlocking quartz grains are more visible and the micas inside the stylolite show high order interference colors.

Figure 3.13 illustrates a micro stylolite in a moderately sorted medium-grained sandstone within the Hugin Formation. Sutured seams are visible between individual quartz grains as a thin dark line, and to the right of the figure the seam is seen to penetrate an individual grain. This stylolite lacks the micas observed in Figure 3.12, but contains clay minerals and fine organic matter. The interlocking texture is not as apparent as shown in Figure 3.12, although it is partly seen in the lower part of the Figure.

In Figure 3.14, the stylolites appear as swarms in a well sorted fine-grained sandstone. The stylolites have a vertical extent of a couple of mm and follow the same horizontal direction as the bedding plane of the formation. Micas are well distributed throughout the sample, showing a high degree of interference colors in cross-polarized light (b). The same intense interlocking texture amongst the detrital grains as observed in Figure 3.12 is also present in this sample. The sample consists of a high amount of fine material, observed as a brown and greenish substance also seen in Figure 3.10.

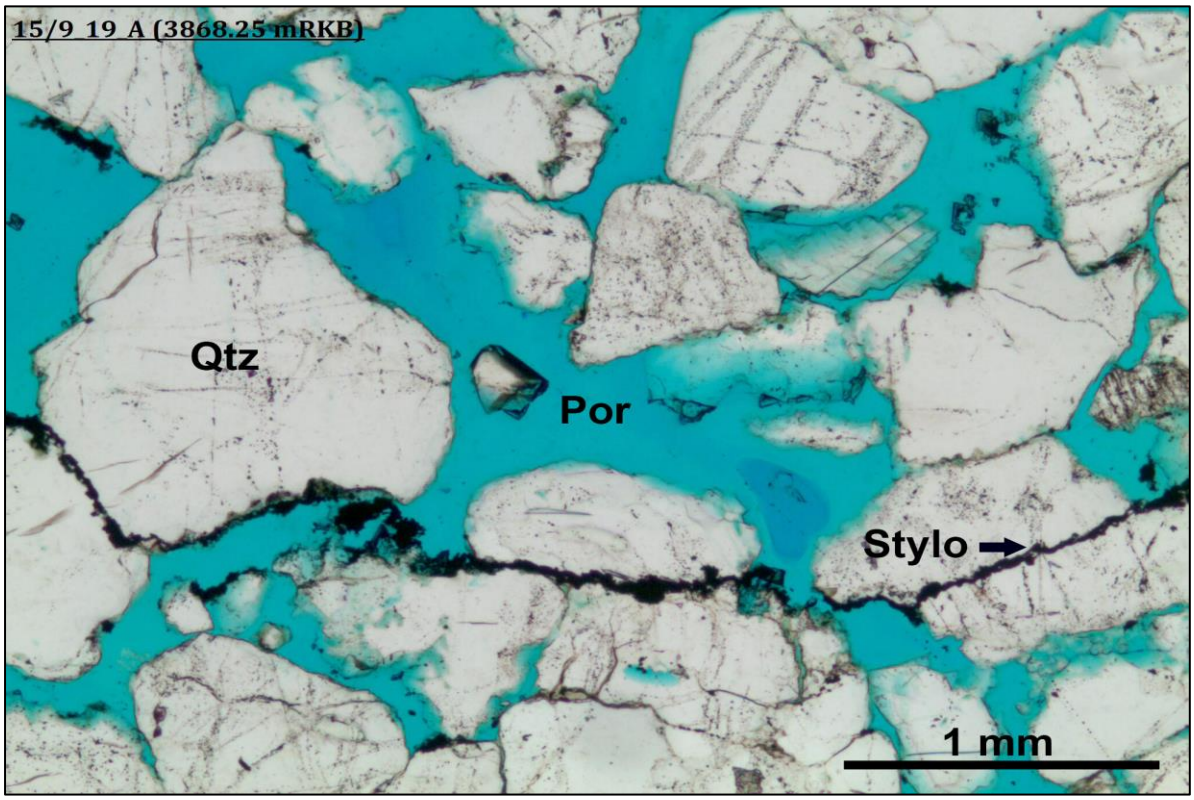

Figure 3.13: Optical micrograph of sample 3868.25 mRKB from well 15/9-19 A. A micro stylolite is seen between individual quartz grains: It penetrates one of the grains in the right of the figure. Stylolite possesses the characteristic jagged surface appearing as a black line in the figure. (Qtz = quartz, Por = porosity, Stylo = Stylolite).

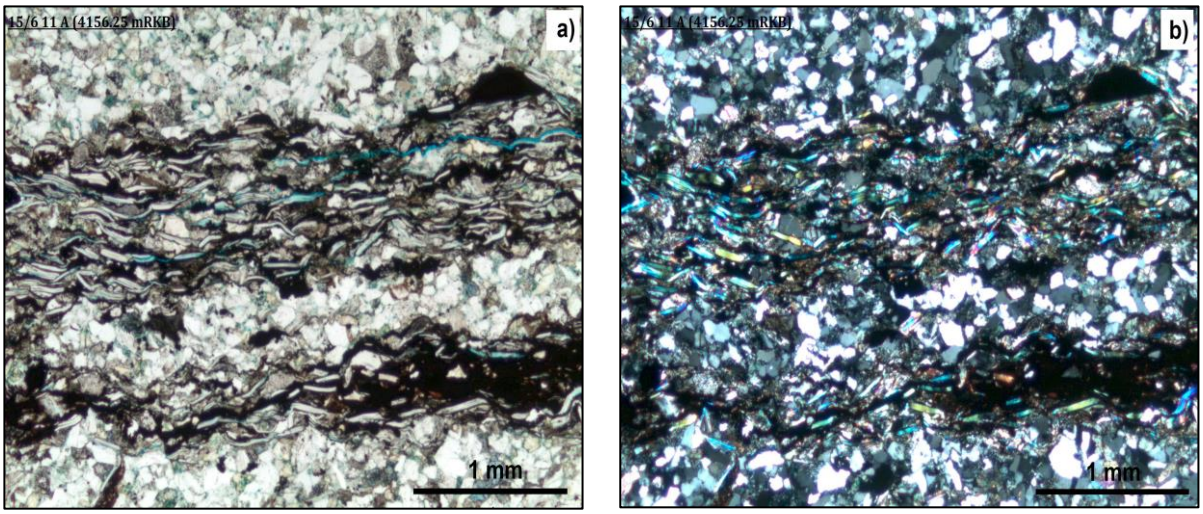

Figure 3.14: Optical micrograph of sample 4156.25 mRKB from well 15/6-11 A. a) Swarms of stylolites in a very fine-grained section of the Hugin Formation sandstone. Stylolites follow the bedding plane, and have a vertical extent of a couple of mm. Typical black zigzag pattern consisting of micas, clay minerals and fine-grained organic material. Image taken with plane-polarized light. b) Same as a) only taken with cross-polarized light.

3.6 Diagenetic minerals

The diagenesis of sandstones is described in Section 1.3, and in the following sections the authigenic minerals of quartz and carbonate cement, pyrite, kaolinite, glauconite, and illite will be described.

Quartz cement

Quartz cement is recognized in samples from all the wells as syntaxial quartz overgrowths on quartz grains. Quartz cement is the most abundant cement type present in the wells studied. The overgrowth can be seen as a rim around the quartz crystals, developing in the same crystallographic orientation and optical continuity as the former detrital quartz grain. At first, the quartz overgrowth will consist of many tiny crystals, which grow together to form a single crystal with well-formed crystal faces. Sometimes quartz cement is hard to distinguish from the detrital quartz grain, since both possess uniform interference color. In order to form the cement, a significant amount of dissolved quartz must be available in pore water. The sources and processes behind quartz cement will be described further in Chapter 4 and 5. The crystal shapes developed are mostly euhedral, often forming prism or pyramid shapes (Fig. 3.15).

Figure 3.15 illustrates quartz cement as syntaxial overgrowths. In the marked area, the cement is filling the pore spaces between the grains, leaving a reduced volume for fluids to occupy. This will lower both the porosity and the permeability, and reduce the reservoir properties. Well 15/3-7 is the deepest of the wells examined. Throughout the entire interval of the well, there is quartz cement present with the characteristic crystal shape illustrated in Figure 3.1. The cement is generally not in contact with the detrital quartz grain, but separated by a thin ”dust ring”; small pores between the cement and the grain containing minerals and organic matter which is visible in Figure 3.15. Where the grains are locked together, the cement is not so easy to visualize. Sometimes scanning electron microscopy (SEM) is needed to distinguish between the grain and the cement, but in this case the cement is readily apparent.

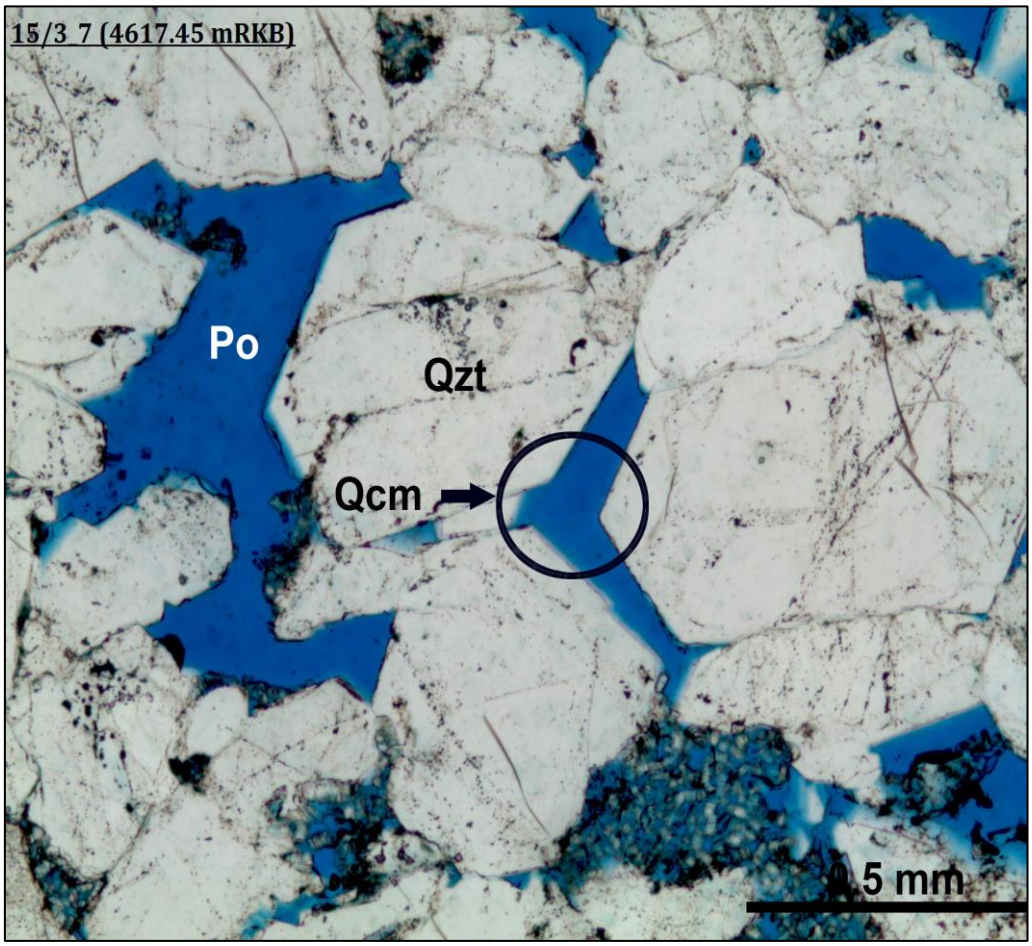

Figure 3.15: Optical micrograph from well 15/3-7. In the marked area, quartz cement is visible as syntaxial overgrowth occupying space in between the grains. Both porosity and permeability are reduced as a result of this process.

Figure 3.16 is provided illustrate the quartz cement more clearly. The cement is occupying a significant amount of space, and the porosity is decreased as a result. In addition to the cement, residual hydrocarbon is present, visible as black rims surrounding the grains.

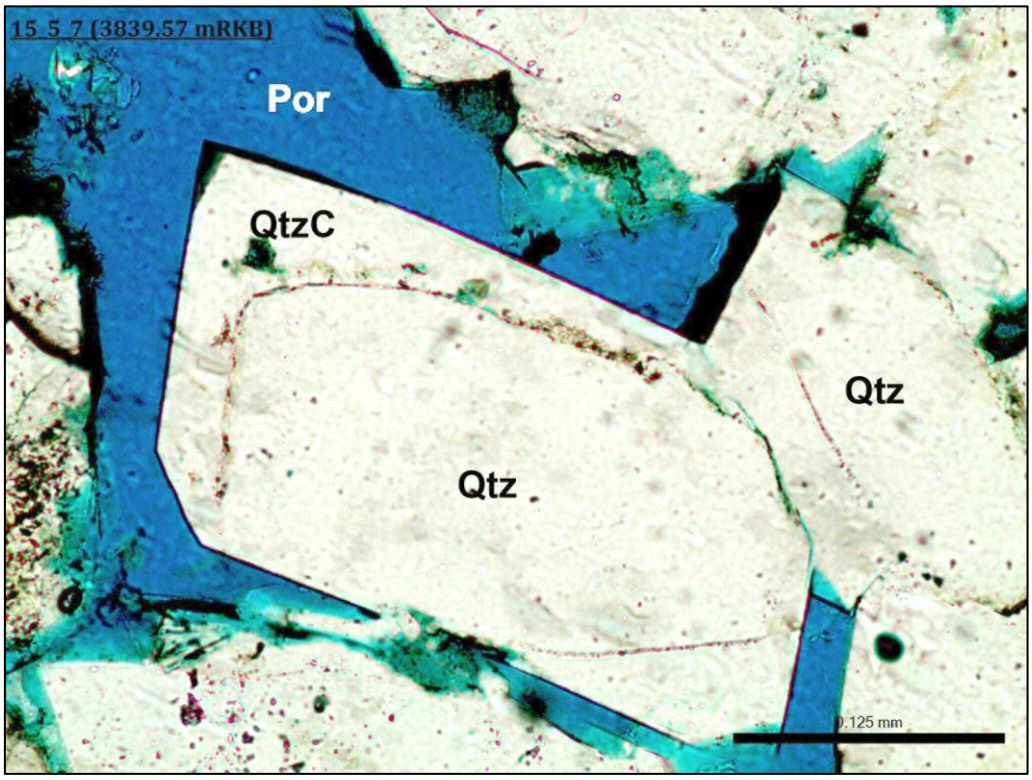

Figure 3.16: Optical micrograph from well 15/5-7. Sample 3839.57 mRKB shows the quartz cement especially well in plane-polarized light. The ”dust rings” differentiates the detrital quartz grains from the cement. The black rim around the cement is probably residual hydrocarbons.

In all the wells examined, quartz cement is present in a varying amount. The cement is not always clearly visible, as seen in Figures 3.15 and 3.16, but its presence can be proven by other methods. Clay mineral coatings can inhibit the quartz overgrowth, but this was not seen in any of the examined samples. Regarding the core photos, quartz cement can be distinguished by its slightly whitish appearance compared to non-cemented sections. Based only on the core photos, quartz cement can be mistaken for calcite cement since they both appear whitish, but in general the calcite cement is whiter than the quartz cement. With thin sections available for the same intervals, it is possible to distinguish the two types of cement. Figure 3.17 shows core photos of an interval in well 15/3-7, containing zones of both calcite- and quartz cement. The calcite cement appears more whitish then the quartz cement.

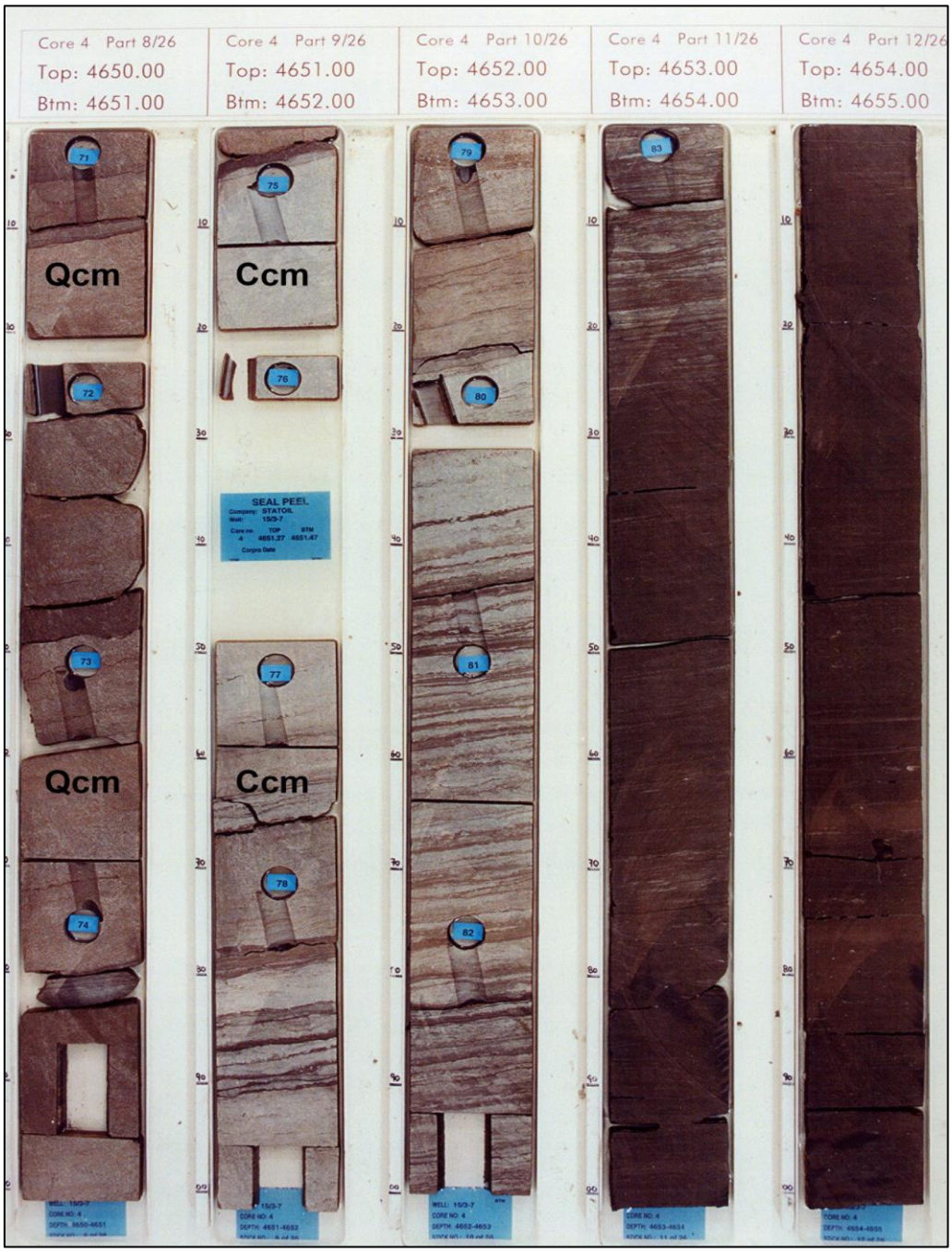

Figure 3.17: Core photos from well 15/3-7 illustrating quartz cemented (Qcm) and calcite cemented (Ccm) zones. The quartz cemented zones are not as whitish as the calcite cemented zones, making it possible to distinguish between them.

Carbonate cement

Carbonate cement is present in all the wells studied and, after quartz, it is the most abundant cement type in the Hugin Formation. The samples from well 15/5-7 and 15/6-11 A are stained with potassium ferricyanide, used alongside other methods, to distinguish between ferrous and non-ferrous calcite. Calcite cement occurs as poikilotopic crystals through most of the formation. In plane-polarized light the calcite minerals are colorless, while in cross-polarized light, calcite has very high interference colors. In the Hugin Formation, the calcite cement occurs as calcite crystals which formed poikilotopic fabric crystals as they grew from pore to pore. The framework grains appear to "float" in calcite crystals, where the formation is more or less entirely calcite cemented (Fig. 3.19).
Figure 3.18 shows sample 4148.32 mRKB containing calcite cement (stained blue) from well 15/6-11 A: the characteristic shape and blue coloration is clearly visible. The bluish color indicates ferrous calcite, ferrous dolomite (Adams and MacKensey, 2001) or possibly ankerite. To determine if it is calcite ($CaCO_3$) or dolomite ($CaMg(CO_3)_2$), further analyses are required, e.g. Scanning electron microscopy (SEM). In Figure 3.18, the carbonate cement is filling the pore space together with the quartz cement, reducing the amount of space available for fluids to occupy.

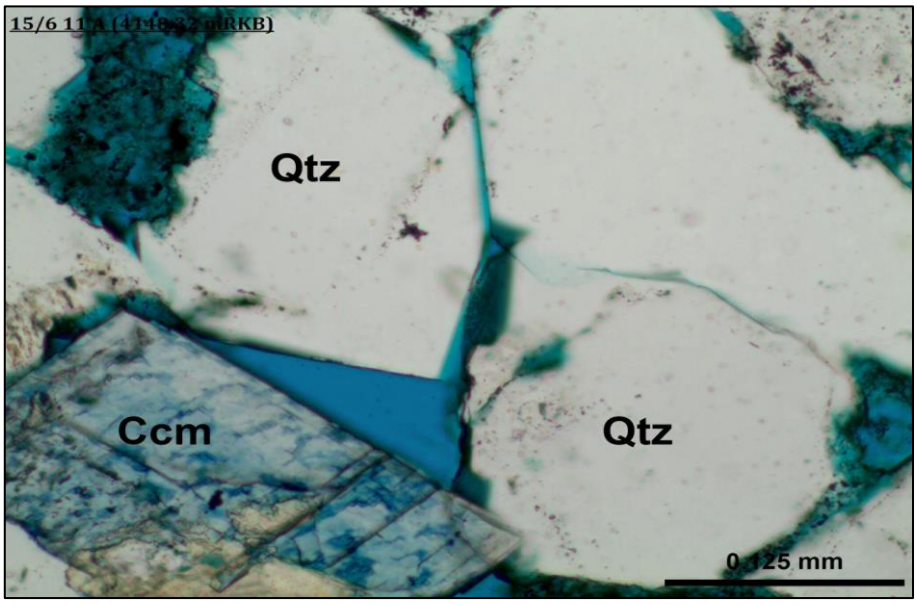

Figure 3.18: Optical micrograph from well 15/6-11 A, which illustrates calcite cement (Ccm), and quartz (Qtz) in plane-polarized light (PPL). The sample from 4148.32 mRKB shows calcite filling the pore spaces. Due to staining, the calcite cement appears blue.

Figure 3.19 displays an optical micrograph of a calcite cemented sample taken from well 15/6-11 A. The cement typically fills all the pores in the sample, leaving no room available for any fluids to occupy, so the sample is almost totally calcite cemented. The extent of the calcite cement present in the different wells is submitted in Tables A.1 to A.5 in the Appendix. All the wells are punctuated with areas of high calcite cement concentration, resulting in decreased porosity and permeability in those areas.

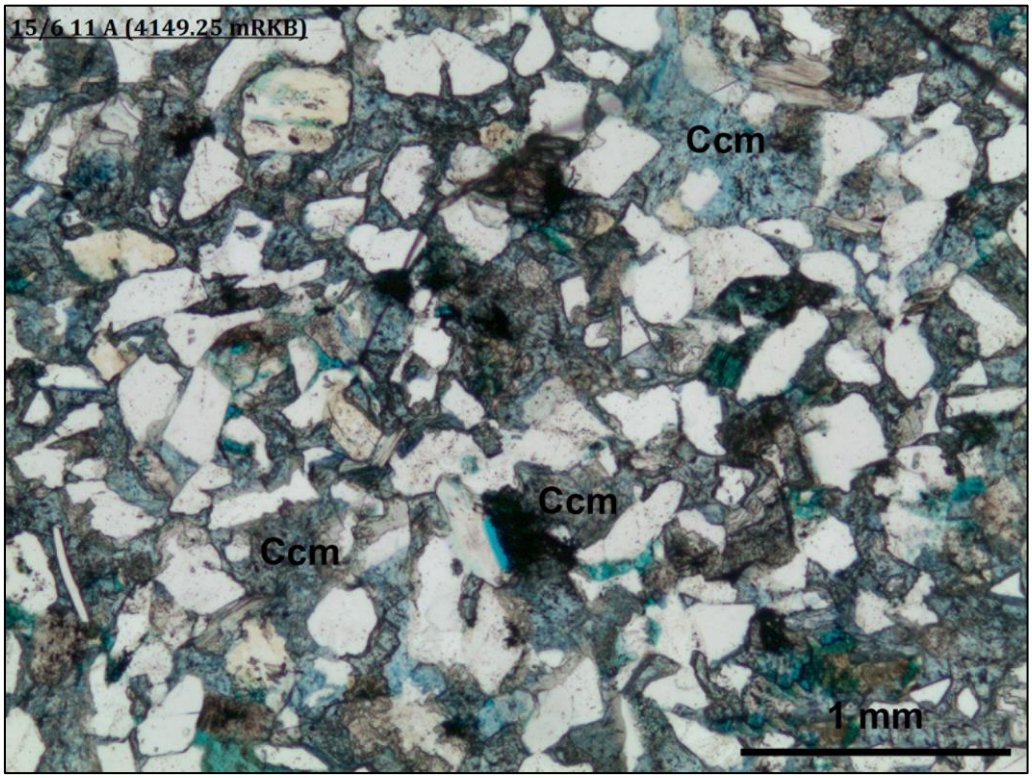

Figure 3.19: Optical micrograph of calcite cement from well 15/6-11 A sample 4149.25 mRKB. The bluish cement (marked with "Ccm") fills all the space in the sample, leaving no room for fluids to occupy. Also present in the figure are the minerals quartz, feldspar and mica; feldspar appears yellowish due to the staining. Mica is present in the lower part to the left, where it appears as a thin, elongated, colorless and white crystal.

Glauconite

Glauconite forms exclusively in marine environments, mostly in shallow water, and is a hydrous potassium iron alumino-silicate mineral with the formula $(K,Ca,Na)_{1.6}$ $(Fe^{3+},Al,Mg,Fe^{2+})_4\,Si_{7.3}Al_{0.7}O_{20}(OH)_4$, (Nesse, 2000). The mineral occurs with a random distribution throughout the formation, and in Figure 3.20a the grain can be seen in the

middle of the image. The characteristic greenish color is seen in plane-polarized light, making the mineral easily identifiable. The brownish color in the middle of the grain is likely a result of oxidation of the ferrous iron in the glauconite. Glauconite is observed in all the wells studied, but since many of the grains are altered and compacted due to the deep burial, some of the grains are not so easily identifiable.

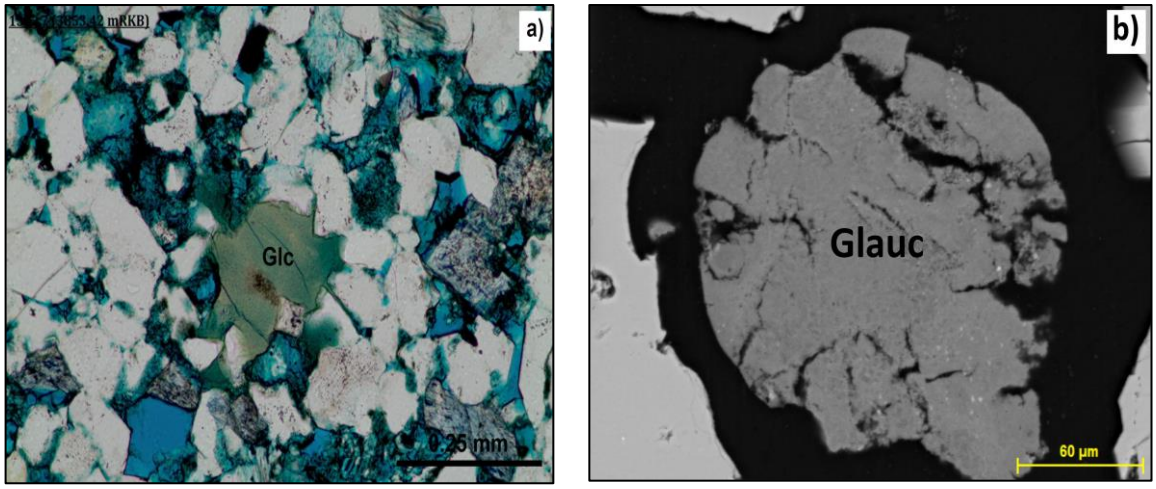

Figure 3.20: a) Optical micrograph from well 15/5-7. Sample 3853.42 shows a glauconite grain in plane-polarized light with the characteristic greenish color. b) Image of a possible glauconite grain from the SEM analyzes.

The EDS analysis (Fig. 4.4) showed spectra containing insufficient amounts of iron, and excessive amounts of aluminum, which made it difficult to determine with absolute certainty that the mineral observed in the samples was glauconite. The iron content of sample 3838.50 mRKB from well 15/9-19 A was 3.78%, and the content of aluminum was 13.05%, which is not synonymous with the mineral assembly of glauconite (Odin and Matter, 1981; Van Houten and Purucker, 1984). Referring to Odin and Matter (1981) the iron content of glauconite varies between 19 to 27%, while the aluminum content stays between 5 and 8%. Van Houten and Purucker (1984) state that the iron content of glauconite constitute more than 15% of the total mineral constituents. The mineral examined in the SEM analysis clearly showed insufficient iron content in order to accurately determine it as glauconite (Fig. 4.4). In this specific case, the grain observed in the SEM analyzes could also be an altered alkali feldspar transforming into a ferric illite, since it is both mineralogically and chemically quite similar to the clay mineral (Odin and Matter,

1981). The sodium present in the sample might be derived from albite twins in the alkali feldspar.

Kaolinite

The kaolinite ($Al_2Si_2O_5(OH)_4$) content is abundant in all wells, except for a small interval in well 15/9-21 S where kaolinite is absent (Tab. A.1 - A.5). The kaolinite grains are small, but easy to identify using an optical microscope since the characteristic plate shaped crystals form a booklet structure (Fig. 3.21). Kaolinite is often transformed into dickite during burial of 2-3 km (Ehrenberg et al., 1993), and then differentiation between the two minerals will be difficult with the use of an optical microscope. Kaolinite is therefore used to refer to the kaolin mineral group, and will not be differentiated.

The clay mineral occurs as pore-filling aggregates, or as replacement of detrital grains (mostly feldspar grains in the samples studied). The kaolinite crystals possess a perfect cleavage, appear white in plane-polarized light and have low order brown to black interference colors. It is the typical booklet structure which makes it possible to identify the mineral using the optical microscope. Dissolved feldspar grains, partly filled with kaolinite and associated with pore filling aggregates of kaolinite, are present throughout the entire Hugin Formation.

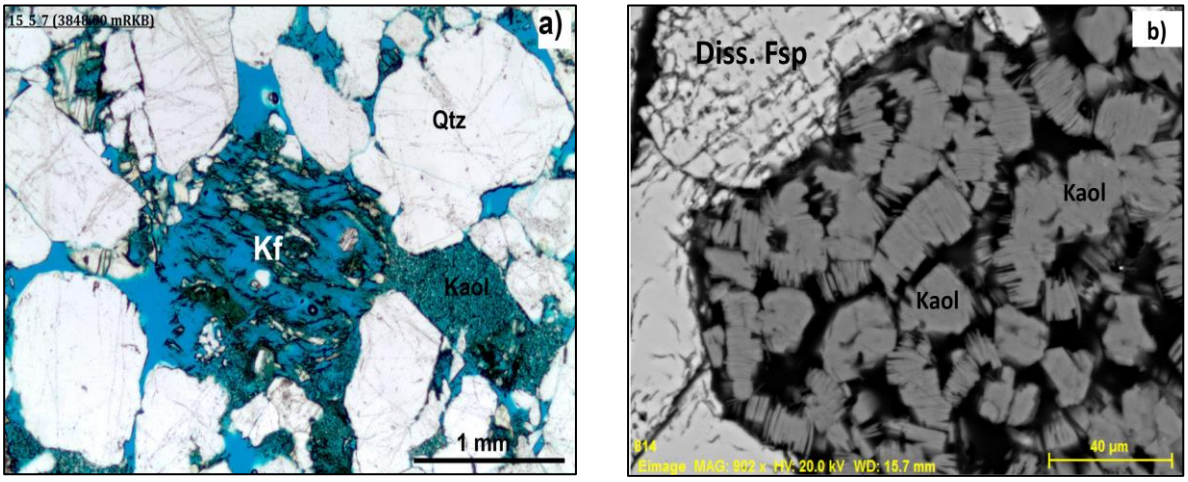

Figure 3.21: SEM image and optical micrograph from well 15/5-7. a) Kaolinite (Kaol) present together with a dissolved alkali feldspar (Kf) grain in the middle of the image. It is possible that the kaolinite, filling the porse space between the quartz (Qtz) grains, is derived from dissolved feldsparb) SEM image of kaolinite (Kaol) present with the characteristic booklet structure, surrounded by a dissolved feldspar grain in the top left corner of the image.

In Figure 3.21, the kaolinite crystals fill the voids in between the quartz grains in the samples. The characteristic booklet structure is present in both images, and image (a) shows a dissolved alkali feldspar grain. The kaolinite, present in image (a), was probably derived from the dissolution of the feldspar grain, and it is therefore replacing the detrital grain. Kaolinite also appears as pore-filling crystals, also shown in the SEM image in Figure 3.21b.

Illite

Illite was not recognized under the optical microscope, but was identified by SEM analysis of two selected samples with abundant matrix. The mineral appears as pore-filling greenish/brownish aggregates (Fig. 3.10), and is described in the tables as brown and green clay, representing the matrix content of the Hugin Formation. In Figure 3.22, the SEM images show the illite clay mineral with different magnifications. In the image to the left, illite clearly fills the pore spaces in between the detrital grains, while in the right hand image the platy and fibrous illite crystals are visible due to the higher magnification. The EDS spectra verify the presence of illite in the sample, presented in Figure 4.3.

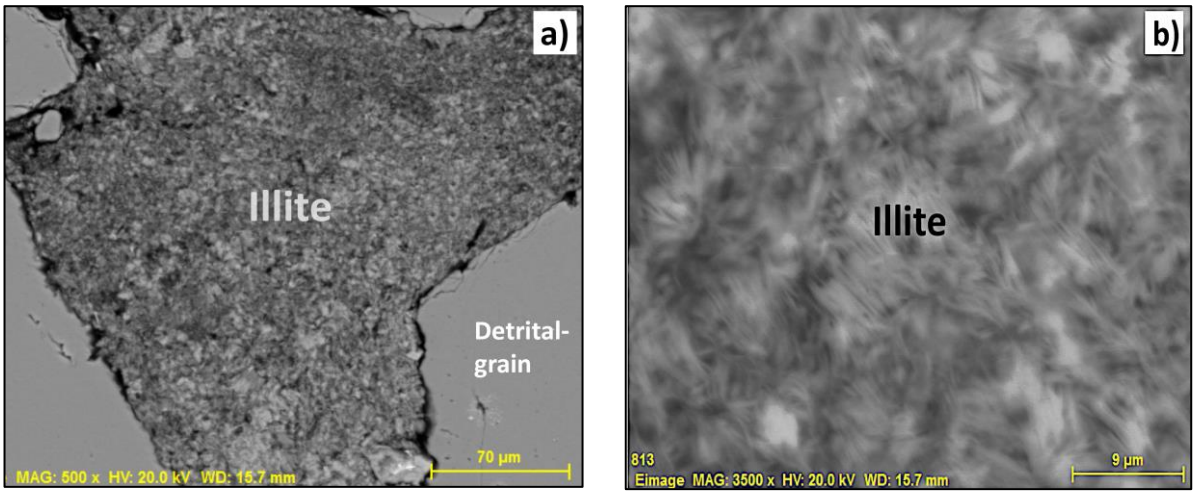

Fig. 3.22: SEM images of illite from well 15/5-7. a) Illite clearly appears as a pore-filling substance in between detrital grains (most likely quartz grains). It appears as a highly abundant substance throughout the entire well. b) Illite shown with a higher magnification. In such view illite is characterized by sheet-like flakes with fibrous texture, which can bridge large pores and restrict the reservoir properties.

Pyrite

Pyrite is observed in all the wells examined in the Hugin Formation, as intergranular cement which forms cubic shaped crystals. These crystals often cluster together to fill the pore spaces in between framework grains and act as pore-filling aggregates (Fig. 3.23). Pyrite is often associated with stylolites, where pyrite is incorporated into part of the matrix which otherwise contains organic matter, insoluble material and mica. Inside the stylolites, the pyrite can occur as micro crystals but also appears as larger crystals, similar to the size of the detrital grains in the samples.

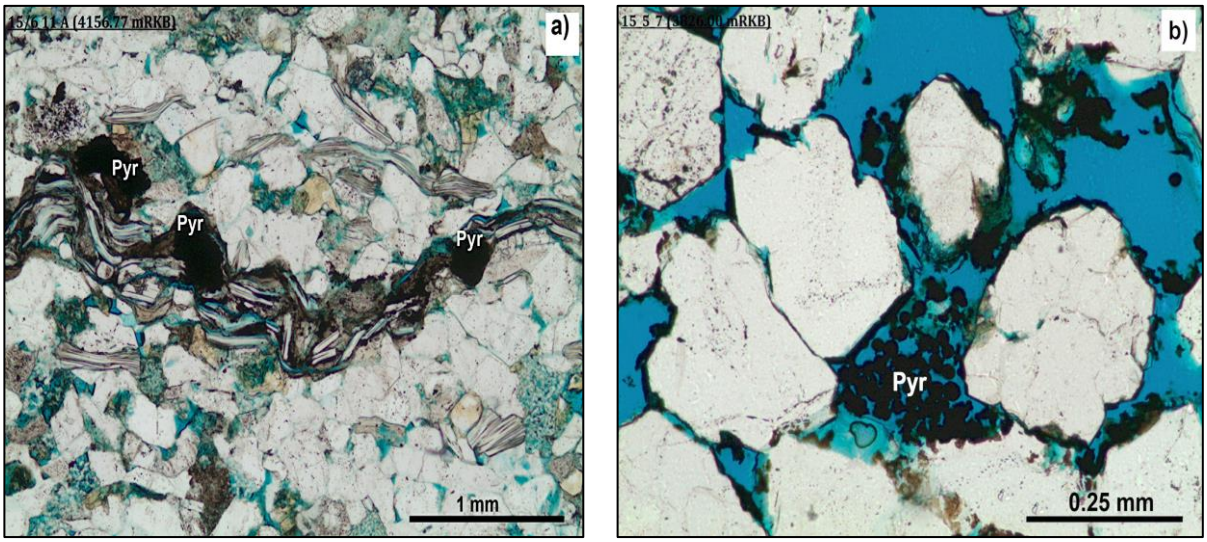

Figure 3.23: Optical micrograph from well 15/6-11 A (a), and well 15/5-7 (b). a) Pyrite (Pyr) seen in stylolite as black crystals. b) Clusters of small pyrite (Pyr) grains seen as a pore filling substance (matrix).

4 Results

The petrography of the sandstones from the wells 15/3-7, 15/5-7, 15/6-11 A, 15/9-19 A and 15/9-21 S was described in Chapter 3. The results of the textural description, framework grains, and diagenetic minerals from the petrography are presented in Appendix A (Tab. A.1, A.2, A.3, A.4, and A.5), and the results from the modal analyzes, are presented in Table 4.1, 4.2, and 4.3. The results will be analyzed and investigated in this chapter, with the sandstones' classifications and maturity described in Section 4.1, and the loss of porosity due to compaction and cementation described in Section 4.2.
The results from the SEM analyses will be presented in Figure 4.1, 4.2, 4.3, and 4.4. The Energy dispersive spectra (EDS) will be presented together with the backscattered electron images (BEI) to better view the different authigenic minerals, which are ankerite, kaolinite, and illite. Also included in the figures are tables with the individual breakdown of different elements in the samples. The authigenic minerals will be further discussed in Chapter 5.

4.1 Petrographical analysis

The petrographical analysis is presented in Tables in Appendix A, where the different framework and diagenetic minerals are presented. The textural description is also available with features such as grain size, sorting, and roundness. All the samples provided from Statoil ASA possessed good quality.

4.2 Modal analysis

Table 4.1: Modal analyzes of the samples from the Hugin Formation in well 15/3-7. The values given for all the samples are in %. (Qtz = quartz, Fsp = feldspar, Mu = muscovite, HM = heavy minerals, Cht = chert, SchQ = schistose quartz, Qtzt = quartzite, B. Cly = brownish clay, G. Cly = greenish clay, Qcm = quartz cement, Ccm = calcite cement, Pyr = pyrite, Glc = glauconite, Kaol = kaolinite, Pri = primary porosity, Sec = secondary porosity, Tot = total porosity, Core = porosity from core plugs).

Well 15/3-7		**Detrital grains**				**Rock fragments**			**Matrix**		**Diagenetic minerals**			**Authigenic clay**		**Porosity**			
Sample depth (mRKB)	**Grain size (mm)**	**Qtz**	**Fsp**	**Mu**	**HM**	**Cht**	**SchQ**	**Qtzt**	**B. Cly**	**G. Cly**	**Qcm**	**Ccm**	**Pyr**	**Glc**	**Kaol**	**Pri**	**Sec**	**Tot**	**Core**
4610.00	0.20	68.7	-	-	-	-	0.3	3.7	-	1.0	11.7	-	-	-	4.3	7.3	3.0	10.3	13.8
4613.25	0.30	65.5	-	-	-	0.3	-	4.9	2.6	-	6.9	-	-	-	4.6	9.3	5.6	14.9	11.6
4615.25	0.50	72.4	-	-	-	-	0.3	4.3	1.0	0.7	10.3	-	-	-	3.0	4.6	3.4	8.0	12.1
4616.75	0.40	67.7	0.3	-	-	-	-	4.3	0.3	1.0	9.3	-	-	-	7.3	6.3	3.4	9.7	12.5
4617.45	0.40	65.0	0.3	-	-	0.3	0.7	4.4	3.0	0.3	10.7	-	-	-	4.7	6.3	1.0	7.3	7.99
4650.00	0.20	73.1	1.3	0.7	0.3	1.3	-	3.0	2.7	2.0	8.0	-	-	-	3.3	3.3	1.0	4.3	10.8
4766.50	0.80	66.1	3.7	-	-	1.0	-	1.3	1.7	0.6	12.6	0.3	-	-	5.3	1.7	5.6	7.3	7.2
4775.30	0.25	71.6	2.7	1.7	0.3	1.0	-	0.7	1.3	0.4	13.0	-	-	-	3.0	3.0	1.3	4.3	6.8
4775.50	0.35	72.3	3.9	0.7	0.3	0.3	-	1.3	2.9	-	11.4	-	0.3	-	2.9	2.8	0.9	3.7	5.4
4785.70	0.20	75.6	3.0	0.7	0.3	-	-	1.7	-	0.3	6.3	-	-	-	3.1	3.0	4.7	7.7	13.5

Table 4.2: Modal analyzes of the samples from the Hugin Formation in well 15/9-19 A. The values given for all the samples are in %. (Qtz = quartz, Fsp = feldspar, Mu = muscovite, HM = heavy minerals, Cht = chert, SchQ = schistose quartz, Qtzt = quartzite, B. Cly = brownish clay, G. Cly = greenish clay, Qcm = quartz cement, Ccm = calcite cement, Pyr = pyrite, Glc = glauconite, Kaol = kaolinite, Pri = primary porosity, Sec = secondary porosity, Tot = total porosity, Core = porosity from core plugs).

Well 15/9-19 A		**Detrital grains**				**Rock fragments**			**Matrix**		**Diagenetic minerals**			**Authigenic clay**		**Porosity**			
Sample depth (mRKB)	**Grain size (mm)**	**Qtz**	**Fsp**	**Mu**	**HM**	**Cht**	**SchQ**	**Qtzt**	**B.Cly**	**G.Cly**	**Qcm**	**Ccm**	**Pyr**	**Glc**	**Kaol**	**Pri**	**Sec**	**Tot**	**Core**
3840.25	0.25	62.7	5.3	-	-	-	-	5.0	3.2	6.8	3.3	-	-	-	0.7	9.0	4.0	13.0	21.0
3845.50	0.22	63.6	4.0	-	-	-	-	3.3	2.4	5.3	4.0	-	-	-	0.7	11.7	5.0	16.7	23.6
3850.50	0.20	60.8	4.7	1.0	0.0	-	-	0.7	4.0	2.6	4.5	4.7	1.0	-	2.0	10.3	3.7	14.0	22.0
3857.50	0.20	64.8	5.7	0.7	-	-	-	0.7	2.0	2.7	4.7	-	0.3	-	1.7	11.3	3.4	16.7	22.8
3862.40	0.45	62.3	3.0	0.3	-	1.0	-	6.0	0.7	3.0	4.0	-	-	-	1.7	13.7	4.3	18.0	24.4
3868.25	0.30	65.4	3.3	-	-	1.0	0.7	5.3	1.0	2.0	3.3	-	0.3	-	1.7	11.3	4.7	16.0	22.2
3873.50	0.50	61.3	2.6	-	-	1.0	0.7	8.0	0.6	4.7	4.6	-	0.7	-	1.0	12.0	2.9	14.9	23.6
3885.55	0.30	66.6	2.0	-	-	-	-	3.7	2.0	2.7	3.0	-	-	-	3.7	14.0	2.3	16.3	20.7
3898.55	0.35	68.5	3.8	0.3	-	1.0	-	1.7	1.0	2.2	2.6	-	1.6	-	4.8	10.8	1.7	12.5	17.1
3900.50	0.40	72.3	2.7	-	-	-	-	2.7	1.7	1.6	1.6	-	-	-	0.7	14.3	2.4	16.7	20.4

Table 4.3: Modal analyzes of the samples from the Hugin Formation in well 15/6-11 A. The values given for all the samples are in %. (Qtz = quartz, Fsp = feldspar, Mu = muscovite, HM = heavy minerals, Cht = chert, SchQ = schistose quartz, Qtzt = quartzite, B. Cly = brownish clay, G. Cly = greenish clay, Qcm = quartz cement, Ccm = calcite cement, Pyr = pyrite, Glc = glauconite, Kaol = kaolinite, Pri = primary porosity, Sec = secondary porosity, Tot = total porosity, Core = porosity from core plugs).

Well 15/6-11 A		**Detrital grains**				**Rock fragments**			**Matrix**		**Diagenetic minerals**			**Authigenic clay**		**Porosity**			
Sample depth (mRKB)	**Grain size (mm)**	**Qtz**	**Fsp**	**Mu**	**HM**	**Cht**	**SchQ**	**Qtzt**	**B.Cly**	**G.Cly**	**Qcm**	**Ccm**	**Pyr**	**Glc**	**Kaol**	**Pri**	**Sec**	**Tot**	**Core**
4150.45	0.20	41.5	7.5	2.0	-	0.5	-	2.0	-	2	4.5	23.0	2.0	-	3.5	7.5	4.0	11.5	14.3
4152.00	0.20	61.1	11.8	5.2	-	-	-	0.5	-	2.8	2.8	1.4	-	-	5.2	3.3	5.7	9.0	11.8
4154.75	0.18	50.0	12.5	2.5	-	-	0.5	0.5	-	2.5	3.5	7.5	1.0	-	4.0	9.0	6.5	15.5	18.2
4155.00	0.20	54.5	14.9	2.5				0.5	0.5	4.0	3.5	5.4	-	-	3.5	6.9	4.0	10.9	18.9
4158.75	0.18	59.0	9.0	4.5	-	-	-	2.0	-	2.0	5.5	1.0	-	-	5.0	7.0	5.0	12.0	16.2
4159.75	0.20	60.5	13.0	4.0	0.5	-	-	-	-	2.0	2.5	1.5	-	-	3.5	6.0	6.5	12.5	16.2
4160.50	0.18	58.5	14.5	0.5	-	-	-	2.5	-	-	3.0	5.0	-	-	4.0	4.0	8.0	12.0	18.8
4169.00	0.22	61.0	9.5	3.5	-	-	0.5	0.5	-	1.0	2.0	11.5	0.5	-	2.5	3.5	3.5	7.0	13.9
4173.50	0.20	64.0	7.5	-	-	-	-	0.5	-	1.5	3.5	5.0	0.5	-	2.5	7.5	7.5	15.0	15.8
4174.00	0.14	65.5	10.0	1.5	-	-	-	0.5	-	0.5	3.0	7.0	1.0	-	1.0	4.0	6.0	10.0	15.7

4.3 SEM analysis

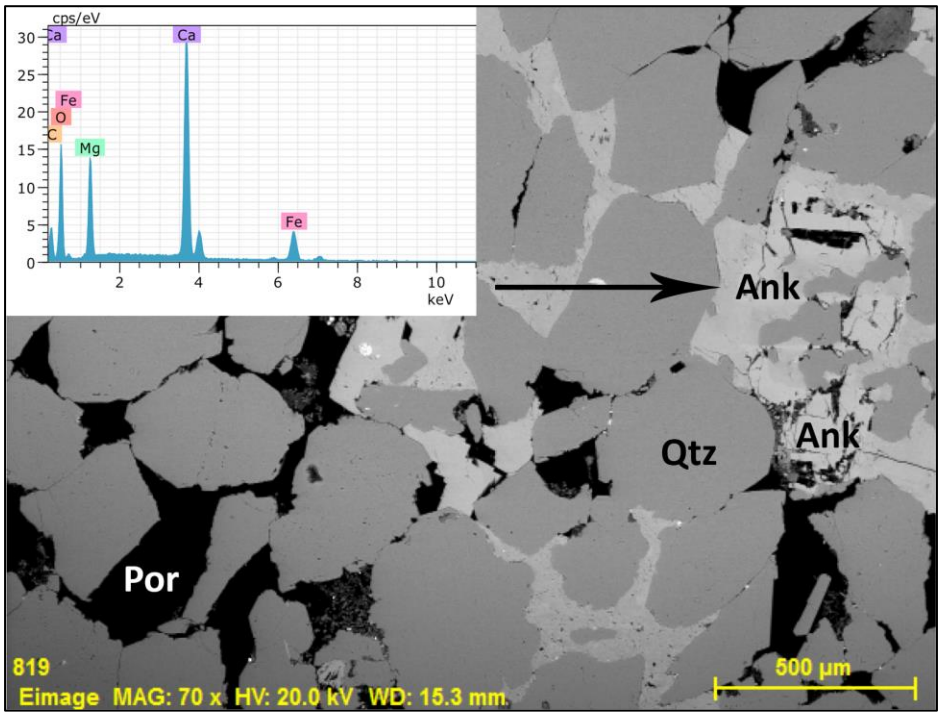

Figure 4.1: A SEM image and EDS spectrum of the authigenic mineral ankerite from well 15/9-19 A, sample 3838.50 mRKB. Ankerite fills the pores in between the quartz grains.

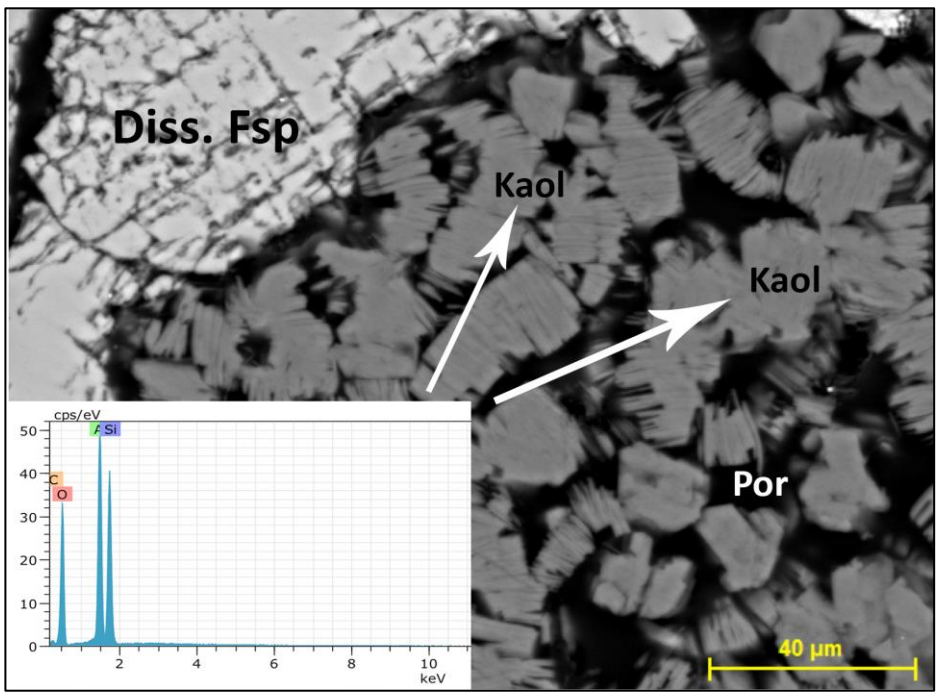

Figure 4.2: Showing a SEM image and EDS spectrum of the authigenic clay mineral kaolinite in well 15/5-7, sample 3826.0 mRKB. Kaolinite (with characteristic booklet structure) fills the pore spaces. The Al symbol is partly hidden in the image.

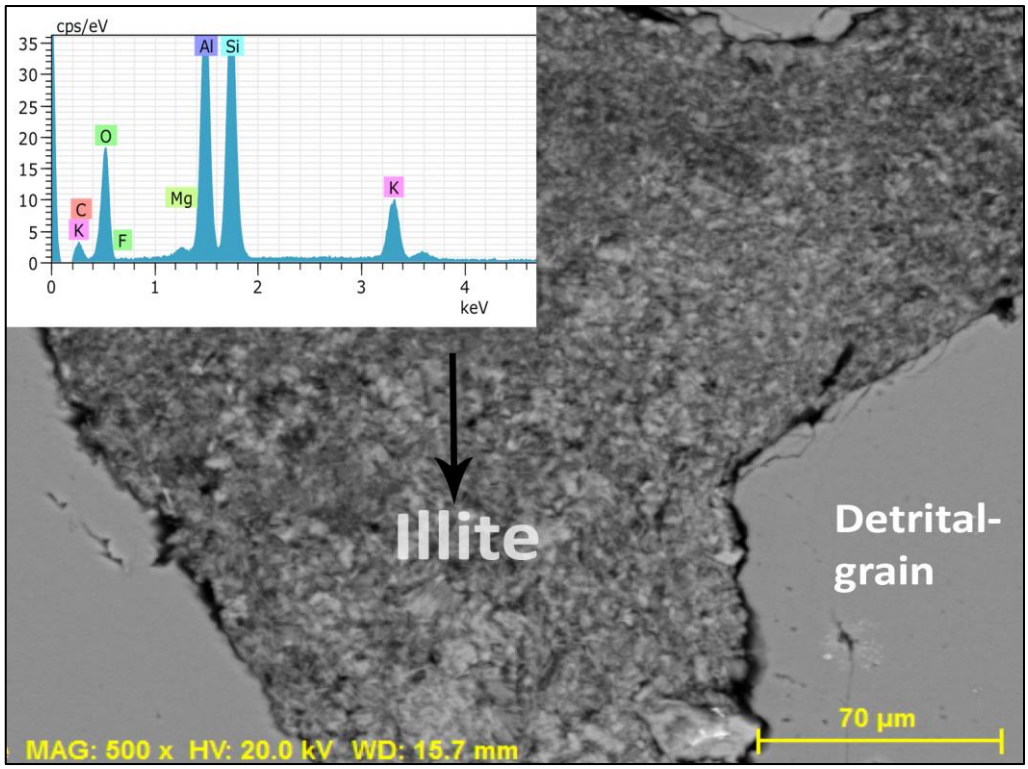

Figure 4.3: A SEM image and EDS spectrum of the authigenic mineral illite from well 15/5-7, sample 3826.0 mRKB. Illite fills the pores in between the detrital grains.

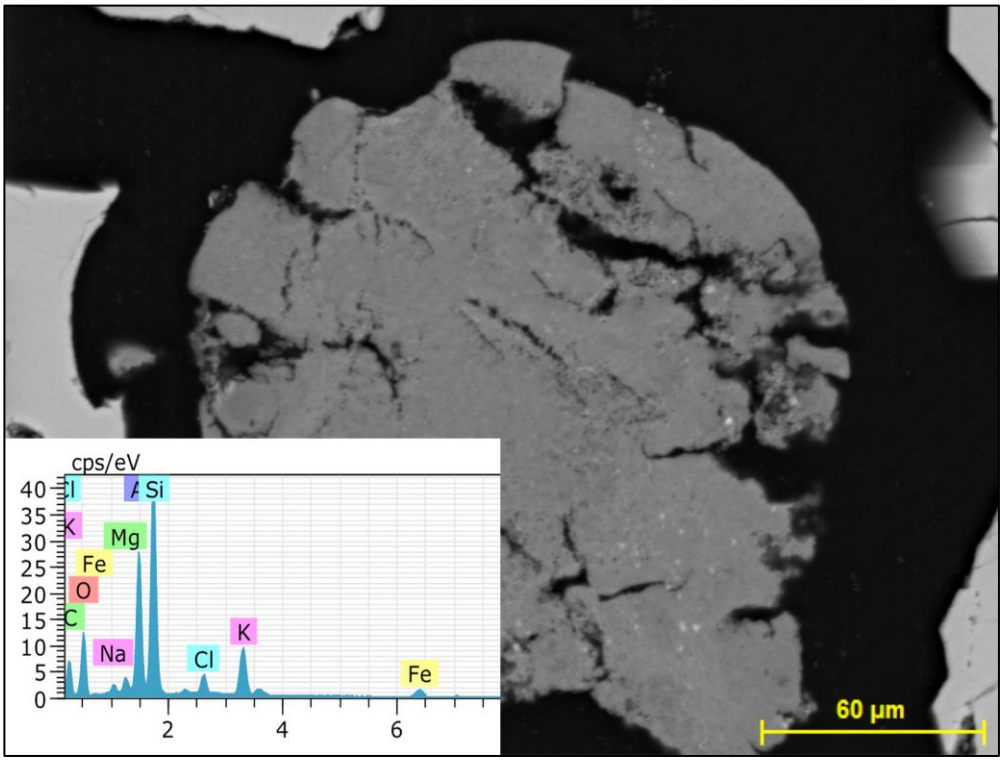

Figure 4.4: A SEM image and EDS spectrum of the possible authigenic mineral, glauconite, from well 15/9-19 A, sample 3838.50 mRKB. The grain could also be an altered feldspar, transformed into ferrous illite.

4.4 Sandstone classification

The sandstones studied consist of matrix, framework grains and diagenetic minerals in varying amounts. The sandstone classification refers to Dott's classification from 1964 (Fig. 4.5).

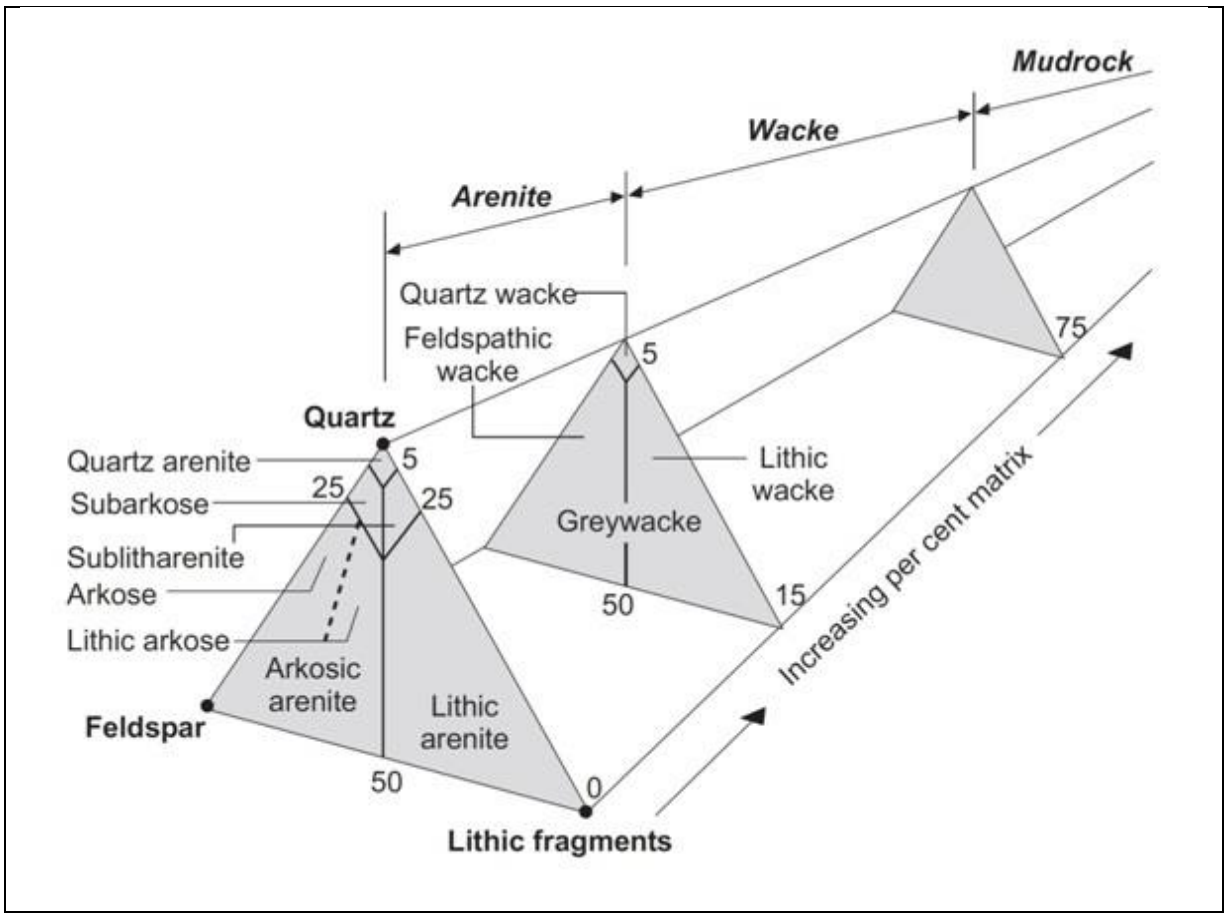

Figure 4.5: Classification of sandstones (Dott, 1964). Sedimentary rocks are divided into mudrock, wacke and arenite depending on the matrix content. Wacke and arenite also have subgroups, depending on the quartz, feldspar, and lithic fragments in the samples.

If the matrix content is between 0 and 15%, the sandstone is classified as an arenite, if the matrix content is between 15 and 75% it is classified as a wacke, and it is classified as a mudstone if it exceeds 75% (Fig. 4.5), (Dott, 1964). All the samples studied are classified as arenites after the modal analyses, since they consist of less than 15% matrix (Tab. A.1, A.2, A.3, A.4, A.5).

The sandstones from the Hugin Formation in wells 15/3-7, 15/6-11 A and 15/9-19 A, are presented as ternary plots in Figure 4.6, based on data from the modal analysis (Tab. 4.1, 4.2 and 4.3). The percentage of quartz (Qtz), feldspar (Fsp), and rock fragments (such as muscovite, heavy minerals, chert, schistose quartzite, quartzite, and pyrite), is calculated and listed in Table 4.4. Each of the wells is described below, regarding the mineralogical (4.5.1) and textural (4.5.2) maturity.

Table 4.4: Samples from well 15/3-7, 15/9-19 A, and 15/6-11 A displaying the percentage content of quartz (Qtz), feldspar (Fsp) and rock fragments (Lith). , which are classified as quartz arenites, subarkoses and sublitharenites after Table 4.1, 4.2, and 4.3. The data in this table is further used in Figure 4.6.

Well 15/3-7					**Well 15/9-19 A**					**Well 15/6-11 A**				
mRKB	**mRSF**	**Qtz (%)**	**Fsp (%)**	**Lith (%)**	**mRKB**	**mRSF**	**Qtz (%)**	**Fsp (%)**	**Lith (%)**	**mRKB**	**mRSF**	**Qtz (%)**	**Fsp (%)**	**Lith (%)**
4610	4483	94.5	-	5,5	3840	2940	85.8	7.3	6.9	4150	3592	74.5	13.5	11.7
4613	4486	92.6	-	7.4	3845	2946	89.7	5.6	4.7	4152	3594	77.7	15.0	7.3
4615	4488	94.0	-	6.0	3850	2950	89.1	6.9	4.0	4154	3596	79.4	19.8	0.8
4616	4489	93.6	0.4	6.0	3857	2957	89.7	7.9	2.4	4155	3597	75.3	20.6	4.1
4617	4490	91.9	0.4	7.7	3862	2962	85.8	4.1	10	4158	3600	79.2	12.1	8.7
4650	4523	95.3	1.7	3.0	3868	2969	86.0	4.3	9.7	4159	3601	77.5	16.7	5.8
4766	4639	91.8	5.1	3.1	3873	2974	82.5	3.4	14	4160	3602	77.0	19.0	4.0
4775	4648	91.8	3.4	4.8	3885	2986	92.1	2.8	5.1	4169	3611	80.8	12.6	6.6
4775	4648	91.4	4.9	3.7	3898	2999	89.0	4.9	6.1	4173	3615	88.3	10.3	1.4
4785	4658	93.0	3.7	3.3	3900	3001	93.0	3.5	3.5	4174	3616	83.4	12.7	3.9

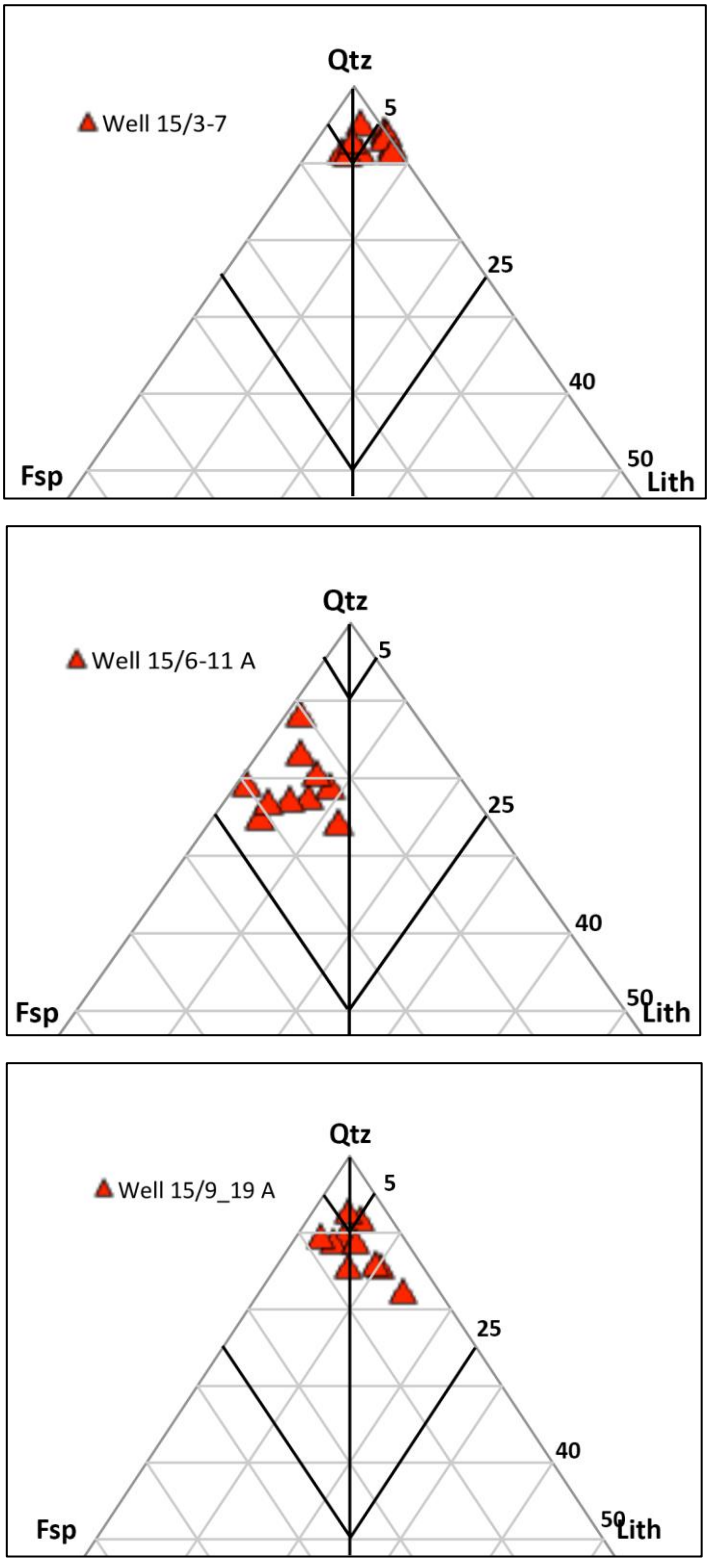

Figure 4.6: Samples from Well 15/3-7, 15/9-19 A, and 15/6-11 A presented in a ternary diagram after Dott(1964). The samples from Well 15/3-7 are classified as quartz arenites. The samples from well 15/9-19 A are classified as subarkoses and sublitharenites, except of one sample, which is classified as quartz arenite. All the samples from well 15/6-11 A is classified as subarkoses.

4.5 Maturity of the sandstones

The mineralogical maturity of sandstones can be divided into two different categories; compositional maturity and textural maturity. If sandstone consists of mainly quartz grains, the sandstone can be classified as compositionally mature. However, if the sandstone mainly consists of unstable grains (such as feldspar, mica, or rock fragments), the sandstone is classified as compositionally immature (Boggs, 2006). Regarding the textural maturity, sandstone is immature if it contains a high content of matrix, and shows low degree of rounding and sorting (Boggs, 2006). Referring to Boggs (2006), the scale of textural maturity goes from immature to supermature (Fig. 4.7).

4.5.1 Compositional maturity

The content of feldspar and rock fragments in the samples from well 15/3-7 and 15/9-19 A is rather low, and distinctly higher in well 15/6-11 A which contains less mature sandstones (Tab. 4.4), (Fig. 4.6). The matrix content is less than 15 % for all the studied wells (Tab. 4.1, 4.2, and 4.3).

Well 15/3-7 contains the most compositionally mature sandstone of the three wells, with no feldspar present in the upper samples, and very low feldspar content (0.4-1.7%) down to 4650 mRKB (Tab. 4.4). The feldspar content increases from 4766.50 to 4785.70 mRKB, with values varying between 3.4 and 5.1%. The rock fragment values are quite constant, varying between 3.0-7.7 %. The data from the modal analyses for well 15/3-7 indicate that the sandstone is compositionally mature. This combined evidence suggests presence of quartz arenite (Fig. 4.6).

Well 15/9-19 A contains a higher degree of feldspar and rock fragments (Tab. 4.4), making it slightly less compositionally mature than well 15/3-7. The feldspar content varies between 2.8 and 11.7%, and the lithic fragment composition varies between 2.4 and 14.1%. The samples plot as subarkoses and sublitharenites (Fig. 4.6).

All the samples from well 15/6-11 A plot as subarkoses since they contain significant amount of feldspar (Tab. 4.4). The amount of lithic fragments in the samples varies between 0.8 and 11.7%, and the feldspar content varies between 10.3 and 20.6% (Tab. 4.4). Well 15/6-11 A is undoubtedly the least compositionally mature sandstone amongst the studied wells (Fig. 4.6).

4.5.2 Textural maturity

In Tables A.1, A.2, A.3, A.4, and A.5, the degree of sorting and rounding of the grains is presented, together with the data from the modal analyses regarding the matrix content (Tab. 4.1, 4.2, 4.3), Figure 4.7 can be used to classify the textural maturity of the sandstones from the Hugin Formation. The textural maturity is related to the total kinetic input (energy) in the depositional environment, on a scale from low to extreme. Low to moderate kinetic input will result in texturally immature or submature sandstones, whereas moderate to extreme kinetic input will give texturally mature or supermature sandstones (Fig. 4.7).

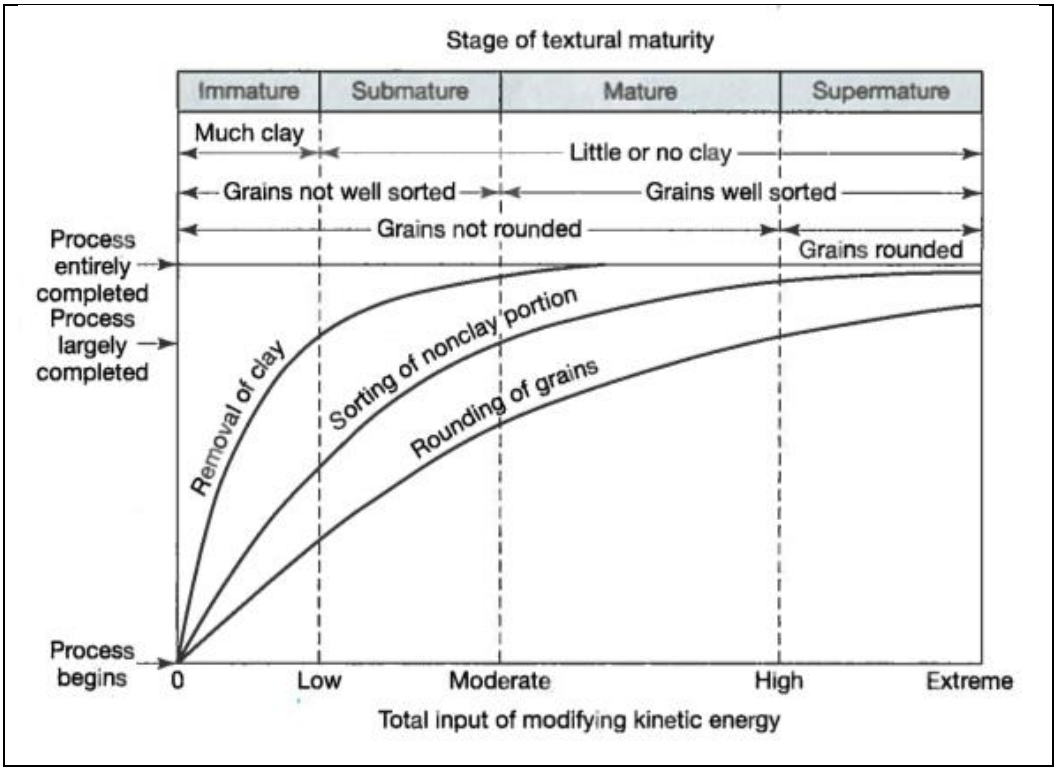

Figure 4.7: Classification of sandstones based on the textural maturity of the grains, and the amount of matrix. The stages of the textural maturity are a function of kinetic input (Boggs, 2006).

The samples from well 15/3-7 consist mainly of subrounded and subangular grains that are well sorted (Tab. A.1). A minority of these grains are moderately, and even poorly, sorted but the roundness is well developed (either subrounded or rounded)for example, sample 4755.10 mRKB and sample 4782.60 mRKB (Tab. A.1). The matrix content observed from the modal analysis displayed a low value ranging from 0.3 to 4.7% (Tab. 4.4). Data from both the petrographical work and the modal analysis indicate a sandstone that is texturally mature.

Well 15/9-19 A consists of grains that are subangular to subrounded, and they are all moderately to well sorted with a few exceptions – for example, 4814.50 mRKB and 4816 mRKB, which are poorly sorted but possess a well-developed roundness of the grains (Tab. A.4). Regarding the matrix content for well 15/9-19 A, the samples have values ranging from 3.0 to 10.0% (Tab. 4.2). Even though they have a higher matrix content compared to wells 15/3-7 and 15/6-11 A, the sandstones of well 15/9-19 A is considered to be texturally mature.

The samples from well 15/6-11 A consist of grains that are subrounded and rounded, and are well to very well sorted (Tab. A.3). Only a minority of the samples are moderately sorted. The matrix content varies between 0.4 and 4.5% (Tab. 4.3). In general, the sandstone displays good reservoir properties and, regarding the textural maturity, it is considered to be mature-to-supermature after Boggs (2006), (Fig. 4.7).

4.6 Porosity and compaction

All buried siliciclastic sandstones will experience loss of porosity,due to both mechanical and chemical compaction, to a varying degree. This is dependent on the rigidity of the framework grains, the framework grain composition, the burial depth, temperature and pore water composition. If the sandstone mostly consists of rigid quartz grains, the porosity loss will be caused by mechanical compaction with increasing burial depth until the grains are in contact with each other. The maximum limit of compaction for well-sorted quartzose sandstones is 26% of the intergranular volume (Paxton et al., 2002). Further porosity loss will then be controlled by chemical compaction, where the contacts between the grains will

develop into sutured, long, or concave/convex contacts. The ions from the dissolved framework grain contacts will migrate to environments where conditions favor precipitation. If the sandstones mostly consist of ductile grains, the intergranular porosity loss is mainly controlled by mechanical compaction (Paxton et al., 2002).

4.6.1 Intergranular volume (IGV)

The intergranular volume (IGV) is an indicator of mechanical and chemical compaction, where intergranular volume (%) = intergranular porosity (%) + intergranular cement (%) + depositional matrix (%), (Paxton et al., 2002).

The components presented in Table 4.1, 4.2 and 4.3 provide the basis for IGV calculations of the Hugin Formation sandstones. The cement components are quartz, calcite, and pyrite. Grain replacements -(such as kaolinite) are not included after Paxton et al. (2002). All the wells have experienced both mechanical and chemical compaction due to the deep burial. Referring to Paxton et al. (2002), any changes in IGV after reaching the depth of approximately 2600 m for quartzose sandstones, is almost entirely because of chemical compaction. Since the studied wells are all placed at greater depths, and significantly higher temperatures, the IGV is resultant of chemical compaction differences.

The IGV values are given in percentage, based on the results from the modal analysis, and are presented in Table 4.5, 4.6 and 4.7.

Table 4.5: Calculated intergranular volume (IGV) for the Hugin Formation in well 15/3-7 based on modal analysis (Tab. 4.1). (B. Cly = Brown clay, G. Cly = Green clay, Qcm = quartz cement, Ccm = calcite cement, Pyr = pyrite).

Well 15/3-7									
Sample depth (mRKB)	Vertical depth (mRSF)	Grain size (mm)	Matrix		Diagenetic minerals			Primary porosity	IGV (%)
			B. Cly	G. Cly	Qcm	Ccm	Pyr		
4610.00	4483.00	0.20	-	1.0	11.7	-	-	7.3	20
4613.25	4486.25	0.30	2.6	-	6.9	-	-	9.3	18.8
4615.25	4488.25	0.50	1.0	0.7	10.3	-	-	4.6	16.6
4616.75	4489.75	0.40	0.3	1.0	9.3	-	-	6.3	16.9
4617.45	4490.45	0.40	3.0	0.3	10.7	-	-	6.3	20.3
4650.00	4523.00	0.20	2.7	2.0	8.0	-	-	3.3	16.0
4766.50	4639.50	0.80	1.7	0.6	12.6	0.3	-	1.7	5.9
4775.30	4648.30	0.25	1.3	0.4	13.0	-	-	3.0	17.7
4775.50	4648.50	0.35	2.9	-	11.4	-	0.3	2.8	15.4
4785.70	4658.70	0.20	-	0.3	6.3	-	-	3.0	9.6

Table 4.6: Calculated intergranular volume (IGV) for the Hugin Formation in well 15/9-19 A based on modal analysis (Table 4.2). (B. Cly = Brown clay, G. Cly = Green clay, Qcm = quartz cement, Ccm = calcite cement, Pyr = pyrite).

Well 15/9-19 A									
Sample depth (mRKB)	Vertical depth (mRSF)	Grainsize (mm)	Matrix		Diagenetic minerals			Primary porosity	IGV (%)
			B. Cly	G. Cly	Qcm	Ccm	Pyr		
3840.45	2940.95	0.25	3.2	6.8	3.3	-	-	9.0	22.3
3845.50	2946.00	0.22	2.4	5.3	4.0	-	-	11.7	23.4
3850.50	2950.95	0.20	4.0	2.6	4.5	4.7	1.0	10.3	27.1
3857.50	2957.90	0.20	2.0	2.7	4.7	-	0.3	11.3	21.0
3862.40	2962.50	0.45	0.7	3.0	4.0	-	-	13.7	21.4
3868.25	2969.00	0.30	1.0	2.0	3.3	-	0.3	11.3	17.9
3873.50	2974.90	0.50	0.6	4.7	4.6	-	0.7	12.0	22.6
3885.55	2986.00	0.30	2.0	2.7	3.0	-	-	14.0	21.7
3898.55	2999.05	0.35	1.0	2.2	2.6	-	1.6	10.8	18.2
3900.50	3001.05	0.40	1.7	1.6	1.6	-	-	14.3	19.2

Table 4.7: Calculated intergranular volume (IGV) for the Hugin Formation in well 15/6/11 A based on modal analysis (Table 4.3). (B. Cly = Brown clay, G. Cly = Green clay, Qcm = quartz cement, Ccm = calcite cement, Pyr = pyrite).

Well 15/6-11 A									
Sample depth (mRKB)	**Vertical depth (mRSF)**	**Grainsize (mm)**	**Matrix**		**Diagenetic minerals**			**Primary porosity**	**IGV (%)**
			B. Cly	**G. Cly**	**Qcm**	**Ccm**	**Pyr**		
4150.45	3592.45	0.20	-	2	4.5	23.0	2.0	7.5	37.0
4152.00	3594.00	0.20	-	2.8	2.8	1.4	-	3.3	10.3
4154.75	3596.75	0.18	-	2.5	3.5	7.5	1.0	9.0	23.5
4155.00	3597.00	0.20	0.5	4.0	3.5	5.4	-	6.9	18.3
4158.75	3600.75	0.18	-	2.0	5.5	1.0	-	7.0	15.5
4159.75	3601.75	0.20	-	2.0	2.5	1.5	-	6.0	12.0
4160.50	3602.50	0.18	-	-	3.0	5.0	-	4.0	12.0
4169.00	3611.00	0.22	-	1.0	2.0	11.5	0.5	3.5	18.5
4173.50	3615.50	0.20	-	1.5	3.5	5.0	0.5	7.5	18.0
4174.00	3616.00	0.14	-	0.5	3.0	7.0	1.0	4.0	15.5

Well 15/3-7 possesses IGV values from 5.9 to 20.3%, with the majority of the samples between 15 and 20% (Tab. 4.5). Sample 4785.70 mRKB contains a lower IGV than the rest, with an IGV of 9.6%. A closer look at the thin section reveals that the quartz grains are strongly interlocked with each other, indicating a high content of quartz cement in the sample. Missing dust rings in the thin section made the interpretation of the quartz cement difficult, which could have resulted in an underestimation of the IGV.

Well 15/9-19 A possesses slightly higher IGV values from 17.9 to 27.1%, with most samples having values above 20% (Tab. 4.6). The highest values are due to calcite cementation, (e.g. at sample 3850.50 mRKB).

Well 15/6-11 A possesses IGV values from 12.0 to 37.0%, with the majority between 12.0 and 23.5% (Tab. 4.7). Samples 4150.45 mRKB and 4154.75 mRKB possess higher IGV values compared to the rest. Calcite cementation is responsible for the high readings seen in these samples (Tab. 4.7).

Comparing well 15/3-7 and 15/9-19 A, the amount of quartz cement is almost double in the samples from well 15/3-7. An explanation can be that the sandstones have experienced a

higher temperature, due to the 1.6 km deeper burial. Despite differences in the mineralogical composition and primary porosity, the IGV is quite similar even though the sandstones differ quite much in vertical depth (Fig. 4.8).

As for well 15/6-11 A, the IGV is a bit lower. The higher feldspar content might have resulted in more mechanical compaction. Another difference is the content of calcite cement in sample 4150.45 mRKB. Calcite will inhibit mechanical compaction, resulting in the higher IGV values. Compared with non-calcite samples from related depths, they will have lower IGV values.

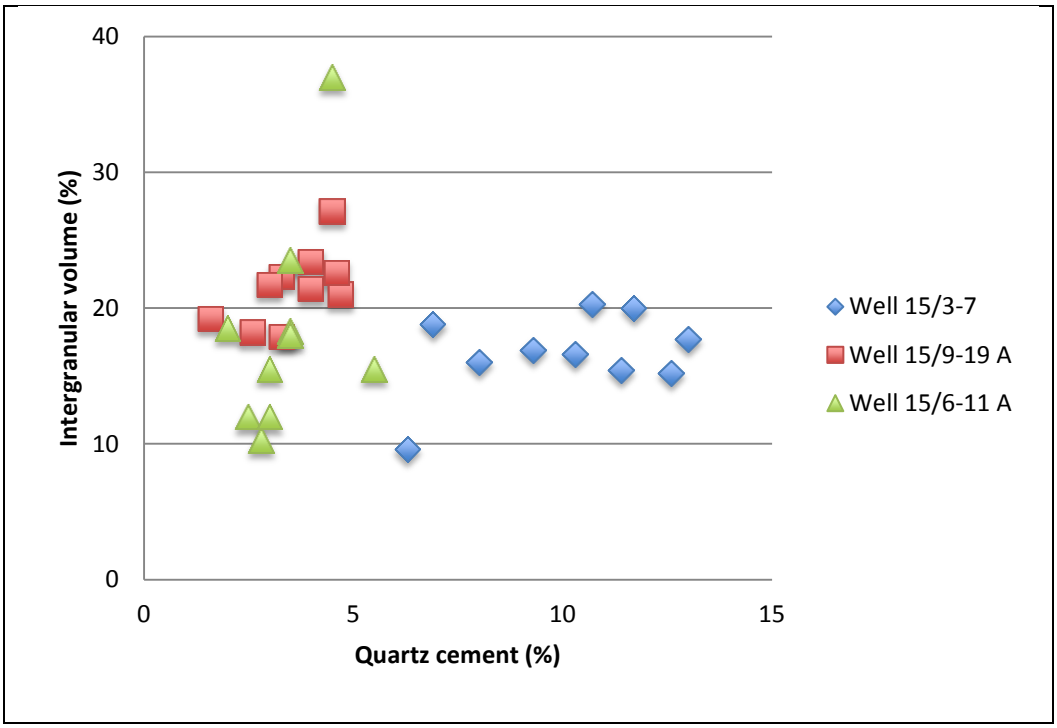

Figure 4.8: Crossplot of data from well 15/3-7, 15/9-19 A and 15/6-11 A, showing trends of quartz cement versus intergranular volume.

An interesting discovery from the IGV measurements is that the values are not widely dispersed even though there are large depth differences. Grain-to-grain pressure solution would have caused the IGV to decrease with increased depth, but this is not observed (Fig. 4.8). This could indicate that the reason for the worsened reservoir quality due to quartz cementation is caused by dissolution at stylolites and clay laminaes. The IGV results from this work support conclusions from similar work done on the same area (Maast et al., 2011).

5 Discussion

The paragenetic sequence and the diagenesis will be discussed in this chapter. There will be a presentation of the permeability and porosity related to true vertical depth (mRSF), in addition to a presentation of the permeability versus porosity for the core plug data. Porosity from the core plugs will be compared with the modal analyzes for the wells 15/3-7, 15/6-1 A, and 15/9-19 A. The aim is to discover any diagenetic trends related to depth, mainly the abundance of quartz cement as a function of different factors (such as grain size, lithology, maturity, and the abundance of stylolites). Processes related to the formation of the stylolites, and how they interfere with the distribution of quartz cement, will be investigated. Quartz cement inhibitors, such as different clay coatings together with oil emplacement, will be discussed. Other diagenetic minerals such as calcite cement, kaolinite and illite will be discussed, and which role these authigenic minerals play in the characterization of the reservoir property. The overall picture of the reservoir quality of the Hugin Formation will also be covered in this chapter.

5.1 Paragenetic sequence

The paragenetic sequence is the order of the different diagenetic minerals developed in the sediments. Some of the minerals develop in the eogenetic regime while others develop in the mesogenetic regime. The paragenetic sequence for wells 15/3-7, 15/5-7, 15/6-11 A, 15/9-19 A and 15/9-21 S is presented in Figure 5.1. The interpretation is based on petrographical methods.

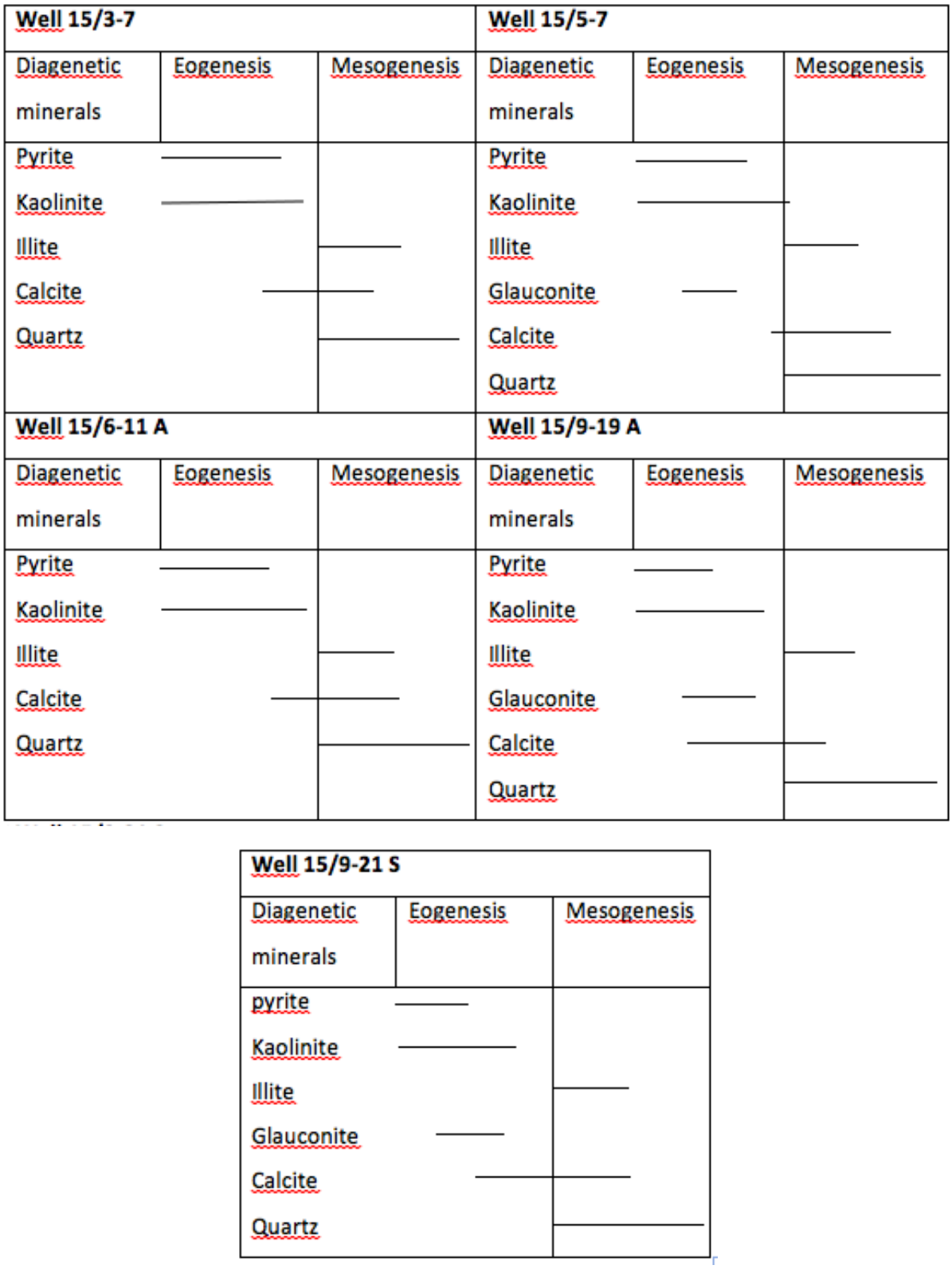

Figure 5.1: Paragenetic sequence of well 15/3-7, 15/5-7, 15/6-11 A, 15/9-19 A and 15/9-21 S. The diagenetic minerals are pyrite, kaolinite, glauconite, calcite and quartz and illite. Pyrite, kaolinite and glauconite are developed in the eogenetic regime, while calcite is formed in both the eogenetic and the mesogenetic regime. Quartz cement and illite are developed in the mesogenetic regime.

5.2 Diagenetic minerals

The diagenetic minerals were described in Chapter 3, and their occurrence will be covered in the following sections. Quartz overgrowths will also be discussed further in Section 5.4. The diagenetic minerals were precipitated from pore waters during the eogenetic and mesogenetic regime. Diagenetic changes in a sandstone reservoir are mainly controlled by mineralogy/texture, fluid composition, geothermal gradients and pressure gradients.

5.2.1 Pyrite

Pyrite is the earliest formed authigenic mineral, and is present in all the wells (Tab. A.1, A.2, A.3, A.4, A.5). Well 15/3-7 shows the lowest amount of pyrite, while well 15/6-11 A and 15/9-19 A both possess a significant amount of pyrite. The pyrite crystals occur both as cement and single crystals, either dispersed randomly in the sediments, but often seen in relationship with stylolites. The pyrite is entrapped inside the stylolites, together with other insoluble minerals, forming the characteristic stylolite zigzag pattern.

5.2.2 Authigenic clay

Kaolinite occurs in all the wells in varying amounts, mainly as pore-filling aggregates, but also as replacement of detrital grains. For further descriptions see Chapter 3.
In some of the calcite cemented samples, kaolinite is absent. In such cases it could look like calcite cement pre-dated the kaolinite in the paragenetic sequence, but that is not the case. It is believed that the kaolinite pre-dates the calcite precipitation for all the wells, as kaolinite crystals have been found as inclusions in both calcite cement and quartz overgrowths.
Since the Hugin Formation consists of near shore, shallow marine sandstones (Vollset et al., 1984), it may have been exposed to considerable amounts of meteoric waters flushing through the sediments, which may have contributed to dissolution of unstable minerals such as alkali feldspar. Kaolinite crystals are also observed in contact with partly-dissolved

alkali feldspar grains, which support this interpretation. The chemical reaction of the dissolution of alkali feldspar and formation of kaolinite is given in Bjørlykke (2010):

Equation 3:

$$2K(Na)AlSi_3O_8 \text{ (feldspar)} + 2H^+ + 9H_2O = Al_2Si_2O_5(OH)_4 \text{ (kaolinite)} + 4H_4SiO_4 + K^+(Na^+)$$

The reaction can only take place in an open system, since it needs a constant flux of water to remove the K^+ ions and the silica. Such conditions exist in fluvial and shallow marine environments, such as the Hugin Formation.
Normally the released silica will not precipitate at low temperatures, so for the kaolinite to remain stable, the pore waters need to be diluted with respect to silica and K^+ ions. Since the kaolinitization of feldspar requires a constant water flux through the sediments, the reaction is limited to a certain burial depth, since the permeability decreases with increased depth. Bjørlykke (1998) suggests that the dissolution of feldspar and formation of kaolinite is pervasive at depths shallower than 10m, but might still occur down to burial depths of approximately 100m. On the other hand, Worden and Burley (2003) claim that the dissolution of feldspar grains and the formation of kaolinite occurs at depths up to 4500m, producing so called “diagenetic quartz arenites”. In such cases, the meteoric waters need to penetrate deep into the basins, which is not really likely since several impermeable layers would inhibit a high water flux through the sediments. The depths and temperatures are still debated amongst workers related to the formation of kaolinite in the North Sea. Studies of the Brent sandstone shows that kaolinite forms from the precursor mineral feldspar (Bjørlykke, 1998), and for the Hugin Formation the similar trend is observed related to the formation of kaolinite.

Illite occurs in the Hugin Formation and is recognized in all the wells studied (Tab. A.1 - A.5). Illite forms at temperatures over 70 ˚C (Worden and Burley, 2003), in formation waters containing potassium (K^+), and it may form in addition to quartz by the reaction :

Equation 4:

$Al_2Si_2O_5(OH)_4 + KAlSi_3O_8 = KAl_3Si_3O_{10}(OH)_2 + 2SiO_2 + H_2O$

Illite forms by the reaction between kaolinite and feldspar, also known as illitization of kaolinite. A strong trend of increasing illite is seen with an increase of temperature (Giles et al., 1992), and the formation may occur at temperatures even above 130-140 ˚C (Bjørlykke et al., 1986; Ehrenberg, 1990). It has been observed that partly dissolved alkali feldspar is closely associated with kaolinite in the Hugin Formation. The illite seen in the formation has most probably been developed due to illitization of kaolinite (Equation 4). This hypothesis is congruent with work done by others (Bjørlykke, 1998; Bjørlykke, 2001). Bjørlykke (2001), states that the validity of the reaction is dependent on the presence of alkali feldspar, in order to supply the potassium needed for the formation of illite. Actually, this phenomenon is observed in most cases of illite formation in sandstones in the North Sea area (Bjørlykke, 2001). In order to recognize if illite is formed by clastic or authigenic kaolinite (Eq. 4), the appearance of the mineral needs to be investigated. The petrographical work shows the kaolinite crystals are strongly related to the presence of feldspar. It shows that the illite seen in the Hugin Formation can be caused by authigenic kaolinite. If the amount of alkali feldspar is low in the sediments, kaolinite will be relatively stable even in deep burials. In well 15/3-7, this could explain the higher permeability observed, as discussed in Section 5.2.1. Illite could also have been developed from dissolving smectite by the reaction (Bjørlykke et al., 1995):

Equation 5:

Smectite + K^+ = Illite + silica (via mixed – layer minerals).

Since no smectite is observed in the samples, it is unlikely that this reaction is valid for the Hugin Formation. The climate during deposition would not have been conducive to the formation of smectite, since the conditions where warm and humid when the formation was deposited.

5.2.3 Glauconite

Glauconite is observed in well 15/5-7, 15/9-19 A and 15/9-21 S where it appears in a granular form (Fig. 3.20b). Since glauconite is formed in marine environments, it is apparent that the formation of the mineral occurred during the early stage of the eogenetic regime. Since Hugin Formation mainly consists of shallow marine sandstones (Folkestad et al., 2008), it is natural to believe that the mineral should be present in all the wells, which is not the case. The occurance of glauconite will be further discussed using a sequence stratigraphical approach in Section 5.2.4.

5.2.4 Kaolinite and glauconite in a sequence stratigraphic correlation

The formation of ***kaolinite*** must be seen in close relationship with the sequence boundaries related to system tracts. Kaolinite tends to increase towards the top of highstand system tracts (HST) and at sequence boundaries in general (Ketzer et al., 2003). If the system tract consists of progradational or aggradational parasequences, the amount of kaolinite might be considerably high. During a sea level fall at a HST, the meteoric head will be at its greatest, and since the mixing zone moves towards the basin, the meteoric recharge area will be considerably enlarged, and the formation of kaolinite will increase. An interesting discovery is that the Hugin Formation was mostly developed during a transgression, hence during deposition of retrogradational parasequences. Referring to Ketzer et al. (2003) the content of kaolinite in transgressive system tracts (TST) is highly restricted. This is not synonymous with the distribution of kaolinite seen in the Hugin Formation. However, during the overall transgression, or “the drowning of the Brent delta”, some progradational sequences are observed within the Hugin Formation (Folkestad et al., 2008). Even though the sediments are deposited during a TST, some of the individual progradational parasequences within the system tract can explain the kaolinite seen in the formation. Also, if the samples studied in this thesis mainly consist of proximal deposits, the possibility of finding kaolinite is much higher, despite the fact that the Hugin Formation consists of sediments deposited during a transgression. Kaolinite can cause production problems in reservoirs and will be further discussed in Section 5.5.

Referring to Ketzer et al. (2003), ***glauconite*** is often associated with condensed sections during a transgression, hence it is naturally found in TST. The condensed sections are associated with marine environments with reduced or negligible clastic sedimentation, where it forms at the transition zone between oxidized and reduced conditions (Bjørlykke, 2001). Unlike Ketzer et al. (2003), Amorosi (1995) states that the formation of glauconite is not diagnostic of a specific system tract, but can be located in addition to TST, in condensed sections in both lowstand system tracts (LST) and HST. With respect to the prevalence of the mineral throughout the examined wells, it is believed that the cores were not only cut at condensed sections due to the limited amount of glauconite found in the samples.

5.2.5 Calcite cement

Calcite cement is distributed amongst all the wells studied. The formation of calcite cement is the dominant porosity-reducing process, together with the mechanical compaction. Carbonate cement precipitates when the solubility of calcium carbonate decreases in the pore waters, often controlled by an increase in temperature and concentration of bicarbonate ions (HCO_3^-). With a simultaneous decrease in the CO_2 content, conditions are favorable for calcite precipitation (Boggs, 1992).

For the precipitation of calcite cement there must clearly be sources of calcium in the sediments during deposition and burial. In shallow marine sandstones, such as the Hugin Formation, the only significant source of calcite cement (hence calcium) is biogenic carbonate (Walderhaug and Bjørkum, 1998). Original biogenic carbonate, present in the sandstone, will be dissolved locally and redistributed by diffusion. Biogenic carbonate is less stable than calcite cement, so when a calcite nucleus has formed, calcite continues to precipitate around the nucleus until the concentration in the pore waters no longer favors precipitation. Biogenic carbonate will than dissolve and continue to precipitate around the same nucleus, until it is fully consumed or all the available pore space within the sandstone is filled with cement.

Calcite cement is observed with no typical trend related to depth, as is observed for the quartz cement. The precipitation of calcite has occurred in both the eogenetic and the mesogenetic regime. In some samples, calcite cement post-dates quartz cement (Fig. 5.1a

and b) or at least overlaps with the quartz cement, and in other samples the calcite cement precipitated at an early stage of the eogenetic regime. In the case of early precipitation, no primary porosity remains due to the calcite filling all the pores in the sediments. No mechanical compaction was observed in such samples, suggesting that the precipitation must have happened in the eogenetic regime. Regarding the later precipitation in the mesogenetic regime, in addition to the calcite post-dating quartz cement, the calcite is observed as iron rich.

The iron rich calcite or dolomite is an evidence of late stage precipitation, hence a precipitation in the mesogenetic regime (Adams et al., 2001). In order to distinguish between the two different minerals (as mentioned in Section 3.6), further analysis had to be introduced, and SEM was applied to sample 3838.50 from well 15/9-19 A, containing carbonate cement. In the examined sample, the electron dispersive spectra (EDS) showed the spectra assigned for ankerite (Welton, 1984), (Fig. 4.1). The cement mineralogy is related to the pore water composition during deposition. The precipitation of ankerite (ferrous dolomite) favors conditions where the sulphate content is low, resulting in lower precipitation of pyrite, and the available Fe^{2+} ions may form ankerite in a late eogenetic, or mesogenetic regime. Since the Hugin Formation consists of sandstones deposited in shallow marine environments, the formation of ankerite seen in this case will probably be the latest formed mineral after calcite and siderite (Worden and Burley, 2003).

In late diagenesis, such as described regarding the Brent sandstone from the Statfjord Field, the formation of ankerite is a common feature (Bjørlykke, 2001). Bjørlykke (2001) suggests the formation of ankerite could be through a reaction between calcite and siderite presented in the following equation:

Equation 6:

$CaCO_3$ (calcite) + $FeCO_3$ (siderite) = $CaFe(CO_3)_2$ (ankerite)

The reaction after Bjørlykke (2001), is simplified since ankerite will also include magnesium ($Ca(Mg,Fe)(CO_3)_2$), (Nesse, 2000).

Ankerite can also be formed from bicarbonate through produced organic-matter reactions (Boggs, 1992). When the depth of burial reaches the zone of methanogenesis, Fe- reduction

and microbial fermentation can together form iron-rich carbonates through the precipitation of ankerite.

5.2.6 Quartz cement

Quartz cementation is entirely restricted to the mesogenetic regime. A general trend is observed through the petrographic work, which is an increase of quartz cement precipitated with an increase of depth (Tab. 4.1, 4.2, 4.3), (Fig. 5.2). Some points in well 15/3-7 show anomalous low readings regarding the amount of quartz cement (6 to 8%), which is caused by calcite filling the pores. The rest of the points from the wells, which do not contain any calcite cement, show a clear trend as mentioned above. One reason for the higher amount of quartz cement, related to deeper burials, could be e.g. higher temperatures, different grain sizes, or different mineralogical compositions. Since no specific change related to the grain size or mineralogy is discovered in the samples, it is reasonable to assume that the higher amounts of quartz cement in the samples is caused by the deeper burial, hence higher temperatures.

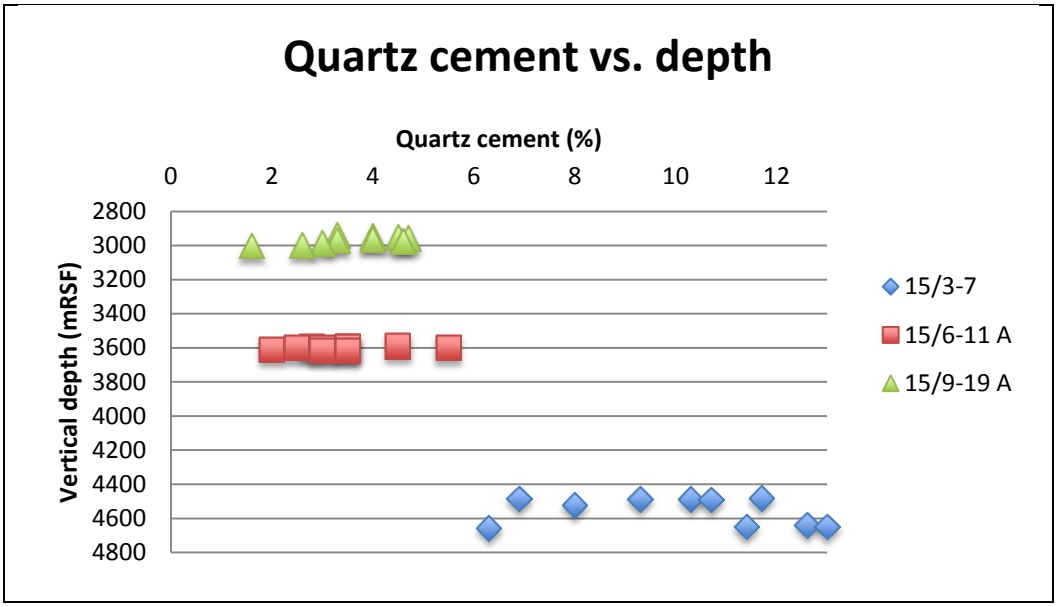

Figure 5.2: Illustrates the amount of quartz cement compared to depth (mRSF) for well 15/3-7, 15/9-19 A, and 15/6-11 . There is a general increase of quartz cement with an increase of depth, which is commonly seen for the wells in the Hugin Formation. The points with the lowest amounts of quartz cement in well 15/3-7, are caused by calcite cement present in the samples.

The porosity trend presented in Figure 5.3, obtained from the core plugs, is a linear function of depth which correspond to the trend found by other workers, e.g. Selley (1998), (Fig. 5.5). The trend identified correspond to the petrographic work (Tab. A.1, A.2, A.3, A.4, A.5) and is also seen in the modal analyzes (Tab. 4.1, 4.2, 4.3). The distribution of quartz cement will be further discussed in Section 5.3.

An explanation regarding the reduced porosity related to depth could be the increased amount of quartz cement precipitated in the pore spaces with increased burial depths. Figure 5.4 shows quartz cement versus porosity, and clearly there is a trend of reduced porosity with increased amounts of quartz cement in the samples. The data is obtained from the modal analysis presented in Tables 4.1, 4.2 and 4.3.

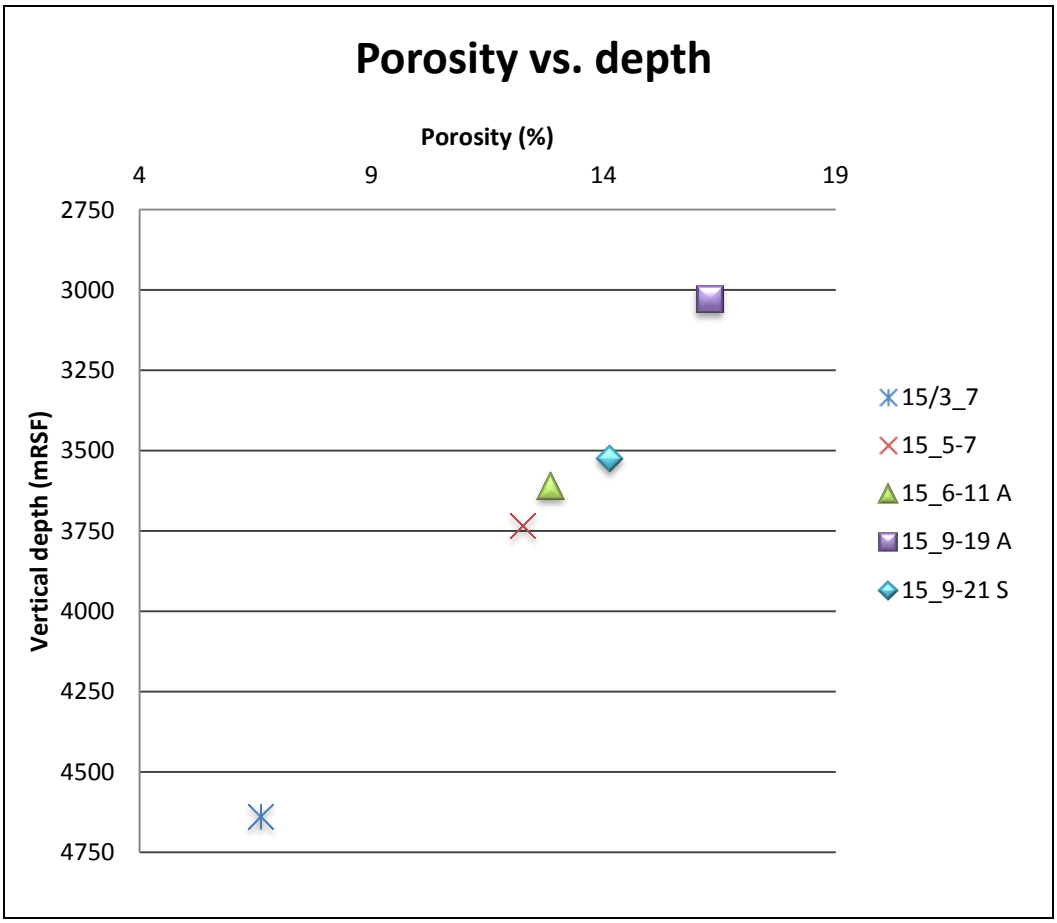

Figure 5.3: Illustrates the average porosity versus depth for well 15/3-7, 15/5-7, 15/6-11 A, 15/9-19 A and 15/9-21 S. Clearly the porosity is a linear function of depth, which is a trend similar to other studies done on reservoirs in the southern part of the Viking Graben (Bjørlykke et al., 1989). The porosity decreases with increasing depth. (The plot is based on data from core plugs provided of Statoil ASA).

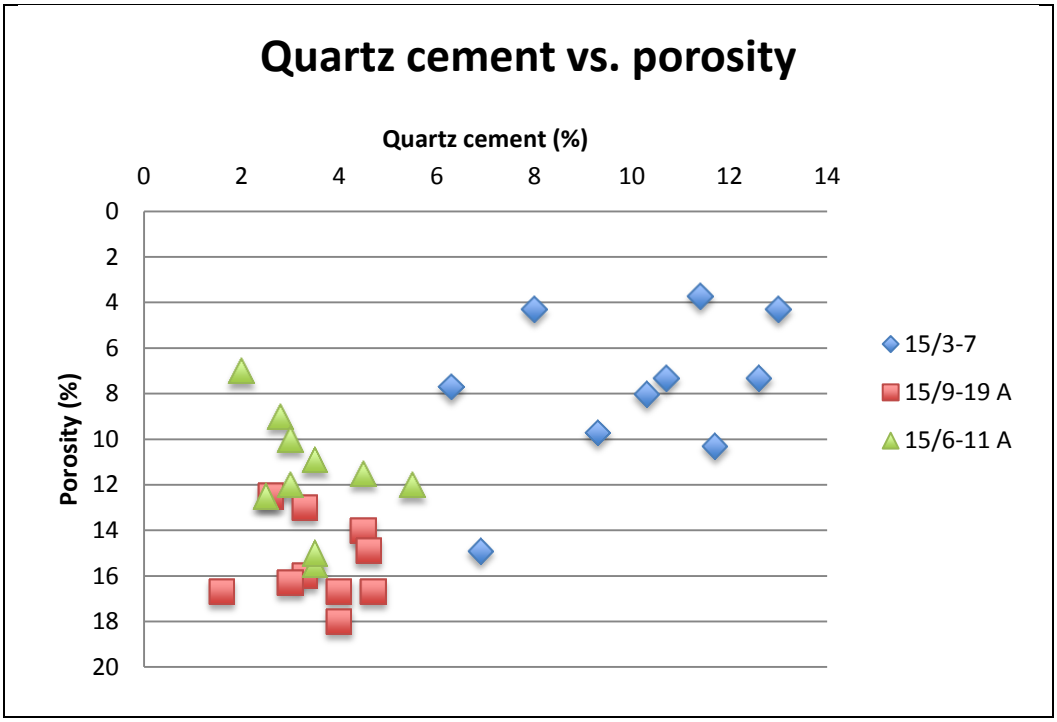

Figure 5.4: Crossplot of data showing the correlation between quartz cement and porosity for well 15/3-7, 15/9-19 A and 15/6-11 A. There is a general trend of reduced porosity while the amount of quartz cement increases. (The plot is based on data obtained from the modal analysis).

The modified Figure 5.5 from Selley (1998), illustrates how the porosity gradients decrease with increasing mineralogical maturity. The quartz arenitic and arkosic sandstones from the Hugin Formation are shown for comparison with Selley's work. The rigid grains in the samples cause an increased stability against mechanical compaction in the formation. Selley (1998) claims that the texture also affects the porosity gradient. Poorly sorted sandstones, with abundant clay, compact more and lose porosity faster than e.g. quartz arenites. In addition, the geothermal gradient and different pressure regimes, will affect the gradient. On the other hand, chemical compaction causes the quartz arenites to lose more porosity than arkoses due to a higher degree of development of quartz cement (McBride, 1989; Dutton and Diggs, 1990).

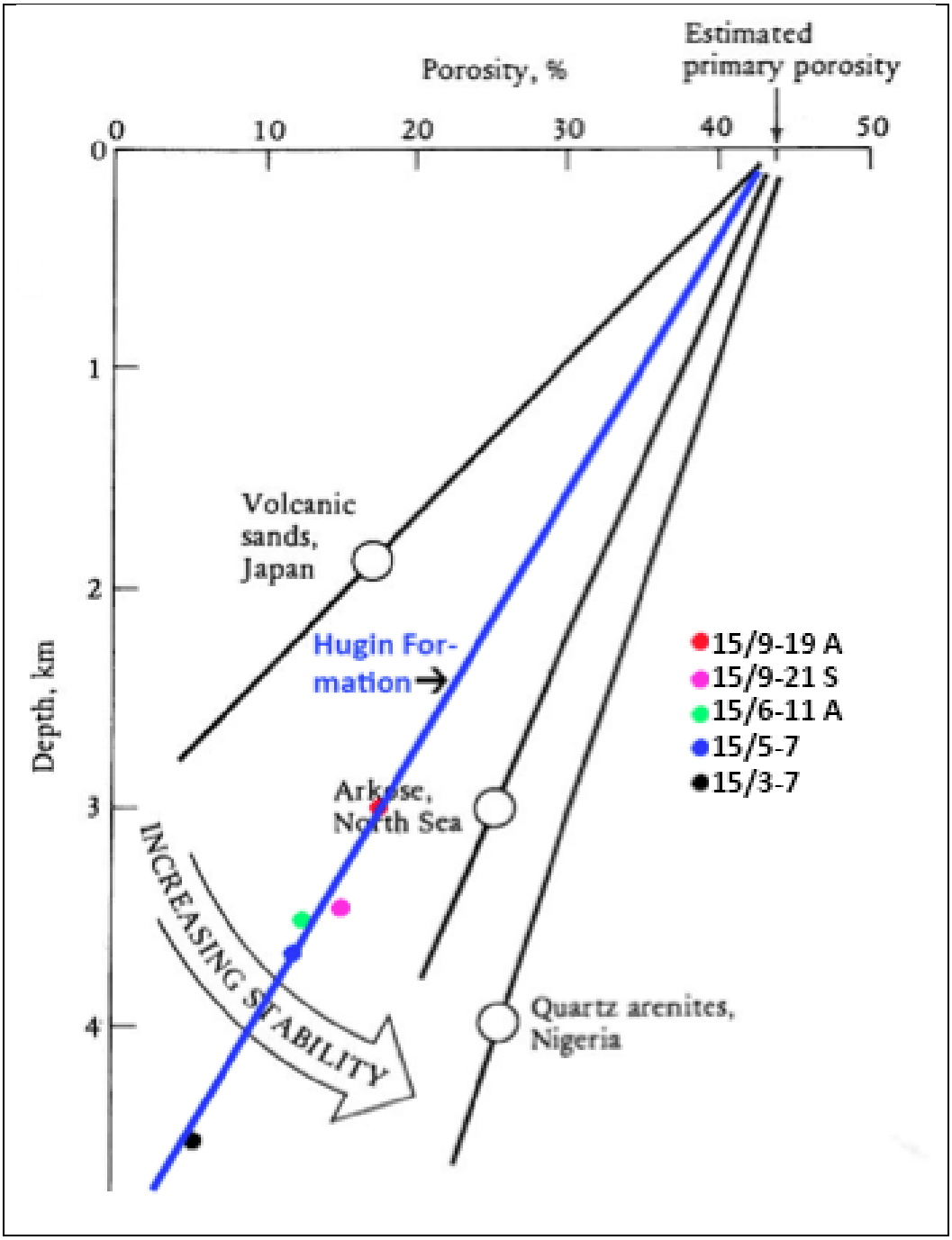

Figure 5.5: The figure is modified after Selley (1998), showing increasing stability regarding preservation of porosity seen as a function of lithology related to depth. The blue line indicates the Hugin Formation represented with the wells 15/3-7, 15/5-7, 15/6-11 A, 15/9-19 A and 15/9-21 S. As observed the line falls nearly on the line of the North Sea arkoses from the work of Selley (1998). The indicated lower stability related to Selleys work might be because the depth used for his presentation is wellbore depths (mRKB) and not true vertical depth (mRFS), which this work is based on. Selley (1998), could also have limited the effect of chemical compaction, or been overly optimistic in his presentation of the porosity data.

In Figure 5.5, the blue line represents the Hugin Formation and it is plotted beneath the trend line for the North Sea arkoses. This observation is interesting since it is reasonable to believe that the trend line would correlate closely with the line of the arkoses, or actually fall in between the line of arenites and arkoses, based on the modal analyzes, hence the maturity of the sandstones. If the results from Selley's studies are based on wellbore depths (mRKB) instead of true vertical depths (mRSF), the line indicating the Hugin Formation would then have plotted further to the right since the depths from this work are based on true vertical depths (mRFS). Selley's plot is also very general with respect to chemical compaction. Both lines, in respect to the arenites and arkoses, should be curved as a result of more intensive chemical compaction related to burial depth. The Hugin Formation has experienced significant amounts of chemical compaction, hence the lower porosities seen in Figure 5.5. Another uncertainty is that the arenites in Selley's work are from Nigeria, and might not be representative for the North Sea arenites. Selley (1998) might also have been overly optimistic in respect to his observations regarding the porosities. More recent studies of the Hugin Formation (Maast et al., 2011) found porosity values which coincided with the results of this work (Fig. 5.16). Variations in the porosity caused by diagenetic processes is a complicated issue, and will be discussed in a later section.

5.3 Diagensis related to porosity and permeability

In the following sections the porosity and permeability will be discussed, and the data obtained from core plugs provided by Statoil ASA will be examined and presented. The average values of porosity and permeability will be discussed first, and then the results from the individual wells will be presented with corresponding data. In Section 5.2.6, the porosity data from the core plugs will be compared to the modal analyzes.

The sandstone porosity in the Hugin Formation for wells 15/3-7, 15/5-7, 15/6-11 A, 15/9-19 A, and 15/9-21 S, is an approximately linear function of depth (Fig. 5.3) already described above, with a trend that is quite similar to other reported sandstone reservoirs in the northern part of the North Sea (Bjørlykke et al., 1989).

Regarding the permeability, it is found to be high at depths shallower than approximately 3600 mRFS but there is a drastic reduction in the permeability at greater depths (Fig. 5.6). Since the scale for the permeability is a logarithmic scale, it is apparent that there is a significant decrease over a few hundred meters.

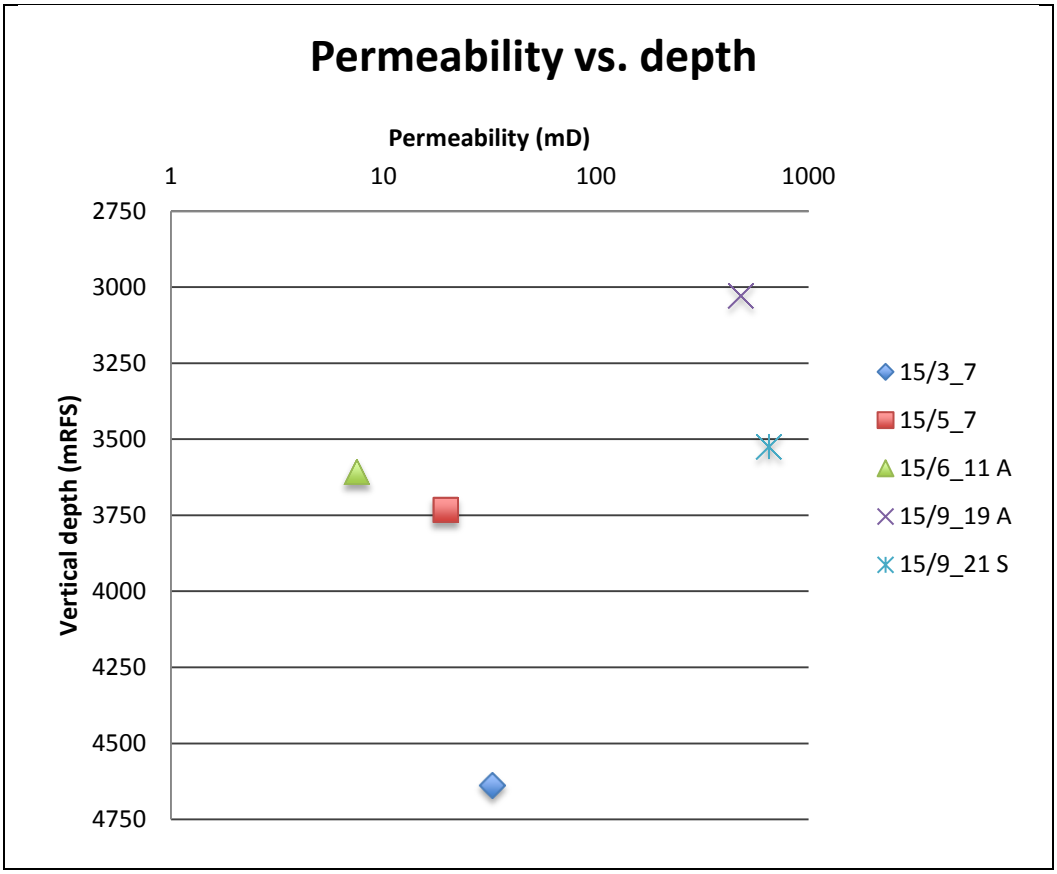

Figure 5.6: Illustrates average permeability versus vertical depth (mRFS) for well 15/3-7, 15/5-7, 15/6-11 A, 15/9-19 A and 15/9-21 S. At depths shallower than approximately 3600 mRFS permeabilities are relatively high, but at greater depths there is a drastic reduction in the permeability. (The plot is based on data from core plugs provided of Statoil ASA).

The plot of permeability against the porosity (Fig. 5.7) reveals a trend of decreasing porosity at a constant permeability at shallow depth, indicated with a black horizontal line, grading into a decreasing trend of permeability at nearly a constant porosity at greater depths, indicated with a black vertical line. The average permeability value for well 15/3-7 is greater (Fig. 5.6, and 5.7), compared to wells 15/5-7 and 15/6-11 A. One explanation is the difference in grain sizes. The average grain sizes are larger in samples from well 15/3-7

compared to the other wells, which is probably one reason for the anomalous difference seen regarding the permeability values of well 15/3-7 (Fig. 5.14). The lower amount of illite could provide another explanation.

Porosity measurements give a more reasonable result considering the depth difference between the wells. The deepest well, well 15/3-7, is the least porous while the most shallow well possesses the highest porosity.

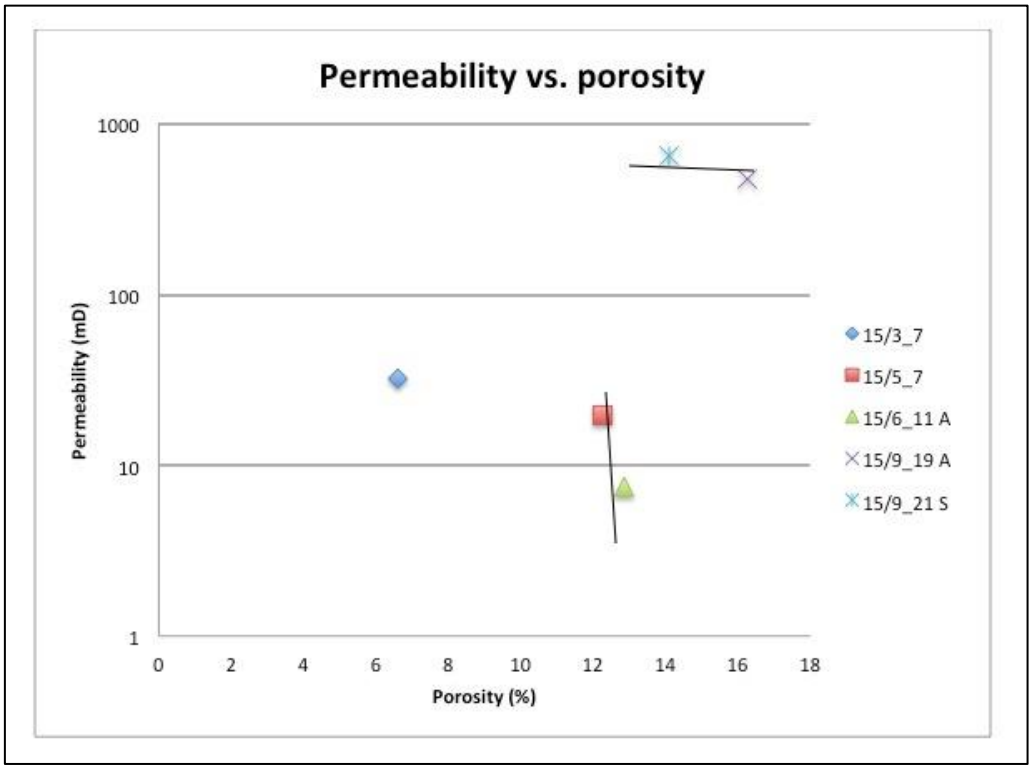

Figure 5.7: Illustrates the average permeability versus the average porosity for well 15/3-7, 15/5-7, 16/6-11 A, 15/9-19 A and 15/9-21 S. There is a non-linear trend of decreasing porosity with nearly a constant permeability at shallow depths, but with greater depths the trend is grading into a field of decreasing permeability at a nearly constant porosity, except from the anomalous high permeability in well 15/3-7. The higher permeability seen in well 15/3-7 is most likely due to a larger average grain size (The plot is based on data from core plugs provided of Statoil ASA).

The basis of the presented data seen above, can be studied in more detail in Figure 5.8, 5.9, and 5.10, 5.11 and 5.12 below. The data from the individual wells is presented, and a more detailed description will be given in Section 5.2.1 to 5.2.5, in order to give a better description of the different patterns seen for the samples of the Hugin Formation.

Figure 5.8: Illustrates three different plots for well 15/3-7. Porosity vs. vertical depth (mRSF), permeability vs. vertical depth (mRSF), and permeability vs. porosity. Referring to text for a more detailed description of the different plots. The gap seen in two of the plots are because of lack of data. All plots are produced with data provided by Statoil ASA.

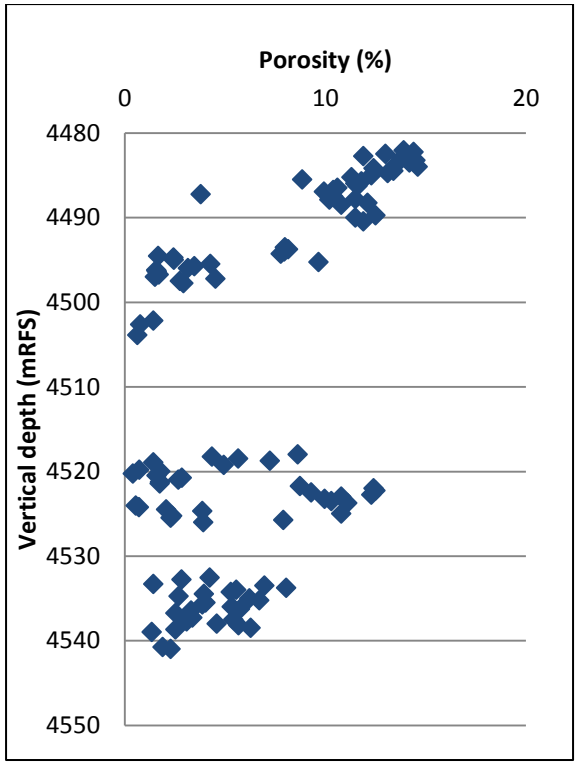

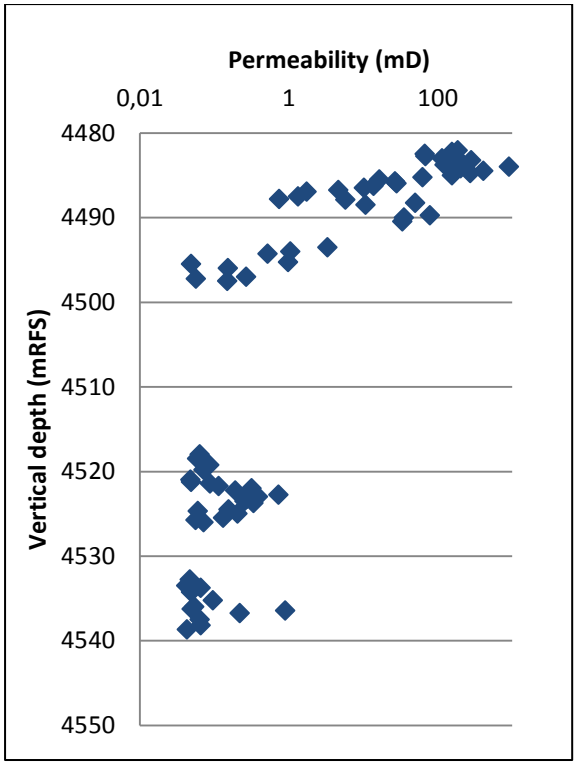

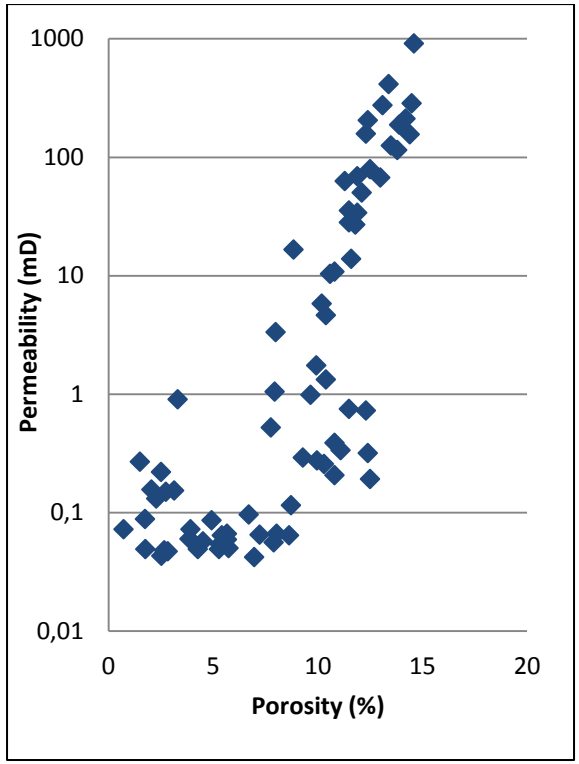

Figure 5.9: Illustrates three different plots for well 15/5-7. Porosity vs. vertical depth (mRSF), permeability vs. vertical depth (mRSF), and permeability vs. porosity. Refer to text for a more detailed description of the different plots. All plots are produced with data provided by Statoil ASA.

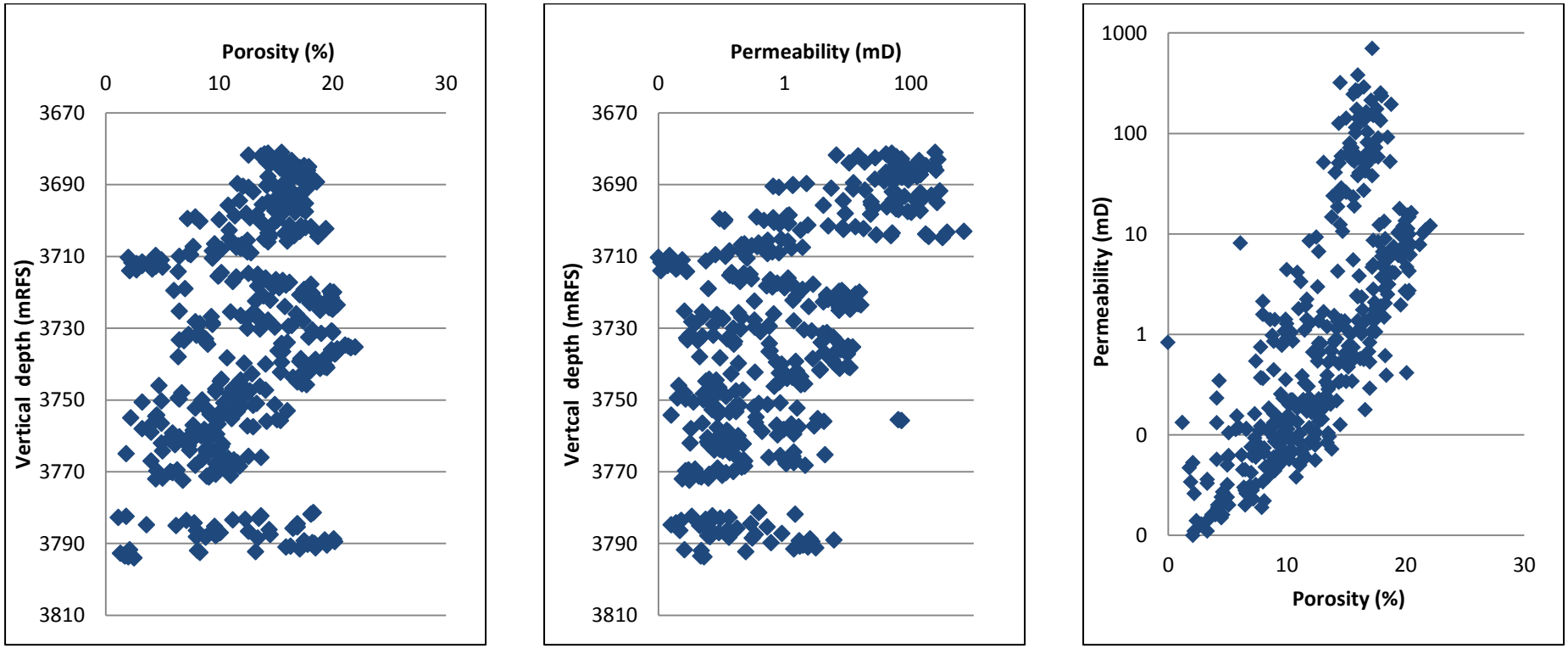

Figure 5.10: Illustrates three different plots for well 15/6-11 A. Porosity vs. vertical depth (mRSF), permeability vs. vertical depth (mRSF), and permeability vs. porosity. Refer to text for a more detailed description of the different plots. All plots are produced with data provided by Statoil ASA.

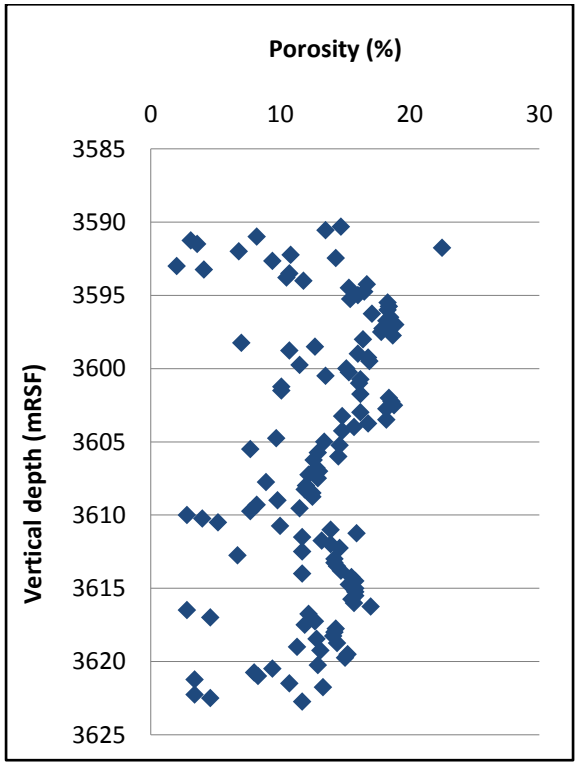

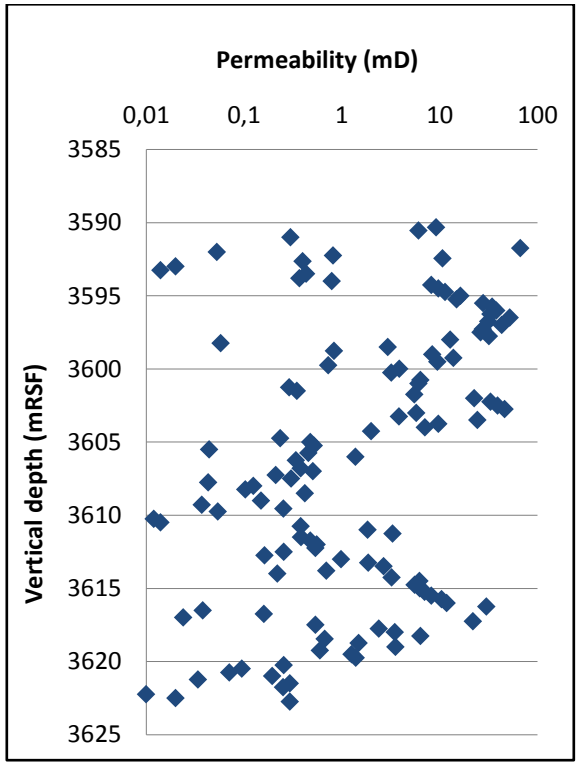

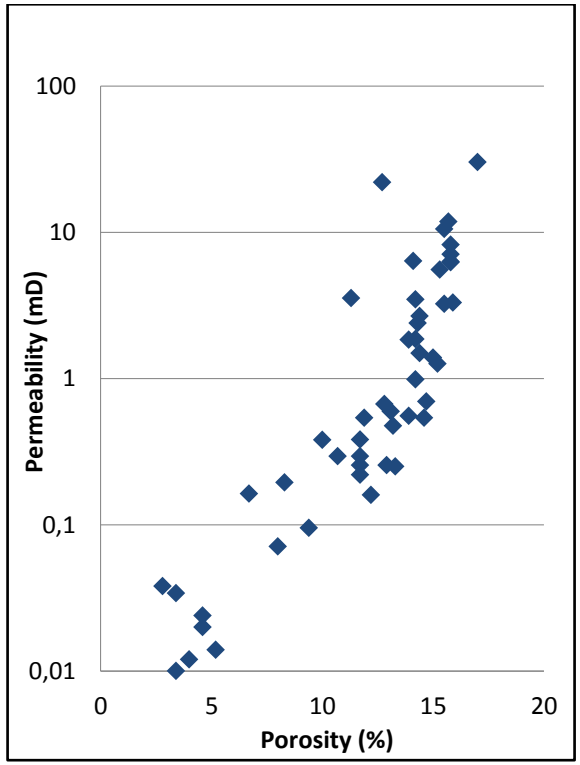

Figure 5.11: Illustrates three different plots for well 15/9-19 A. Porosity vs. vertical depth (mRSF), permeability vs. vertical depth (mRSF), and permeability vs. porosity. Refer to text for a more detailed description of the different plots. All plots are produced with data provided by Statoil ASA.

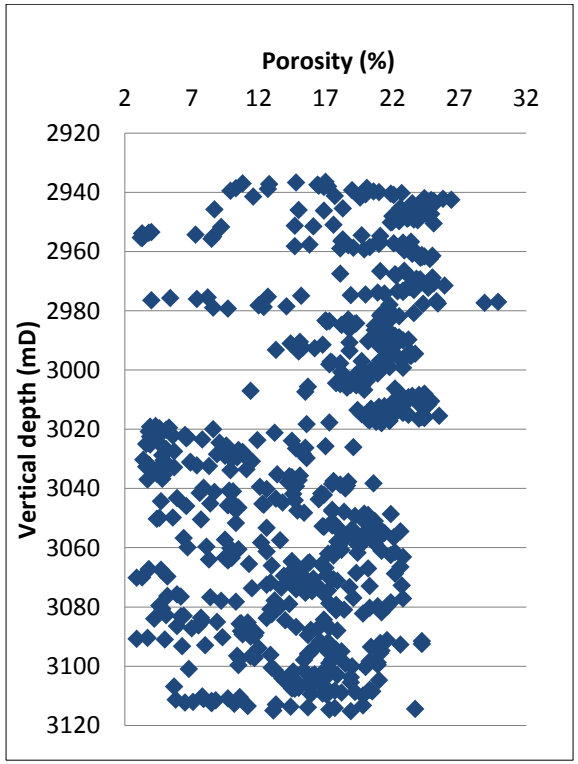

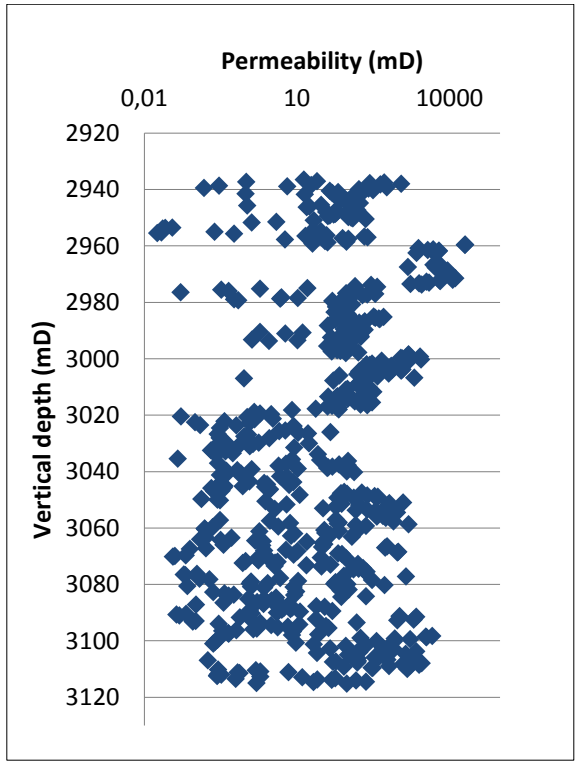

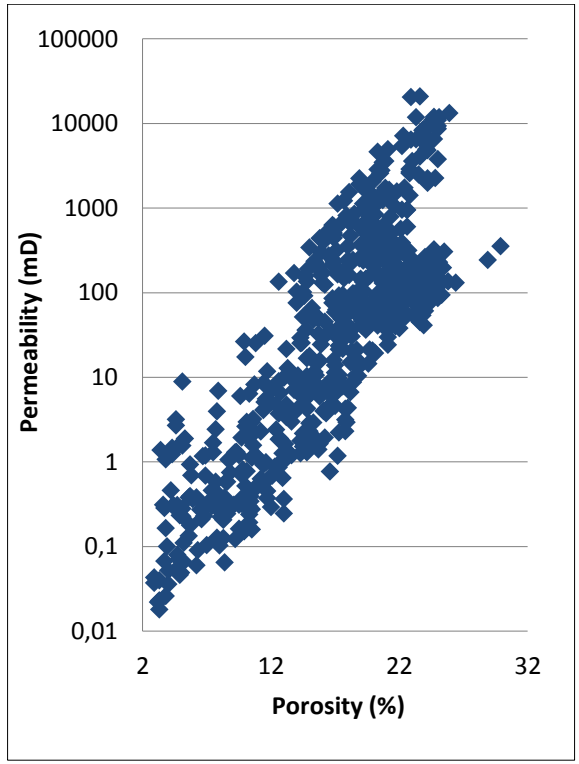

Figure 5.12: Illustrates three different plots for well 15/9-21 S. Porosity vs. vertical depth (mRSF), permeability vs. vertical depth (mRSF), and permeability vs. porosity. Refer to text for a more detailed description of the different plots. All plots are produced with data provided by Statoil ASA.

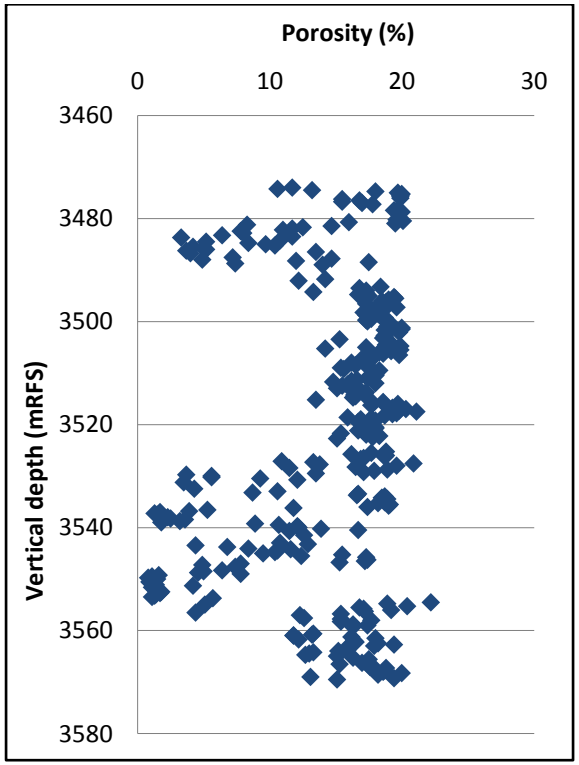

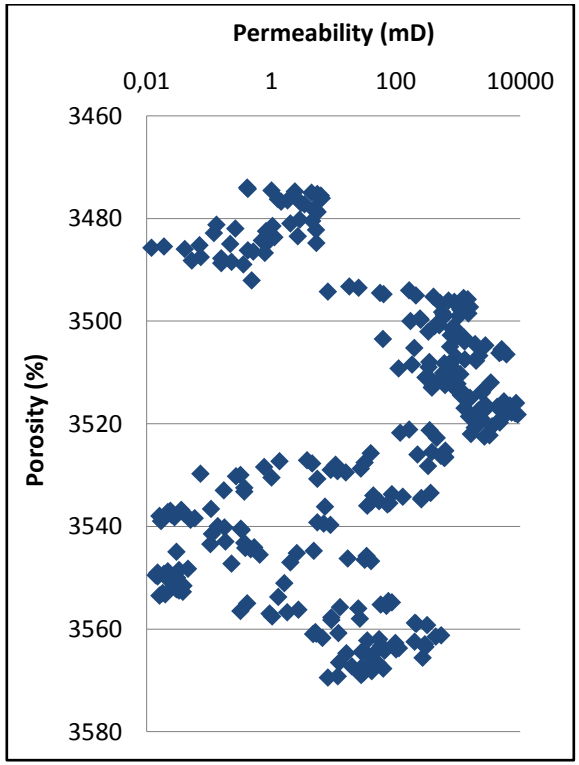

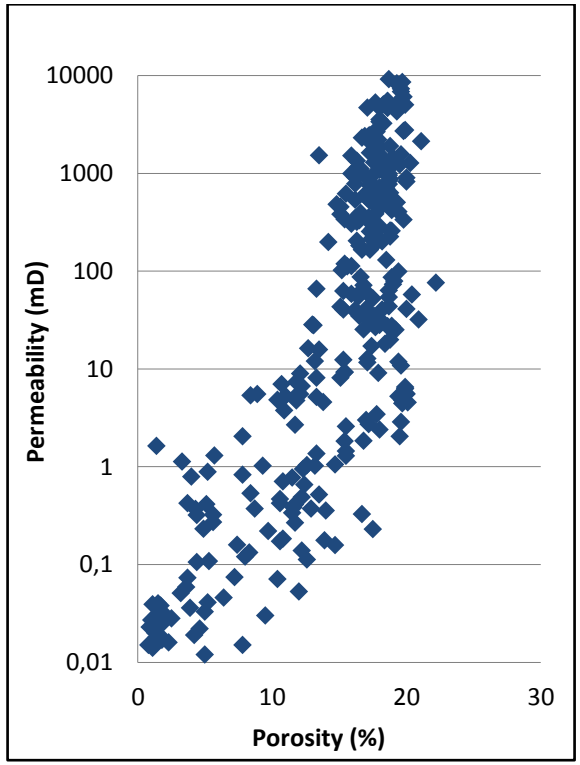

5.3.1 Well 15/3-7

Figure 5.8 illustrates both the permeability and the porosity related to depth, and it also contains a permeability-porosity plot. The gap seen between 4500.00 and 4520.00 mRSF is due to missing data for that specific interval.
To assist the analysis of the data based on core plugs, thin sections are available in the depth ranges of 4482.06 to 4495.00 mRSF, and 4523.00 to 4525.00 mRSF.
Between 4495.00 and 4505.00 mRSF, there is a cluster of points indicating a very low permeability. Based on thin sections and core photos, the anomaly is caused by pore-filling calcite cement in the sandstones. The same trend is seen around the depth of 4520.0 mRSF, but this cannot be verified by thin sections. However, core photos indicate calcite cementation for those points reaching a porosity value of less than approximately 4%. Some of the points plot far to the left, with a relatively high porosity compared to samples at minor depths, e.g. at the depth of 4522 mRSF. Any deviations from a linear trend which indicate excessive porosity values can be a result of over pressured zones or porosity enhancing processes (such as grain coatings). In this case, the gas water contact (GWC) was established at 4787.00 mRKB (Homepage NPD), and at the depth of 4610.00 mRKB (4485.00 mRSF) the formation was found to be water bearing. If the reservoir is filled with gas nearly up to the water-bearing zone at 4610.00 mRKB, it is possible that the high readings around 4525.00 mRSF are due to hydrocarbons present in the formation. Some workers (Marchand et al., 2002) believe that oil or gas emplacement in original water-filled sandstones inhibits quartz cementation and hence preserves the porosity. This could be the case for well 15/3-7.
When it comes to the permeability, the amount of available data is smaller but in general there is a decrease related to depth. Some of the points in Figure 5.8 with relatively low permeability values (for example, between 4490.00 and 4500.00 mRSF) are caused by some calcite cementation which affects the porosity as described above. However, the overall picture relating to permeability is that it is general higher than in wells 15/5-7 and 15/6-11 A - an interesting discovery, since this core is placed much deeper. Sandstones in well 15/3-7 possess a greater average grain size (Fig. 5.14) compared to the two other wells examined, and shows less authigenis clays filling the pore spaced. The low feldspar content would also

result in lower production of diagenetic clay minerals, hence a possible lower production of the fibrous illite crystals. This could be the reason for the higher permeability values seen in Figure 5.6 and 5.7.

Another reason for the lower porosity and permeability values seen in the cores at the depth range between approximately 4520.00 and 4540.00 mRSF (4647.00 – 4667.00 mRKB) could be a higher amount of clay laminaes in the sandstones. Referring to Figure B.2 (Appx.), this specific interval consists of argillaceous sandstones rather than the cleaner sandstones found at burial depths between 4480.00 and 4495.00 mRSF (4610.00 – 4622.00 mRKB), (Fig. B.1). The higher clay content could have resulted in greater mechanical compaction, causing a general reduction in reservoir quality. The finer material would also reduce the permeability, which is seen in these samples.

The permeability versus porosity plot also indicates the same trend already observed, namely a general deterioration of the reservoir properties in relation to depth.

5.3.2 Well 15/5-7

In well 15/5-7, some of the trends observed in well 15/3-7 are identified for both porosity and permeability measurements. Low permeability and porosity values in the interval studied (Fig. 5.9) is caused by calcite cementation, similar to well 15/3-7, and also reflects higher content of clay, which is observed in the core photos. Thin section microscopy shows that the interval at approximately 3700.00 mRSF is cemented by calcite. Further down there is a combination of calcite and clay responsible for the low permeability, while the higher permeability readings are due to cleaner sand. Also to be mentioned is the considerably higher porosity and permeability in this well compared to well 15/3-7. The shallower depth is one explanation, and it is probable that the entire interval of well 15/5-7 analyzed is within the oil zone. An early infill of oil to the reservoir may have resulted in better preservation, and hence higher values regarding the permeability and porosity (Marchand et al., 2002). Also observed in some of the samples possessing the highest porosity values, is a larger grain size compared to those with lower values.

To conclude, regarding the porosity and permeability plots related to depth, calcite and clay are responsible for the low readings.

Regarding the plot of permeability versus porosity, an interesting trend is observed, or more accurately, two interesting trends are observed. Figure 1.7 shows different porosity-permeability trends for different lithologies. The two linear trends seen in well 15/5-7 can be explained using Glover's plot (Fig. 1.7). The uppermost trend line corresponds to the cleaner sandstone while the lower line corresponds to a sandstone containing more clay. This is verified in the core photos. Clay-cemented sandstones possess a high porosity which is mainly due to microporosity. The permeability is lower than expected because of the increased tortuosity, compared to a cleaner sandstone.

5.3.3 Well 15/6-11 A

The data points in the porosity are widely spread out (Fig. 5.10), with no distinct trend as a function of depth. The points showing less than 10% porosity reflect presence of calcite and quartz cement, in combination with stylolites. This is confirmed by the thin sections and core photos. Due to the wide diversity of the points, any distinct trendlines related to lithologies are hard to predict.
In the permeability plot, the points between 3590.00 and 3595.00 mRSF and 3605.00 and 3610.00 mRSF have very low values, between 0.01 and 0.2mD. As previously explained, the reason is an increase of calcite cement and quartz cement seen in those intervals compared to the rest of the plot with less such diagenetic infill. Some of the points stand out, with high permeability values between 3615.00 and 3620.00 mRSF. Studying the data obtained from the thin sections reveals that the explanation is larger grain sizes for those samples.
When it comes to the porosity-permeability plot, the trend is clear - a linear trend of decreasing reservoir properties related to greater depth.

5.3.4 Well 15/9-19 A

Well 15/9-19 A possesses excellent reservoir properties, with respect to both porosity and permeability (Fig. 5.11). Low readings in the porosity plot are caused by variations in calcite cement and exceptionally high readings reflect a combination of clean sand, large grain sizes and well sorted sandstone. Since the points are widely scattered, a trend line is difficult to identify. The same dispersion is seen in the permeability plot. The thin section data is

limited, ending at the depth of 3019.00 mRSF. Using core photos below that depth shows that the low readings are related to calcite cementation, together with an increase of quartz cement. Regarding the porosity-permeability plot, the trend is linear with a decrease of the reservoir properties at greater depths.

5.3.5 Well 15/9-21 S

No thin sections or core photos are provided above 3494.00 mRSF, making the reliability of any predictions uncertain. Lithology descriptions are available for the missing section, provided by Statoil ASA. This data, together with data from thin sections and core photos, provide enough data to interpret the entire interval illustrated in Figure 5.12. Low readings for both porosity and permeability are caused by calcite cementation and sections of finer material (mostly clay laminaes) infiltrating the formation. The excellent reservoir property is depreciated because of this, and the distinguishing pattern of low values for both porosity and permeability is seen between 3475.00 and 3495.00 mRSF, and 3530.00 and 3560.00 mRSF. An almost linear trend is seen for the porosity-permeability plot. In general, the reservoir properties deteriorate with increasing depths.

5.3.6 Comparison core plugs and modal analyzes

The difference in porosity for various depths, between core plugs and modal analyzes, has been evaluated, and the results are presented in Figure 5.12. The wells examined are 15/3-7, 15/9-19 A, and 15/6-11 A, and in addition to porosity, the grain sizes are also included in the examination. In order to describe or explain the differences observed between core plug measurements and modal analyzes, the grain size is a parameter which can used for this purpose. Regarding the permeability, no such comparison between core plugs and modal analyzes was possible, since permeability measurements from modal analyzes have not been produced.

The porosity values from the modal analyzes is generally lower than the core plug measurements. This trend may be caused by the microporosity, which is not measured sufficiently in the modal analyzes. When the grain size decreases, finer material is present in

the sediments and the proportion of microporosity increases relative to the total porosity. By point counting of thin sections, the porosity detected is more likely to be the effective porosity, rather than the total porosity which also includes microporosity. This trend is seen in well 15/3-7 where the grain size is significantly larger then in 15/9-19 A and 15/6-11 A. The degree of microporosity will be lower due to grain size, and the difference between point counted porosity and porosity from core plugs will not vary significantly. The values do actually coincide at several depths, particularly where the average grain size is largest (Fig. 5.13). Also seen in the figure are the higher core plug measurements, compared to modal analyzes, at lower grain sizes - a trend similar to the other wells studied.

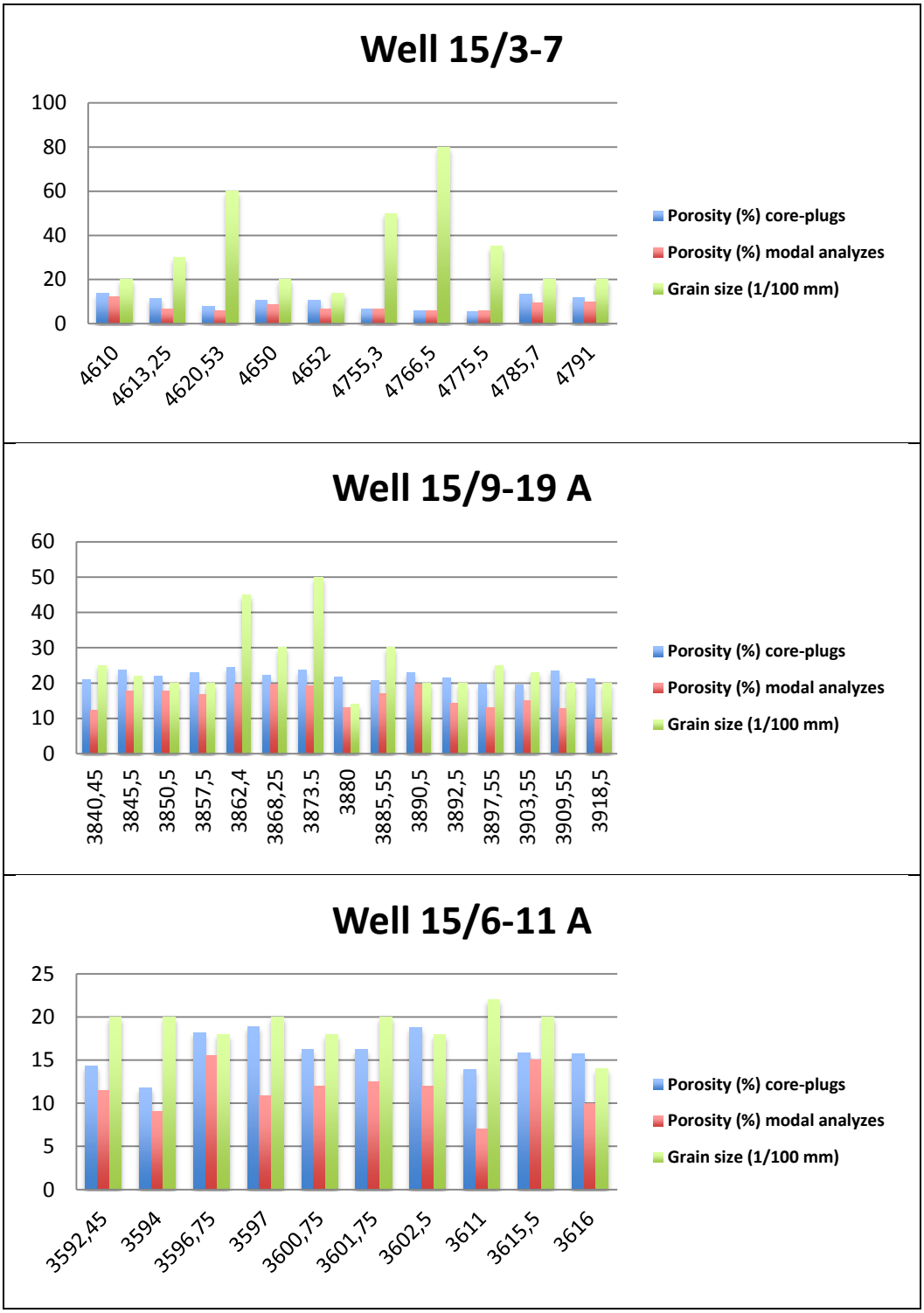

Figure 5.13: Histogram presentation of the porosity (%) from core plugs and modal analyzes, together with grain sizes for well 15/3-7, 15/9-19A, and 15/6-11 A. The depth is given in mRSF. For well 15/3-7, the porosity between core plugs and modal analyzes correspond when the grain sizes are relatively large, while with decreasing grain size the difference increases. The same trend is not as apparent for the other wells

5.4 Development of quartz cement

In the following sections the development of the quartz cement will be discussed. Only those processes relevant for the Hugin Formation will be focused on, namely the mineralogy and grain size, alkali feldspar and kaolinite reactions, and stylolitization.

Quartz is a commonly occurring cement in the Hugin Formation (Tab. A.1, A.2, A.3, A.4 , A.5), where it grows as optically continuous overgrowths on detrital quartz grains (Fig. 3.16). Quartz arenites, and quartzose sandstones belonging to passive-margin basins, such as the sandstones of the Hugin Formation, contain significant amounts of quartz cement compared to other basins (McBride, 1989), for example. rift basins. Sandstones of rift basins (arkoses) and collision-margins (lithic arenites) only contain a small percentage of quartz cement, while passive–margin basins possess higher percentages such as the basin studied. The solubility of silica increases with pH, so silica cement occurs where alkaline fluids have migrated through the sediments and precipitated in the pores in between the framework grains. Quartz cement may originate from several sources, but is restricted to temperatures greater than approximately 90˚C (Bjørkum et al., 1998). Walderhaug (1994) ascertains that quartz cementation in Jurassic sandstones from the Norwegian continental shelf has taken place at temperatures between 75˚C and 165˚C. By studying fluid inclusions, Walderhaug (1994) found that inclusions trapped at temperatures below 100˚C belonged to sandstones placed in the temperature window of 75-100˚C for tens of millions of years. At more rapid burials, quartz cement was seldom found at temperatures less than 100˚C.
There are multiple sources for the silica to originate from, such as pressure solution, conversion of clay minerals during burial, mainly smectite to illite, decomposition/kaolinization of feldspar, dissolution of volcanic glass (McBride, 1989), kaolinite and alkali feldspar reactions (Bjørlykke, 2001), and dissolution of detrital quartz grains at stylolites (Oelkers et al., 1996). The different sources of silica, and models for the development of quartz cement that are relevant to the studied wells from the Hugin Formation, are discussed below.

5.4.1 Mineralogy/ grain size

The grain size in the Hugin Formation from wells 15/3-7, 15/5-7, 15/6-11 A, 15/9-19 A and 15/9-21 S varies from coarse to very fine (Tab. A.1, A.2, A.3, A.4, A.5), but grains are mainly fine to medium. The grains are subangular to subrounded, locally rounded and mostly well sorted. The sandstones from well 15/3-7, 15/9-19 A, and 15/6-11 A are classified as quartz arenites, subarkoses/sublitharenite and subarkoses respectively. They are all both texturally and mineralogically mature, though two of the wells contains smaller amounts of feldspar and lithic fragments.

The grain size may influence the amount of quartz cement precipitated in the formation. Quartz overgrowths can be more common for beds or laminae that hold a particular grain size. Generally, workers have found that finer–grained sandstones often possess more quartz overgrowths than coarser-grained beds (McBride, 1989), and observations by Walderhaug (1996) supports this. Small grain size gives a larger surface area for nucleation, so when the surface area increases, the amount of quartz cement will also increase, because a larger area is available for precipitation (Walderhaug, 1996). Simulations done by Walderhaug also showed that finer-grained sandstones became cemented faster than coarser-grained sandstones. This fact is supported by other workers, e.g. Heald and Renton (1966). McBride (1989) specifies that this trend does not necessarily apply to all formations. It is important to be aware of several other factors, such as degree of fluid flux and the permeability of the formation, when trying to establish a rule of thumb regarding quartz cement related to grain size. A more permeable formation will have the potential to provide a higher fluid flux of oversaturated pore waters in respect to silica, which may lead to greater quartz cementation. The general understanding though is still that quartz cementation increases with decreasing grain size. Another interesting observation, by James et al. (1986) and Anderson and Pichard (1971), is related not only to grain size but also to the grain structure, e.g. undulosity and polycrystallinity. The quartz grain structure can influence the precipitation of greater amounts of quartz cement in finer-grained formations, since they possess fewer polycrystalline and undulose quartz grains. It has been discovered that polycrystalline quartz grains contain thinner quartz overgrowths than monocrystalline quartz grains (Worden and Morad, 2000). The reason for this is probably the competitive

growth between separate and differently orientated quartz nuclei on the surface of the polycrystalline quartz grain.

The grain size alone does not necessarily explain the differential content of quartz cement in the Hugin Formation, since the amount of quartz cement does not correlate with the grain size in all the wells. Figure 5.14 shows that the hypothesis holds for two of the wells, 15/9-19 A, and 15/6-11 A, but for well 15/3-7 the opposite is true. Trend lines applied to the plots indicate that with a decrease in grain size, the amount of quartz cement increases for well 15/9-19 A and 15/6-11 A, but in well 15/3-7 there is an increase of quartz cement with an increase of grain size. The plot is based on the results from the modal analyzes (Tab. 4.1, 4.2 and 4.3).

Since this is contradictory to the earlier work of e.g. Walderhaug (1996), Heald and Renton (1966), several other possibilities have been explored in order to find an explanation. Average porosities and permeability values for the same depths of the modal analyzes (Tab. 4.1, 4.2 and 4.3) have been produced to examine any differences which can explain the anomaly seen in well 15/3-7 (Fig. 5.15). The permeability and porosity values used in Figure 5.14 are based on core plug measurements, while the average grain size is based on the petrographical work.

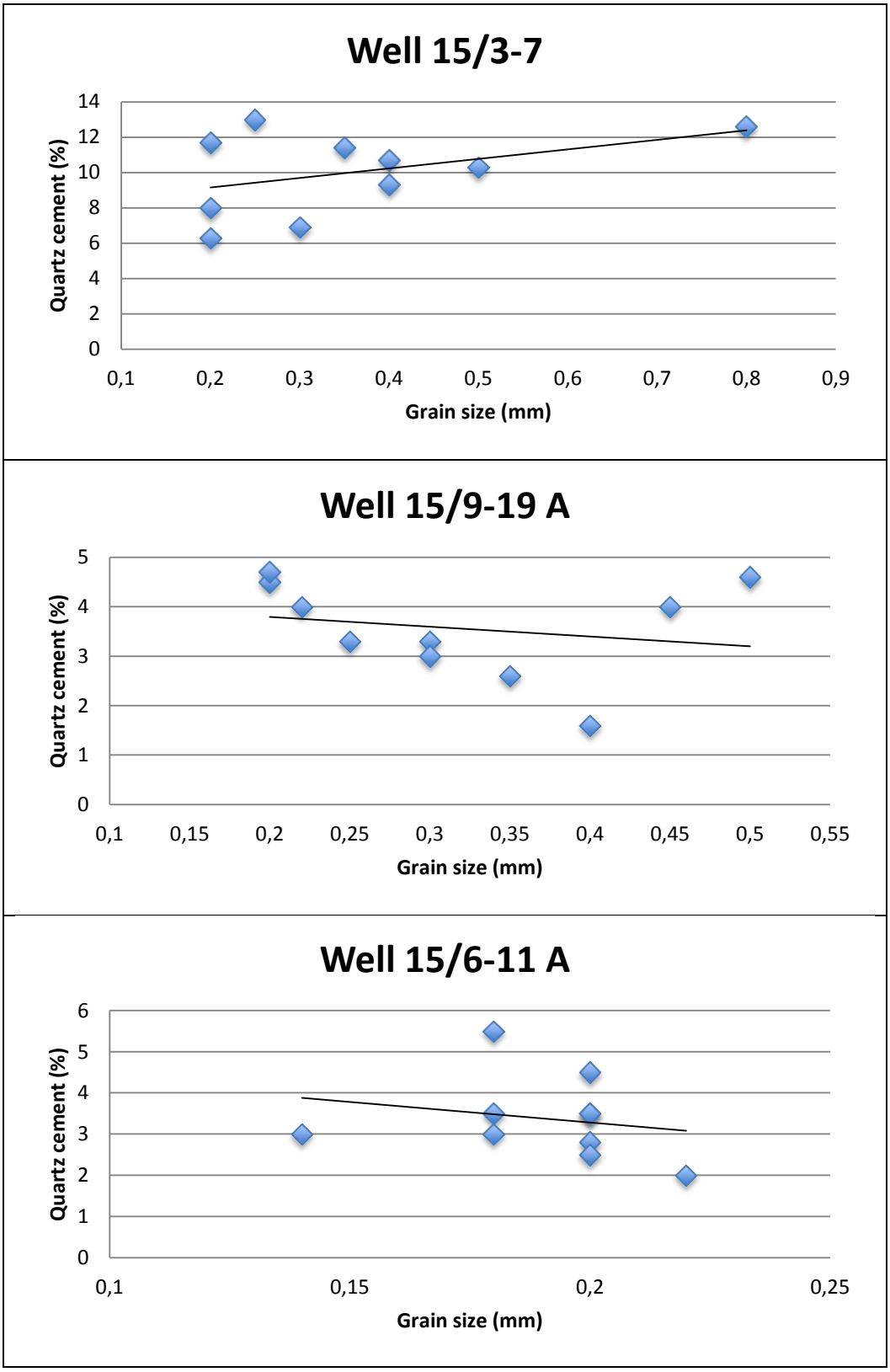

Fig 5.14: Quartz cement vs. grain size plots for well 15/3-7, 15/919 A, and 15/6-11 A. For well 15/9-19 A and 15/6-11 A there is an increase of quartz cement with decreasing grain size, but for well 15/3-7 there is an opposite trend, a decrease of quartz cement with a decreasing grain size.

Figure 5.15 reveals that the difference in the porosity is not significant enough to explain the anomaly seen related to the amount of quartz cement and grain size for well 15/3-7. On the other hand, the difference in permeability is quite significant and could be one of the reasons for the observed trend. Referring to McBride (1989), such an event could be the case. A higher fluid flux, due to larger grain sizes, will allow more water to circulate through the formation, which could be the reason for the greater amount of quartz cement seen in well 15/3-7.

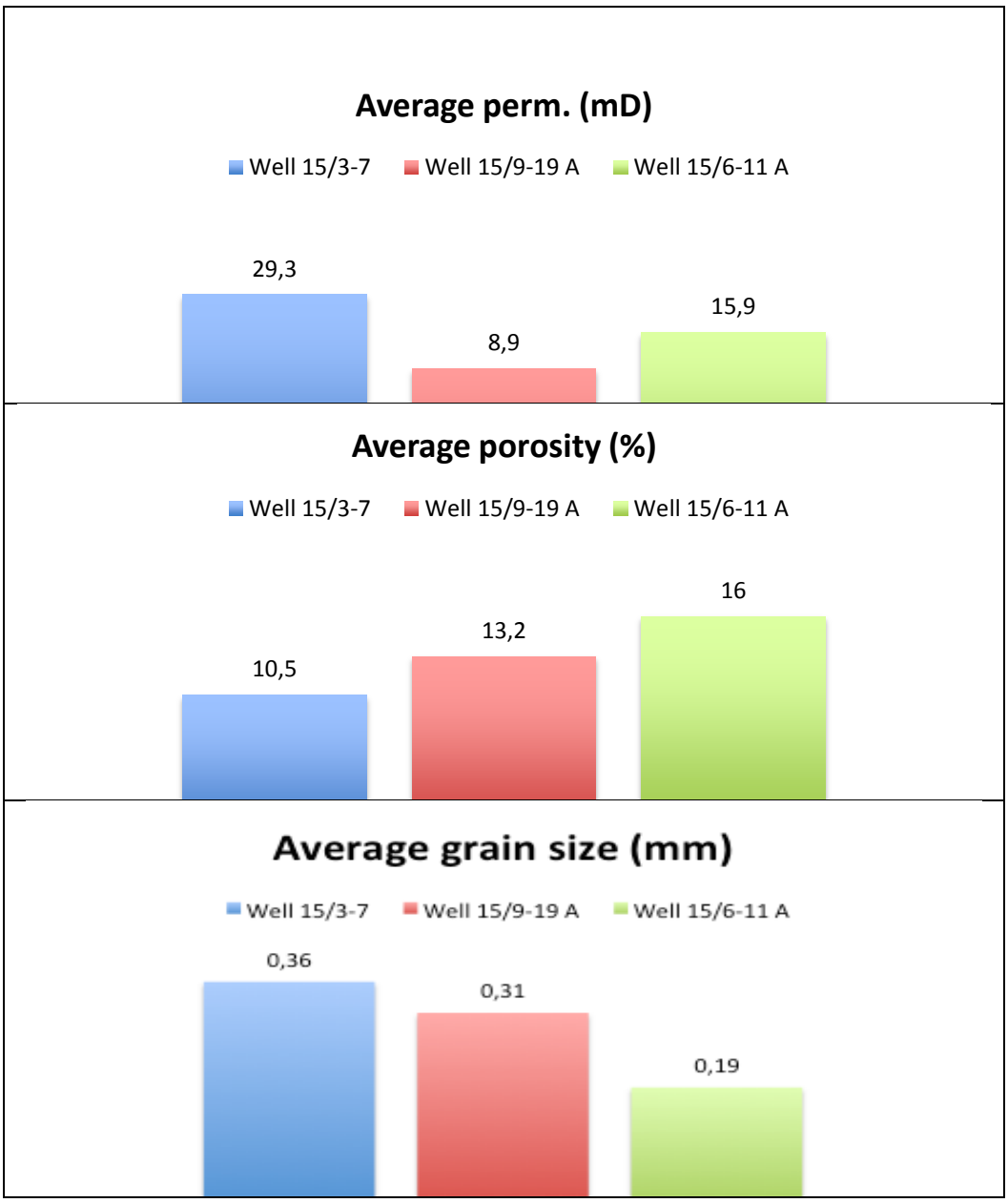

Figure 5.15: Illustrates the average permeability values, porosities and average grain size for well 15/3-7, 15/9-19 A, and 15/6-11 A.

Another aspect to be considered, related to the higher amount of quartz cement in well 15/3-7, is the mineralogy. As determined by the modal analyzes, the lithology was different for well 15/3-7 then for well 15/9-19 A and 15/6-11 A (Fig. 4.6). Well 15/3-7 is more mature than the two other wells examined, and falls in the category of a quartz arenite. It is common to find more quartz cement in clean sandstones, such as arenites, compared to other lithologies, for example, arkoses (Boggs, 1992). This supports the discovery, made by Dutton and Diggs (1990), that the amount of quartz cement decreased exponentially with increased matrix content in the sandstones of Travis Peak, East Texas. Walderhaug (1996) made a kinetic model for the effect of the framework grain composition, to compare the differences in porosity and degree of quartz cementation as a function of time for quartz arenites and arkoses of similar initial porosity. The final result was that the quartz arenite had a higher rate of quartz cementation and a higher loss of porosity than the arkose. This could also be the reality for the Hugin Formation based on the same model (Walderhaug, 1996). This would explain the higher amount of quartz cement seen in well 15/3-7 based on lithology, independent of the grain size.

5.4.2 Alkali feldspar/ kaolinite reactions

Quartz cement appears in all samples from the Hugin Formation, together with kaolinite, illite and partly-dissolved alkali feldspar. There are several possibilities in which the alkali feldspar and kaolinite reactions can contribute to the development of quartz overgrowth on quartz grains. This work focused on two reactions, since they were most relevant for the source of the quartz cement regarding the Hugin Formation. Previously mentioned in Section 5.3.2, the decomposition or kaolinitization of feldspar (Eq. 3) is one source, and the other source is the reaction between alkali feldspar and kaolinite (Eq. 4) forming illite. Equation 3 implies that for each mole of feldspar altered to kaolinite, two moles of silica are released, which may be a source of quartz overgrowths (Siever, 1957). However, some of this silica will be used in the development of authigenic clay minerals, so the source of quartz to precipitate from this reaction will be limited. Another possibility is related to the illitization of kaolinite (Eq. 4).

For well 15/3-7, the content of feldspar is lower compared to wells 15/9-19 A and 15/6-11 A. Nevertheless, well 15/3-7 contains a significant amount of dissolved feldspar, so the initial amount of feldspar may have been larger. It is worth noting that well 15/3-7 is the most deeply buried, which could explain the lower feldspar content due to alteration. Some intervals in well 15/3-7 contain higher amounts of clay laminaes, described as argilleous sand in Figure A.1, presented in the Appendix. Such laminaes could contribute to the increased amounts of quartz cement seen in the sandstones of well 15/3-7, due to quartz dissolution on grain contacts between quartz and clay.

5.4.3 Stylolites and quartz cementation

The content of quartz cement in the samples from the Hugin Formation varies in abundance, but all samples contain euhedral quartz overgrowths, except the fully calcite cemented samples. Since no macroscopic analyzes were done, the abundance of stylolites was discovered by microscopic methods. However, some core photos of good quality showed some stylolites, and in such cases the observations could be used to confirm the result seen in the thin sections.

There is a clear trend seen in abundance of stylolites and amount of quartz cement in well 15/3-7. Where the density of the stylolites is highest, the highest amount of quartz cement is seen (Tab. A.1). This relationship is optically observed at several places in the formation, and confirms that the stylolites could be the major source for quartz cement in the Hugin Formation. Other workers (Baron and Parnell, 2005) have also discovered that sandstones from the North Sea containing abundant stylolites are characterized by their highly quartz cemented nature.

The formation of stylolites are coupled to pressure solution, and the pressure solution is commonly divided into two types, hence the intergranular pressure solution and stylolitization (Baron and Parnell, 2005). The pressure solution seen in the Hugin Formation is mainly associated with stylolitization since only a few cases of intergranular pressure solution are observed. The IGV results from Chapter 4 also confirm this. The silica cement seen in the samples could also result from local quartz dissolution at mica or clay/quartz interfaces, where the silica is transported by diffusion into the interstylolite regions and

precipitated as quartz cement (Oelkers et al., 1996; Bjørkum et al., 1998). The precipitation is controlled by kinetically crystallization reactions. Also discovered in well 15/3-7 is that the amount of quartz cement in the interstylolite regions decreases together with an increase of the porosity for the same interval. Referring to Table A.1, the abundance of stylolites is great at 4776.40 and 4786.20 mRKB, and in between there are no stylolites present. The data from the core plugs show that at the stylolites the porosity is 5.3 and 6.4% respectively, while in the interstylolite region the porosity values increase up to 13.5%. This result is synonymous with the work done by Oelkers et al. (1996), where they found the same trend. Bjørkum et al. (1998) also did a research on Jurassic sandstones and discovered that computed porosities increased with decreasing stylolite densities, the same trend seen in this work. The results from the work done by Oelkers (1996) is relevant for the results seen in this thesis, since some of the sandstones investigated belong to the Hugin Formation. Oelkers et al. (1996) discovered, from the same investigation, that a more even distribution of stylolites throughout the formation corresponds to a steadier amount of quartz cement. No major differences regarding the porosity were seen with that kind of distribution, which is similar to the observations in this thesis.

5.5 Quartz cement inhibitors

The general opinion amongst workers is that quartz cementation can be inhibited by several processes (e.g. grain coatings) and contribute to improvement of the reservoir quality (French et al., 2012; Storvoll et al., 2002). In order to develop quartz cement, the quartz grains need to develop nucleation sites for quartz cement. Monocrystalline quartz grains provide a preferable site for nucleation, rather than polycrystalline quartz grains, and previous work done on Jurassic formations shows that monocrystalline quartz grains are three times more likely to develop quartz overgrowths than polycrystalline grains (James et al., 1986; Lander et al., 2008). The different mineral grain coatings on detrital quartz grains will be discussed in Section 5.5.1, and also the effect of oil emplacement, which can retard the rate of quartz cementation, will be discussed below.

5.5.1 Grain coats

Mineral coatings on detrital quartz grains can inhibit quartz overgrowths by isolating the quartz grain surface for nucleation and precipitation of quartz cement. Circulating waters, oversaturated with quartz, will not be able to precipitate and the result will be less quartz cement in such cases. The thickness and continuity of coats are important, since these factors influence the effectiveness of the coats to inhibit quartz overgrowths. In the presence of discontinuously grain coatings, the quartz cement can form prismatic attachments, also called outgrowths (Lowry, 1956).

Several types of coatings can develop on the detrital quartz grains, e.g. different clay minerals. These clay minerals include chlorite and illite, and both contribute to preservation of the reservoir quality by inhibiting quartz overgrowths. Ehrenberg (1993) found that five Jurassic sandstone reservoirs in the Norwegian sector contain more than 10 to 15% higher porosities compared to regional trends of mean porosity vs. depth. Authigenic chlorite coatings were responsible for the preserved porosity in these reservoirs, and it is likely to be found in similar reservoirs on the Norwegian sector.
Illite coatings are also important in a reservoir quality perspective, since the coatings inhibit quartz cementation. Storvoll et al. (2002) examined the Middle Jurassic Garn Formation offshore Mid-Norway, and found that the porosities were anomalously high compared to porosity-depth trends from the same area. The porosity was preserved due to illite coatings. No illite coatings were to be found in the Hugin Formation during this work.

Microcrystalline quartz can be a source for inhibiting quartz cementation. In previous work, done by Maast et al. (2011), only trace amounts of grain-coating microquartz was found in samples from the Hugin Formation. No such crystals were observed in the Hugin Formation during this work. For more detailed information on the topic, the article by French et al. (2012) is highly recommended.
No specific coatings of clay minerals are observed on quartz grains in the studied samples, which correlates to the work done on the Hugin Formation by Maast et al. (2011). Maast et al. (2011) did find some microquartz on some samples, but in this work no such coatings are recognized. Regarding the development of the quartz cement, such coatings would inhibit

the growth, but in this case the amount of quartz overgrowth is substantial in all the wells. The quartz cement is covered in the next section.

5.5.2 Oil emplacement

It has long been the consensus that entrapment of hydrocarbons in sandstones can inhibit quartz cementation, but the topic is still debated amongst scientists. Some workers claim that quartz cementation continues after oil entrapment, by diffusion along the water film on the detrital quartz grains (Maast et al., 2011), but others claim that oil emplacement retards the quartz cementation (Marchand et al., 2002). The most recent work on the topic (Maast et al., 2012), have discovered that the work done on e.g. the Miller Field by Marchand et al. (2002) which concluded that most quartz cement was seen in the water-leg in the reservoir compared to the oil-leg, was incorrect. Aase and Walderhaug (2005) discovered that this was a misinterpretation, since the difference of quartz cement seen in the Miller Field reservoir was caused by microquartz and not by oil inhibition. Other petrographic data supported this interpretation (Bonell et al., 2006). No abnormalites regarding the porosity or permeability values were seen in general for this work, concerning the hydrocarbon filled parts of the Hugin Formation. The only place in the Hugin Formation seen with some abnormalities, earlier described in Section 5.2.1, is in the oil-leg (gas) for well 15/3-7. Since no microquartz was found in this interval, and work done by Maast et al. (2011) disproving the hydrocarbon inhibition hypothesis of quartz cement, a possible explanation for the higher porosity readings could be a different mineralogical composition. No data from the modal analyzes is available for the specific interval, so definite conclusions cannot be made, except that neither microquartz nor oil entrapment is responsible for the higher porosity seen in the specific interval of well 15/3-7.

5.6 Reservoir quality of the Hugin Formation

The reservoir quality in the Hugin Formation varies between the wells studied, but porosities and permeability values do coincide with previous work done on the topic (Ehrenberg, 1993; Bloch et al., 2001). The Hugin Formation follows the average regional

trend of the North Sea area regarding the porosity, which also is confirmed by Maast et al. (2011). The Hugin Formation data plots some points below the average line for porosities (Fig. 5.16). Average porosities and permeability values (Fig. 5.3, 5.6) form trends related to depth. The porosities from the core plugs vary from 6% in the deepest well at 4675 mRSF to 16% in the shallowest well at 3000m RSF, while the permeability values vary between 10 and 800mD at the same depths. Porosities from this study are compared with the plot done by Maast et al. (2011) illustrated in Figure 5.16, which shows that the Hugin Formation data plots beneath the line of average porosity for the south Viking Graben area. However, the Gudrun Field, represented in well 15/3-7, is already a promising field, estimated to hold around 18 Sm^3 oil equivalents (NPD). The license plan is to develop the field with a stand-alone platform, and export oil and gas via Sleipner and on to Kårstø in northern Rogaland county.

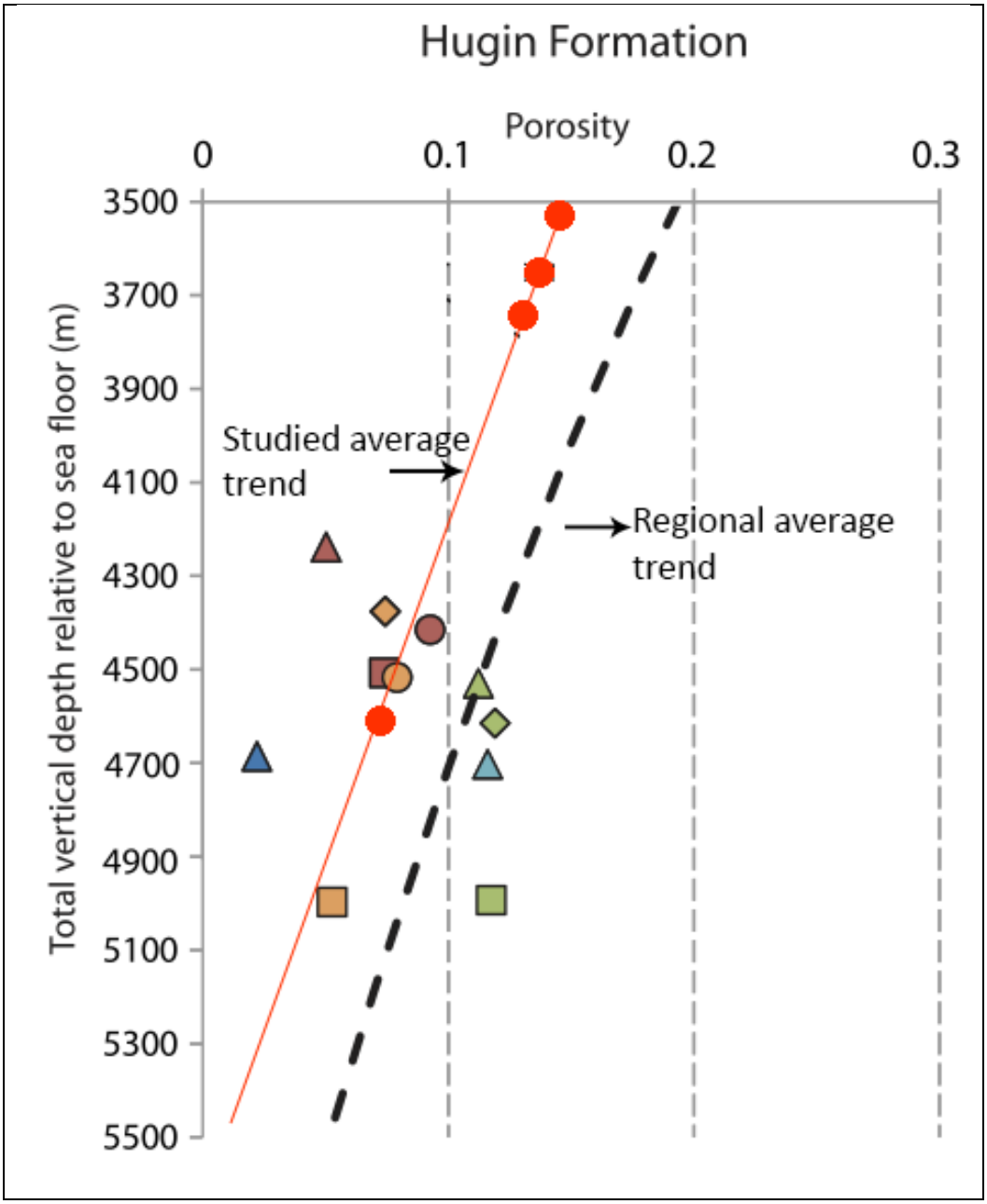

Figure 5.16: Average porosities for wells from the Hugin Formation following the trend of porosities related to depth for the studied area, hence the South Viking Graben. The colored symbols represent average values of porosity for different wells from the study of Maast et al. (2011), all representing the Hugin Formation, and most of the wells fall beneath the line of average porosity. The black line represents the trend line for the wells studied in this thesis representing the Hugin Formation. This work also shows that the average porosity falls beneath the regional average line for porosity.

The deterioration of the reservoir quality is a result of both mechanical and chemical compaction. Diagenesis, such as quartz cementation and calcite cement, is strongly represented in all the wells of the Hugin Formation. Calcite cement can occur, either

dispersed randomly or totally filling the pores in the samples. The petrography discovered both an early infill, resulting in a high IGV, and also a later infill which post-dated some of the quartz cement. In the samples containing calcite, both the porosity and the permeability is low, causing a reduction in reservoir quality.
The quartz cement follows a more specific trend, related to depth. The quartz cement increases with depth due to higher temperatures, and in many of the samples studied the quartz overgrowths totally fills up the pore spaces in between framework grains. In such cases, the porosity and permeability is worsened leaving the sandstones with poor reservoir properties. In the worst cases, the porosity and the permeability hold values at 2-3% and 0.01mD respectively, and in best cases 25 to 27% and 10000mD. Also seen in the Hugin Formation is an abundance of stylolites, which in this case provide the major source of silica for the quartz cementation. Close to the stylolites, the values of both porosity and permeability are close to zero, but in the interstylolite region the values are higher.

Clay coatings, or coatings in general, have not been seen in the Hugin Formation. Any such coatings would have contributed to enhance the reservoir quality. Work done by Maast et al. (2011) reveals that almost none of the studied samples from the Hugin Formation contained coatings, so the results coincided with this work from the same formation.
There is one process which enhances the reservoir properties of the Hugin Formation, which is the secondary dissolution of alkali feldspar. The dissoluted grains are seen in all the wells studied and the the dissolution most probably took place in the eogenetic regime, and the system most likely was open. Also typical for the Hugin Formation is that the area has not been exposed to any uplift or meteoric waters where unstable minerals could have been dissolved (Maast et al., 2011). This indicates that the event took place at an early phase in the eogenetic regime.

Kaolinite can cause production problems for reservoirs because the loosely attached crystals can clog the pore throats. Since the kaolinite crystals are relatively large they will easily assist to the clogging and limit the production rate (Almon and Davies, 1981).
The clay mineral illite also fills the pores in the Hugin Formation sandstones, as the kaolinite does. As opposed to kaolinite, illite has a tendency to strongly reduce the permeability and thus deteriorate the reservoir properties. Illite sometimes grows in the pores as long “hairy”

crystals, which drastically reduces the permeability in the sediments (Almon and Davies, 1981). The crystals are not always easily detected, even by SEM images, but in Figure 3.22b, the fibrous or “hairy” crystals could be recognized. If the crystals develop as described, they grow and reduce the permeability.

The development of illite may also cause production problems. The main problem is that illite bind water to the grains, which can cause high irreducible water saturations. In such cases, reservoirs can be overlooked by the use of petrophysical methods since the high water saturation “hides” hydrocarbon filled reservoirs (Almon and Davies, 1981). When fresh water is present, illite crystals accumulates to further reducing the permeability. If any smectite is present in the formation drilled, oil based mud (OBM) will be preferred, since smectite swells in contact with fresh water (Almon and Davies, 1981).

A general comparison between wells 15/3-7, 15/9-19 A and 15/6-11 A is done below regarding the differences seen in the reservoir properties. Since these wells have been optically examined by modal analyzes, a more detailed description can be done.

The deepest well, 15/3-7, holds the average highest permeability and grain size measurements, but the lowest average porosity of the three wells examined (Fig. 5.14). Already described in previously sections, these results are based on the formations maturity and physical properties, such as grain size. A quartz arenite will have less opportunity to develop authigenic clay (e.g. illite) in order to reduce the average permeability in the rock, since the feldspar content is low. But the porosity will be substantially reduced since the development of quartz cement is more prevalent in such lithologies, compared to the less mature rocks seen in well 15/9-19 A and 15/6-11 A (Fig. 5.13).

Well 15/9-19 A and 15/6-11 A are less mature than well 15/3-7, and are classified as sublitharenite and subarkose respectively. The IGV results revealed that well 15/9-19 A was more texturally immature than 15/6-11 A, but more compositionally mature (Tab. 4.5 to 4.7). This could explain the lower permeability values seen in well 15/9-19 A since the amount of matrix is higher compared to well 15/6-11 A. Well 15/6-11 A, which is more compositionally immature, holds the highest porosity of the two. An explanation could be more developed secondary porosity due to higher degree of dissolved feldspar grains. The increased amount of kaolinite may have resulted in more illitization, but the permeability values observed are higher than in well 15/9-19 A (Fig. 5.14). Most probably, the burial depth of 3600 mRFS is not sufficient to complete the illitization. In summary, it appears as

though the less texturally mature sandstones contribute the most with respect to the lower permeability values seen in the Hugin Formation, because of the matrix, while the less compositionally mature sandstones could preserve the reservoir properties better, even though there is a greater amount of illitization.

To summarize, the authigenic clay minerals do reduce the reservoir properties mainly because of the generally increased tortuosity.

6 Conclusion

The deeply-buried Hugin Formation sandstones are texturally and compositionally mature, and classify as quartz arenites, subarkoses, and sublitharenites. Calcite cement and quartz overgrowths are the main components which reduce the reservoir quality of the formation. A distinct correlation is observed between porosity and abundance of quartz cement versus depth. With increasing depth, the porosity decreases due to larger amounts of precipitated quartz cement. The increase in quartz cement reflects the higher temperatures experienced during burial.

Calcite cementation does not follow any specific trend, but contributes to the reduction of reservoir quality. The porosity values are lower compared to average porosity-depth trends of adjacent areas, and vary between 6 and 16%.

IGV results confirm that the main source of quartz cement is dissolution of detrital quartz grains at stylolites. In contrast, any quartz cement derived from pressure solution at grain contacts would have given lower IGV results, combined with an increase of quartz overgrowths.

Clay mineral reactions could also be a source for the quartz cement, primarily by the illitization of kaolinite. Kaolinite and illite are associated with alkali feldspar in variable amounts throughout the wells, and might be responsible for the illitization. In intervals with low feldspar content, e.g. in well 15/3-7, the reservoir properties are better preserved due to reduced formation of illite. Illite has a negative impact on reservoir quality.

Clay laminaes are responsible for the reduced permeability in some parts of the cores. This results from a higher degree of mechanical compaction, and a larger amount of finer material present in the formation.

Secondary dissolution of alkali feldspar occasionally contributes towards preserving reservoir quality, and thus dissolution is most commonly seen in the subarkoses.

7 References

Adams, A.E., MacKenzie, W.S., 2001: A colour atlas of carbonate cements and rocks under the microscope, pp. 180.

Adams, A.E., MacKenzie, W.S., Guilford, C., 1984: Atlas of sedimentary rocks under the microscope, pp. 104.

Almon, W.R., Davies, D.K., 1981: Formation damage and the crystal chemistry of clays, ch.5, In: Longstaffe, F.J. (eds.), Clays and Resource geologists. Mineralogical Society of Canada, Short Course Handbook 7, p. 81-103.

Amorosi, A., 1995: Glaucony and sequence stratigraphy: A conceptual framework of distribution in siliciclastic sequences. Journal of Sedimentary Research, Vol. B65, No. 4, p. 419-425.

Amyx, J.W., Bass, D.M., Whiting, R.L., 1960: Petroleum Reservoir Engineering. McGraw-Hill Book Company.

Aase, N.E., Walderhaug, O., 2005: The effects of hydrocarbons on quartz cementation: Diagenesis in the Upper Jurassic sandstones of the Miller Field, North Sea, revisited. Petroleum Geoscience, Vol. 11, p. 215-223.

Baron, M., Parnell, J., 2005: Relationships between stylolites and cementation in sandstone reservoirs: Examples from the North Sea, U.K. and East Greenland. Sedimentary Geology 194, p. 17-35.

Bjørkum, P.A., Oelkers, E.H., Nadeau, P.H., Walderhaug, O., Murphy, W.M., 1998: Porosity prediction in quartzose sandstones as a function of time, temperature, depth, stylolite frequency, and hydrocarbon saturation. AAPG Bulletin, Vol. 82, No. 4, p. 637-648.

Bjørlykke, K., Aagaard, P., Egeberg, P.K., Simmons, S.P., 1995: Geochemical constraints from formation water analyses from the North Sea and Gulf Coast Basin on quartz, feldspar and illite precipitation in reservoir rocks. p. 33-50 in : The Geochemistry of reservoir. Cubitt, J.M., England, W.A., (eds.). J. Geol. Soc. London Spec. Publ. 86.

Bjørlykke, K., 2010: Petroleum Geoscience. From Sedimentary Environments to Rock Physics. Springer -Verlag Berlin – Heidelberg, p. 508.

Bjørlykke, K., Ramm, M., Saigal, G.C., 1989: Sandstone diagenesis and porosity modification during basin evolution: Geologische Rundschau.

Bjørlykke, K., 1998: Clay mineral diagenesis in sedimentary basins-a key to the prediction of rock properties. The Mineralogical Society.

Bjørlykke, K., 2001: Sedimentologi og petroleumsgeologi. Gyldendal Yrkesopplæring, p. 211-229.

Block, S., Lander, R.H., Bonell, L., 2001: Anomalously high porosity and permeability in deeply buried sandstone reservoirs: Origin and predictability. AAPG Bulletin, Vol. 86, No. 2, p. 301-328.

Boggs, Jr. S., 1992: Diagenesis of sandstones and shales. Petrology of sedimentary rocks. Macmillian Publishing Co, pp. 659.

Boggs, Jr, S., 2006: Siliclastic sedimentary rocks, ch 5. In: Boggs Jr, S: Principles of sedimentology and stratigraphy. 4th ed, Person Education, Inc, p. 119-158.

Bonell, L., Larese, R.E., Lander, R.H., 2006: Hydrocarbon versus microquartz inhibition of quartz cementation in the North Sea sandstones: Emperical and experimental evidence. Annual AAPG Convention Abstracts, Vol. 15.

Dott, R.H., 1964: Wacke, greywacke and matrix – what approach to immature sandstone classification. Journal of sedimentary petrology, Vol. 34, No. 3.

Dutton, S.P., Diggs, T.N. 1990: Histoty of quartz cementation in the Lower Creaceous Travis Peak Formation, east Texas. Journal of sedimentary petrology, Vol. 60, p. 192-202.

Ehrenberg, S.N., 1993: Preservation of Anomalously High Porosity in Deeply Buried Sandstones by Grain-Coating Chlorite: Examples from the Norwegian Continental Shelf. AAPG Bulletin, No. 7, p. 1260-1286.

Ehrenberg, S.N., Aagaard, P., Wilson, M.J., Fraser, A.R., Duthie, D.M.L., 1993: Depth-dependent transformation of kaolinite to dickite in sandstones of the Norwegian continental shelf. Clay Minerals 28, p. 325-352.

Folkestad, A., Stur, N., 2008: Regressive and transgressive cycles in a rift-basin: Depositional model and sedimentary partitioning of the Middle Jurassic Hugin Formation, Southern Viking Graben, North Sea. Elsevier.

French, M.W, Worden, R., H., Mariani, E., Larese, R. E., Mueler, R.R., Kliewer, C. E., 2012: Microcrystalline quartz generation and the preservation of porosity in sandstones: evidence from the upper createous of the subhercynian basin, Germany. Journal of Sedimentary Research, Vol. 82, p. 422-434.

Giles, M.R., Stevenson, S., Martin, S.V., Cannon, S.J.S., 1992: The reservoir properties and diagenesis of the Brent Group: a regional perspective, p. 289-327 in: Geology of the Brent Group. Morton, A.C., Haszeldine, R.S., Giles, M.R., Brown, S. (eds.). Geol. Soc. London Spec, Paper 61.

Heald, M.T., Renton, J.J., 1966: Experimental study of sandstone cementation. Journal of Sedimentary Petrology, Vol. 36, p. 972-991.

Hook, J.R., 2003: An Introduction to porosity. Petrophysics Tutorial, Vol. 44, No. 3, p. 205-212.

James, W.C., Wilmar, G.C., Davidson, B.G., 1986: Role of quartz type and grain size in silica diagenesis, Nugget Sandstone, south-central Wyoming. Journal of Sedimentary Petrology, Vol. 56, s. 657-662.

Johannesen, E.P., Nøttvedt, A., 2006: Norge omkranses av kystsletter og deltaer, Ch 11, In: Ramberg, I.B., Bryhni, I. and Nøttvedt, A. (eds.) : Landet blir til, Norges geologi. Norsk geologisk forening, Trondheim, Second edition, p. 354-381.

Ketzer, J.M., Morad, S., Amorosi, A., 2003: Predictive diagenetic clay-mineral distribution in siliciclastic rocks within a sequence stratigraphic framework. Int. Assoc. Sedimentol. Spec. Publ. 34, p. 43-61.

Lander, H.R., Larese, R.E., Bonnell, L.M., 2008: Toward more accurate quartz cement models: The importance of euhedral versus noneuhedral growth rates. AAPG Bulletin, Vol. 92, No. 11, p. 1537-1563.

Langeland. H., 1992: Innføring i boreholslogging. Institutt for petroleumsteknologi og anvendt geofysikk. Norges teknisk-naturvitenskaplege universitet.

Lowry, W. D., 1956: Factors in loss of porosity by quartzose sandstones of Virginia. AAPG Bulletin, No. 40, p. 489-500.

McBride, E.F., 1989: Quartz cement in sandstones. Earth Science Reviews 26, p. 69-112.

Marchand, A.M.E., Smalley, P.C., Haszeldine, R.S., Fallick, A.E., 2002: Note of the importance of hydrocarbon fill for reservoir quality prediction in sandstones. AAPG Bulletin, Vol. 86, No. 9, p. 1561-1571.

Maast T.E., Jahren J., Bjorlykke K. 2011: Diagenetic controls on reservoir quality in Middle to Upper Jurassic sandstones in the South Viking Graben, North Sea. AAPG Bulletin, Vol. 95, No. 11, p. 1883 – 1905

Nesse, W.D., 2000: Introduction to mineralogi. Oxford University Press, Inc. 2000, p. 248-249.

Odin, G.S., Matter, A., 1981: De glauconiarum origine. Sedimentology 28, p. 611-641.

Oelkers, E.H., Bjørkum, P.A., Murphy, W.M., 1996: A petrographic and computational investigation of quartz cementation and porosity reduction in North Sea sandstones. American Journal of Science 296, p. 420-452.

Paxton, S.T., Szabo, O., Adjukiewicz, J.M., Klimentidis, R.E., 2002: Construction of an intergranular volume compaction curve for evaluating and predicting compaction and porosity loss in rigid-grain sandstone reservoirs. AAPG Bulletin, Vol. 86, No. 12, p. 2047-2067.

Selley, R.C., 1998: Elements of petroleum Geology. (Second edition). Academic Press, p. 239-299.

Siever, R., 1957: Pennsylvanian sandstones from the Eastern Interior Coal Basin. Journal of sedimentary Petrology, Vol. 27, p. 523-535.

Smith, J.V., Stenstrom, R.C., 1965: Electron-excited luminescence as a petrologic tool. Journal of Geology, Vol. 73, p. 627-635.

Storvoll, V., Bjørlykke, K., Karlsen, D., Saigal, G., 2002: Porosity preservation in reservoir sandstones due to grain-coating illite: a study of the Jurassic garn Formation from the Kristin and Lavrans fields, offshore Mid –Norway. Marine and Petroleum Geology, Vol. 19, p. 767-781.

Torsæter, O., Abtahi, M., 2003: Experimental reservoir engineering laboratory workbook. Department of Petroleum engineering of Science and Applied Geophysics. Norwegian University of Science and Technology.

Van Houten, F.B., Purucker, M.E., 1984: Glauconitic peloids and chamositic ooids – favorable factors, constraints, and problems. Earth Science Rev., Vol. 20, p. 211 - 243.

Vollset, J., Dore, A.G., 1984: A revised Triassic and Jurassic lithostratigraphic nomenclature for the Norwegian North Sea. NPD-bulletin, No. 3.

Walderhaug, O., 1996: Kinetic modelling of quartz cementation and porosity loss in deeply buried sandstone reservoirs. AAPG Bulletin, Vol. 80, No. 5, p. 731-745.

Walderhaug, O., 1994: Temperatures of quartz cementation in Jurassic sandstones from the Norwegian continental shelf-evidence from fluid inclusions. Journal of sedimentary research, Vol. A64, No. 2, p. 311-323.

Website, 2011: http://freepdfdb.com/pdf/petrophysics-msc-course-notes-references-dr-paul-glover-page-i-12163702.html

Wescott,W.A., Ethridge, F.G., 1983: Eocene fan delta – submarine fan deposition in the Wagwater Trough, east – central Jamaica. Sedimentology, Vol. 30, p. 235-245.

Welton, J., 1984: SEM Petrology Atlas. Methods in Exploration Series, AAPG Bulletin, Tulsa, Oklahoma 74102, USA, p. 237.

Wikipedia, 2001: www.wikipedia.org.

Wikipedia, 2011: http://mpgpetroleum.com/fundamentals.html

Worden, R., Morad, S., 2000: Quartz cementation in sandstones. Special Publication 29 of the IAS. Blackwell Science Inc.

Worden, R.H., Burley, S.D., 2003: Sandstone diagenesis: The evolution of sand to stone. In: Burley, S.D. & Worden, R.H. (eds.): Sandstone diagenesis. Recent and Ancient. Blackwell Publishing, p. 649.

References

Appendix

A. Tables

B. Figures

C. Legend

Table A.1: Physical properties and diagenetic minerals of the samples from well 15/3-7. (Ccm = Calcite cement, Qcm = Quartz cement, Kaol = Kaolinite, Pyr = Pyrite, Glc = Glauconite, Cly = Clay, Styl = Stylolite, X = minor, XX = medium, XXX = extensive).

Well 15/3-7											
Vertical depth (mRKB)	**Vertical depth (mRFS)**	**Grainsize (mm)**	**Sorting**	**Roundness**	**Cement**		**Authigenic minerals**			**Matrix**	
					Ccm	**Qcm**	**Kaol**	**Pyr**	**Glc**	**Cly**	**Styl**
4609.06	4482.06	0.40 med	Moderate	Subrounded		x	xx			x	
4610.00	4483.00	0.20 fine	Well	Subrounded		xx	xx				
4611.00	4484.00	0.40 med	Well	Rounded		xx	x			x	
4612.00	4485.00	0.35 med	Well	Subrounded		xx	xxx				
4613.25	4486.25	0.30 med	Moderate	Subrounded		x	xx				x
4614.25	4487.25	0.30 med	Well	Subrounded	x	x	xx	x			
4615.25	4488.25	0.50 med	Well	Rounded		xx	xx			x	
4616.75	4489.75	0.40 med	Well	Rounded		xx	xx			x	
4617.45	4490.45	0.40 med	Well	Subangular		xx	xx			x	
4620.53	4493.53	0.60 coar	Moderate	Rounded		xx	xx			x	
4621.55	4494.55	0.20 fine	Well	Subrounded	xxx	x					
4622.50	4495.50	0.20 fine	Very well	Subrounded	xxx	x	xx			x	
4650..00	4523.00	0.20 fine	Very well	Rounded		xx	xx			xx	
4651.05	4524.05	0.1 v fine	Very well	Angular	xxx	x				x	xx
4652.00	4525.00	0.14 fine	Very well	Subrounded	xx	xx	xx			xx	
4755.10	4628.10	0.70 coar	Poorly	Subrounded		xx	xx	x		xx	
4755.30	4628.30	0.50 med	Moderate	Subroundet		xxx	x			xx	x
4756.00	4629.00	0.50 med	Moderate	Subrounded		xxx	x			xx	
4756.20	4629.20	0.50 med	Well	Subrounded		xxx	x			xx	x
4766.50	4639.50	0.80 coar	Very well	Rounded		xxx	xx				
4775.30	4648.30	0.25 fine	Well	Rounded		xxx	xx			xx	
4775.50	4648.50	0.35 med	Well	Subangular		xxx	x			x	xx
4776.40	4649.40	0.20 fine	Very well	Subrounded		xxx	x			x	xx
4778.00	4651.00	0.40 med	Poorly	Subounded		xx	xx			xx	
4779.50	4652.50	0.20 fine	Moderate	Subrounded	x	xx	xxx			x	
4782.00	4655.00	1.4 v coar	poorly	Rounded	x	x	xxx				
4782.60	4655.60	1.4 v coar	poorly	Subangular	x	xx	xxx				
4785.70	4658.70	0.20 fine	Very well	Subrounded	x	xxx	xx				
4786.20	4659.20	0.25 fine	Well	Subrounded		xxx					xxx
4786.70	4659.70	0.20 fine	Well	Subrounded		xxx	xx				xxx
4791.00	4664.00	0.20 fine	Well	Subangular		xxx	xx				

Table A.2: Physical properties and diagenetic minerals of the samples from well 15/5-7. (Ccm = Calcite cement, Qcm = Quartz cement, Kao = Kaolinite, Pyr = Pyrite, Glc = Glauconite, Cly = Clay, Styl = Stylolite, X = minor, XX = medium, XXX = extensive).

15/5-7											
Vertical depth (mRKB)	**Vertical depth (mRFS)**	**Grainsize (mm)**	**Sorting**	**Roundness**	**Cement**		**Authigenic minerals**			**Matrix**	
					Ccm	**Qcm**	**Kal**	**Pyr**	**Glc**	**Cly**	**Styl**
3826.00	3681.00	0.40 med	Well	Subrounded		x	x	x	x	x	
3826.75	3681.75	0.30 med	Well	Subrounded		x	x	x	x	xx	
3827.57	3682.57	0.24 fine	Well	Subrounded		x	x		x	xx	
3827.80	3682.80	0.20 fine	Very well	Subrounded		x	x		x	xx	
3828.00	3683.00	0.30 med	Well	Subrounded		x	x		x	x	
3829.25	3684.25	0.30 med	Very well	Subrounded		x	x		x	xx	
3831.00	3686.00	0.30 med	Well	Subrounded		x	x		x	xx	
3833.75	3688.75	0.24 fine	Well	Subrounded	x	x	xx		x	xx	
3835.32	3690.32	0.16 fine	Well	Subrounded	x	x	x		x	xxx	x
3837.75	3692.75	0.50 med	Well	Subrounded	x	x	x		x	x	
3839.57	3694.57	0.30 med	Moderate	Subrounded		x	x		x	xx	
3840.50	3695.50	0.30 med	Moderate	Subrounded		x	x		x	x	x
3841.75	3696.75	0.30 med	Moderate	Subrounded		x	xx		x	xx	x
3848.00	3703.00	1.00 coar	Moderate	Subrounded		x	x		x	xx	x
3849.50	3704.50	0.40 med	Poorly	Subrounded	x	x	xx		x	x	
3853.42	3708.42	0.10 v fine	Very well	Subrounded	xx	x	xx	x		xx	x
3861.42	3716.42	0.18 fine	Well	Subrounded	x	x	xx			xx	x
3865.67	3720.67	0.18 fine	Well	Subrounded	x	x	x		x	xx	
3875.67	3730.67	0.10 v fine	Very well	Subrounded	x	x	xx			xx	
3876.00	3731.00	0.10 v fine	Very well	Subrounded	x	x	xx			xx	
3885.52	3740.52	0.10 v fine	Very well	Subrounded	x	x	xx	x		xx	
3897.87	3752.87	0.14 fine	Very well	Subrounded	x	xx	xx			xx	
3912.75	3767.75	0.30 med	Poorly	Subrounded	x	x	x			x	
3913.00	3768.00	0.30 med	Moderate	Subrounded	x	x	x			xxx	x

Table A.3: Physical properties and diagenetic minerals of the samples from well 15/6-11 A. (Ccm = Calcite cement, Qcm = Quartz cement, Kaol = Kaolinite, Pyr = Pyrite, Glc = Glauconite, Cly = Clay, Styl = Stylolite, X = minor, XX = medium, XXX = extensive).

Well 15/6-11 A											
Vertical depth (mRKB)	**Vertical depth (mRFS)**	**Grainsize (mm)**	**Sorting**	**Roundness**	**Cement**		**Authigenic minerals**			**Matrix**	
					Ccm	**Qcm**	**Kaol**	**Pyr**	**Glc**	**Cly**	**Styl**
4148.32	3590.32	0.20 fine	Well	Subrounded	x	x		x		x	x
4148.55	3590.55	0.20 fine	Well	Subrounded		x				x	x
4149.25	3591.25	0.20 fine	Well	Subrounded		x				x	x
4150.45	3592.45	0.20 fine	Well	Subrounded		x		x		x	
4150.65	3592.65	0.20 fine	Well	Subrounded		x				x	
4151.00	3593.00	0.22 fine	Well	Subrounded	xx	x				x	x
4151.50	3593.50	0.20 fine	Moderate	Subrounded	xx	x	xx	x		x	x
4152.00	3594.00	0.20 fine	Well	Subangular		xxx	xx	x		x	
4152.50	3594.50	0.20 fine	Very well	Subrounded		xx	xx	x		x	x
4153.00	3595.00	0.20 fine	Very well	Subrounded		xx	xx	x		x	x
4153.50	3595.50	0.20 fine	Well	Subrounded		x	xx	x		x	
4154.00	3596.00	0.20 fine	Very well	Subrounded	x	xx	xx	x		x	
4154.50	3596.50	0.18 fine	Well	Subrounded	xx	x	xx			x	x
4154.75	3596.75	0.18 fine	Very well	Subrounded	x	x	xx	x		x	
4155.00	3597.00	0.20 fine	Very well	Subrounded	x	x	x	x		x	
4155.27	3597.27	0.19 fine	Well	Subrounded	x	x	xx	x		x	
4155.75	3597.75	0.21 fine	Well	Subrounded	x	x	x			x	
4156.25	3598.25	0.15 fine	Well	Subangular	x	xxx	xx	x		x	x
4156.77	3598.77	0.17 fine	Well	Subangular	x	xxx	x	x		x	x
4157.25	3599.25	0.16 fine	Very well	Rounded	x	xx	xx	x		x	x
4157.75	3599.75	0.18 fine	Well	Subrounded	x	xxx	xx	x		x	
4158.25	3600.25	0.17 fine	Well	Subrounded	x	xxx	xx	x		x	
4158.75	3600.75	0.18 fine	Well	Subrounded	x	xx	xx	x		x	
4159.25	3601.25	0.10 v fine	Very well	Subrounded	x	xxx	xx	x		x	x
4159.75	3601.75	0.20 fine	Well	Subrounded	x	xx	xx			x	x
4160.00	3602.00	0.16 fine	Well	Subrounded	x	xx	xx			x	
4160.50	3602.50	0.18 fine	Well	Subrounded	x	x	xx	x		x	
4160.75	3602.75	0.18 fine	Well	Subrounded	x	x	xx			x	
4161.00	3603.00	0.14 fine	Well	Subrounded	x	xx	xx	x		x	
4161.25	3603.25	0.16 fine	Well	Subrounded	x	xx	xx			x	x
4161.50	3603.50	0.20 fine	Well	Subrounded	x	x	xx	x		x	
4161.75	3603.75	0.20 fine	Well	Subangular	xx	x	xx	x		x	

4162.00	3604.00	0.21 fine	Well	Subrounded	xx	xx	x	x		x	
4162.25	3604.25	0.16 fine	Well	Subangular	xx	xx	x	x		x	
4162.75	3604.75	0.17 fine	Well	Subrounded	x	xxx	x	x		x	x
4163.25	3605.25	0.10 v fine	Moderate	Subangular	xx	x	xx	x		x	
4163.75	3605.75	0.16 fine	Well	Subangular	xx	xxx	x	x		x	
4164.00	3606.00	0.14 fine	Well	Subrounded	xx	xxx	x	x		x	
4164.80	3606.80	0.10 v fine	Very well	Subrounded	x	xxx	x	x		x	x
4165.25	3607.25	0.22 fine	Moderate	Subangular	x	xxx	x	x		x	x
4166.25	3608.25	0.10 v fine	Moderate	Subangular	x	xx	x	x		x	
4167.30	3609.30	0.16 fine	Moderate	Subangular	xx	x	x	x		x	x
4168.75	3610.75	0.16 fine	Very well	Subrounded	xx	x	x	x		x	
4169.00	3611.00	0.22 fine	Moderate	Subrounded	x	x	xx	x		x	
4169.75	3611.75	0.16 fine	Moderate	Subrounded	x	xx	xx	x		x	x
4170.25	3612.25	0.16 fine	Moderate	Subrounded	xx	xx	x	x		x	
4171.50	3613.50	0.14 fine	Poorly	Subrounded	x	xxx	xxx	x		x	x
4172.50	3614.50	0.16 fine	Very well	Subrounded	x	xx	x	x		x	
4173.50	3615.50	0.20 fine	Well	Subrounded	x	xx	x	x		x	
4174.00	3616.00	0.14 fine	Well	Subrounded	x	xx	x	x		x	
4175.25	3617.25	0.50 med	Moderate	Subrounded	x	xx	xx	x		x	
4175.75	3617.75	0.24 fine	Moderate	Subangular	x	xx	xx	x		x	x
4176.75	3618.75	0.10 v fine	Poorly	Subrounded	xx	x	xx	x		x	
4177.50	3619.50	0.10 v fine	Well	Subrounded	xx	x	x	x		x	
4178.50	3620.50	1.00 coar	Poorly	Subangular		x	xx	x		x	
4179.50	3621.50	0.20 fine	Well	Subrounded	x	xxx	x	x		x	
4180.50	3622.50	0.20 fine	Poorly	Subrounded		xxx		x		x	x

Table A.4: Physical properties and diagenetic minerals of the samples from well 15/9-19 A. (Ccm = Calcite cement, Qcm = Quartz cement, Kaol = Kaolinite, Pyr = Pyrite, Glc = Glauconite, Cly = Clay, Styl = Stylolite, X = minor, XX = medium, XXX = extensive).

15/9-19 A											
Vertical depth (mRKB)	**Vertical depth (mRSF)**	**Grainsize (mm)**	**Sorting**	**Roundness**	**Cement**		**Authigenic minerals**			**Matrix**	
					Ccm	**Qcm**	**Kaol**	**Pyr**	**Glc**	**Cly**	**Styl**
3837.55	2938.00	0.25 fine	Moderate	Subangular	x	x		x	x	x	
3838.50	2938.90	0.50 med	Poorly	Subangular	x	x		x	x	x	
3839.40	2939.95	0.40 med	Moderate	Subrounded	x	x		x	x	x	x
3840.45	2940.95	0.25 fine	Well	Subrounded		x	x	x		x	x
3841.45	2942.00	0.18 fine	Well	Subrounded		x	x	x	x	x	x
3842.50	2942.95	0.14 fine	Well	Subrounded		x		x	x	x	x
3843.45	2944.00	0.13 fine	Well	Subangular		x	x	x	x	x	
3844.50	2945.00	0.18 fine	Well	Subangular		x	x	x	x	x	x
3845.50	2946.00	0.22 fine	Well	Subangular		x	x	x	x	x	x
3846.50	2947.00	0.20 fine	Well	Subangular	x	x	x		x	x	x
3847.50	2948.00	0.18 fine	Well	Subrounded	x	x	x	x		x	x
3848.50	2948.90	0.18 fine	Well	Subangular		x	x	x		x	
3849.40	2950.00	0.15 fine	Well	Subangular		x	x	x		x	x
3850.50	2950.95	0.20 fine	Well	Subangular	x	x	x	x		x	
3851.45	2951.70	0.18 fine	Well	Subangular		x	x	x		x	xx
3852.20	2953.90	0.15 fine	Well	Subangular	x	x	x	x		x	x
3854.40	2955.00	0.14 fine	Well	Subangular	xx			x		x	
3855.50	2955.90	0.12 fine	Poorly	Subangular	x			x	x	x	
3856.40	2957.00	0.20 fine	Poorly	Subrounded	x	x		x		x	xx
3857.50	2957.90	0.20 fine	Poorly	Subrounded		x	x	x		x	
3858.40	2959.00	0.15 fine	Well	Subrounded	x	x	x	x		x	x
3859.50	2959.65	0.15 fine	Moderate	Subangular	x	x	x	x		x	x
3860.15	2961.20	0.70 coar	Well	Subrounded		x	x	x		x	
3861.70	2961.90	0.50 med	Well	Subrounded		x		x		x	
3862.40	2962.50	0.45 med	Well	Subrounded		x	x	x		x	
3863.00	2966.65	0.35 med	Well	Subrounded		x	x	x		x	
3867.15	2967.75	0.40 med	Moderate	Subrounded		x	x	x		x	
3868.25	2969.00	0.30 med	Moderate	Subrounded		x	x	x		x	x
3869.50	2969.90	0.45 med	Well	Subrounded		x	x	x		x	
3870.40	2971.00	0.45 med	Well	Subrounded		x	x	x		x	
3871.50	2972.00	0.50 med	Well	Subrounded		x	x	x		x	x
3872.50	2973.00	0.50 med	Moderate	Subrounded		x	x	x		x	x
3873.50	2974.90	0.50 med	Well	Subrounded		x	x	x		xx	

3874.40	2975.00	0.40 med	Well	Subangular		x	x	x		xx	x
3875.50	2976.05	0.25 fine	Moderate	Subangular		x	x	x		xx	x
3876.55	2977.05	0.24 fine	Moderate	Subangular	x	x	x	x		xx	x
3877.55	2978.00	0.25 fine	Moderate	Subangular	x	x	x	x		xx	x
3878.50	2979.00	0.12 v fine	Well	Subrounded	x	x	x	x		xx	
3879.50	2979.50	0.12 v fine	Well	Subrounded	x	x	x	x		x	
3880.00	2980.95	0.14 fine	Well	Subrounded	x	x	x	x		xx	x
3881.45	2981.90	0.14 fine	Well	Subangular	x	x	x	x		xx	
3882.40	2983.00	0.12 v fine	Well	Subangular	x	x	x	x		xx	
3883.50	2984.00	0.12 v fine	Poorly	Subrounded	x	x	x	x		xx	
3884.50	2985.05	0.11 v fine	Poorly	Subrounded	x	x	x	x		xxx	
3885.55	2986.00	0.30 med	Well	Subrounded		x	x			x	
3886.50	2987.05	0.33 med	Well	Subrounded		x	x	x		x	
3887.55	2988.00	0.35 med	Well	Subrounded		x	x	x		x	
3888.50	2989.05	0.20 fine	Well	Subrounded		x	x			xx	x
3889.55	2990.00	0.20 fine	Poorly	Subangular		x	x			xx	x
3890.50	2991.05	0.20 fine	Moderate	Subangular		x	x			xx	x
3891.55	2992.00	0.11 v fine	Well	Subangular		x	x	x		xx	xx
3892.50	2993.00	0.20 fine	Well	Subrounded		x	x	x		x	xx
3893.50	2994.00	0.18 fine	Moderate	Subrounded		x	x			xx	x
3894.50	2995.05	0.12 v fine	Well	Subrounded		x	x	x		xx	
3895.55	2996.00	0.14 fine	Well	Subangular		x	x	x		xxx	x
3896.50	2997.05	0.15 fine	Moderate	Subangular		x	x			xx	
3897.55	2998.05	0.25 fine	Poorly	Subangular		x	x			xx	
3898.55	2999.05	0.35 med	Poorly	Subangular		x	x	x		x	
3899.55	3000.00	0.50 med	Well	Subrounded		x	x			x	
3900.50	3001.05	0.40 med	Well	Subrounded		x	x			x	
3901.55	3002.00	0.22 fine	Poorly	Subrounded		x	x			xx	
3902.50	3003.05	1.05 coar	Poorly	Subrounded		x	x			x	
3903.55	3004.00	0.23 fine	Poorly	Subangular		x	x			xx	
3904.50	3005.05	0.45 med	Moderate	Subrounded	x	x	xx			x	
3905.55	3006.00	0.23 fine	Poorly	Subrounded		x	x			x	x
3906.50	3007.00	0.24 fine	Poorly	Subangular		x	x			xx	xx
3907.50	3007.75	0.22 fine	Moderate	Subangular		x	x	x		xx	xxx
3908.25	3009.05	0.18 fine	Well	Subrounded		x	x			xx	
3909.55	3010.00	0.20 fine	Well	Subangular		x	x	x		xx	
3910.50	3011.05	0.20 fine	Well	Subangular		x	x	x		xx	
3911.55	3012.00	0.16 fine	Well	Subangular		x	x	x		xx	
3912.50	3013.10	0.20 fine	Well	Subangular	x	x	x	x		xx	
3913.60	3014.05	0.17 fine	Well	Subangular	x	x	x	x		xx	

3914.55	3014.95	0.16 fine	Well	Subangular	x	x	x	x		xx	
3915.45	3015.90	0.20 fine	Well	Subangular	x	x	x	x		xx	
3916.40	3017.00	0.16 fine	Well	Subangular	x	x	x	x		xx	
3917.50	3018.00	0.20 fine	Well	Subangular	x	x	x	x		xx	
3918.50	3019.00	0.20 fine	Well	Moderate		x	x	x		xx	

Table A.5: Physical properties and diagenetic minerals of the samples from well 15/9-21 S. (Ccm = Calcite cement, Qcm = Quartz cement, Kaol = Kaolinite, Pyr = Pyrite, Glc = Glauconite, Cly = Clay, Styl = Stylolite, X = minor, XX = medium, XXX = extensive).

15/9-21 S											
Vertical depth (mRKB)	**Vertical depth (mRSF)**	**Grainsize (mm)**	**Sorting**	**Roundness**	**Cement**		**Authigenic minerals**			**Matrix**	
					Ccm	**Qcm**	**Kaol**	**Pyr**	**Glc**	**Cly**	**Styl**
4767.00	3494.00	0.25 fine	Well	Subrounded		x	x		x	x	
4768.00	3495.00	0.25 fine	Well	Subrounded		x	x	x	x	x	
4769.00	3496.00	0.30 med	Well	Subrounded		x	x	x	x	x	
4770.00	3497.00	0.30 med	Well	Subrounded		x	x		x	x	
4771.00	3498.00	0.30 med	Well	Subrounded		x	x		x	x	
4772.00	3499.00	0.28 med	Moderate	Subrounded		x	x	x	x	x	
4773.00	3500.00	0.30 med	Moderate	Subrounded		x	x		x	xx	
4774.00	3501.00	0.35 med	Moderate	Subangular		x	x		x	x	
4775.10	3502.10	0.30 med	Well	Subrounded		x	x		x	x	
4776.00	3503.00	0.35 med	Well	Subrounded		x	x		x	x	
4777.50	3504.50	0.50 med	Very well	Rounded		x					
4778.00	3505.00	0.45 med	Very well	Subrounded		x			x		
4779.00	3506.00	0.80 coar	Well	Subrounded		x	x		x		
4780.00	3507.00	0.50 med	Well	Subrounded		x	x		x	x	
4781.00	3508.00	0.40 med	Well	Subrounded		x	x		x	xx	
4782.00	3509.00	0.50 med	Moderate	Subangular		x	x		x	xx	
4783.35	3510.35	0.40 med	Well	Subrounded		x	x		x	x	
4784.00	3511.00	0.25 fine	Moderate	Subangular		x	xx		x	x	
4785.00	3512.00	0.80 coar	Well	Subrounded		x	xx				
4786.00	3513.00	0.50 med	Moderate	Subangular	x	x	xx				
4787.00	3514.00	0.60 coar	Well	Subrounded	x	x	x			x	
4788.00	3515.00	0.50 med	Well	Subrounded	x	x	x			x	
4789.00	3516.00	0.60 coar	Well	Subrounded		x	xx				
4790.00	3517.00	0.50 med	Moderate	Subangular		x	x			x	x
4791.00	3518.00	0.80 coar	Well	Subrounded		x	xx			x	
4792.00	3519.00	0.50 med	Well	Subrounded		x	x			x	
4793.55	3520.55	0.40 med	Well	Subrounded		x	x			xx	x
4794.15	3521.15	0.60 coar	Well	Subrounded		x	x				
4795.00	3522.00	0.50 med	Moderate	Subrounded		x	xx			x	
4798.25	3525.25	0.32 med	Well	Subrounded		x	xx			x	
4799.00	3526.00	0.80 coar	Poorly	Subrounded		x	x	x		xx	
4800.15	3527.15	0.20 fine	Well	Subrounded		x	x	x		xx	
4801.00	3528.00	0.30 med	Well	Subrounded		x	x	x		xx	

4802.00	3529.00	0.30 med	Well	Subrounded	x	x	x		x	x	
4804.25	3531.25	0.15 fine	Well	Subangular						xxx	
4805.50	3532.50	0.25 fine	Moderate	Subangular						xxx	
4806.00	3533.00	0.40 med	Well	Subrounded		xx	x		x	xx	x
4807.00	3534.00	0.30 med	Well	Subrounded		x	x		x	xx	x
4808.10	3535.10	0.25 fine	Well	Subrounded	x	x	x			x	x
4809.00	3536.00	0.30 med	Well	Subrouned	xxx	x					x
4810.00	3537.00	0.30 med	Well	Subrounded	xxx						x
4811.00	3538.00	0.30 med	Well	Subrounded	xxx						x
4812.00	3539.00	0.25 fine	Poorly	Subangular						xxx	
4813.00	3540.00	0.15 fine	Moderate	Subrounded						xxx	
4814.50	3541.50	0.30 med	Poorly	Subrounded						xxx	x
4816.00	3543.00	0.30 med	Poorly	Subrounded						xxx	x
4817.10	3544,10	0.15 fine	Well	Subrounded						xxx	xx
4818.00	3545.00	0.10 v fine	Well	Subrounded						xxx	xxx
4819.25	3546.25	0.15 fine	Well	Subrounded						xx	xx
4820.00	3547.00	0.25 fine	Poorly	Subrounded	x	x	x			xx	x
4821.30	3548.30	0.50 med	Moderate	Subrounded	xxx						
4822.00	3549.00	0.40 med	Moderate	Subrounded	xxx					x	
4823.00	3550.00	0.35 med	Moderate	Subangular	xxx					x	
4824.10	3551.10	0.35 med	Moderate	Subangular	xxx					x	
4825.00	3552.00	0.38 med	Moderate	Subangular	xxx					x	
4826.00	3553.00	0.32 med	Moderate	Subangular	xxx					x	
4827.55	3554.55	0.23 fine	Well	Subangular		x	xx	x		x	x
4828.00	3555.00	0.40 med	Moderate	Subrounded		x				xxx	
4829.00	3556.00	0.25 fine	Moderate	Subangular		x	x	x		x	x
4830.00	3557.00	0.35 med	Moderate	Subrounded		x	x	x		xx	x
4831.00	3558.00	0.40 med	Moderate	Subrounded		x	x	x		x	x
4832.00	3559.00	0.50 med	Poorly	Subangular		x	x	x		x	x
4833.10	3560.00	0.40 med	Well	Subrounded		x	x			x	x
4834.00	3561.00	0.50 med	Well	Subrounded		x	x	x		xx	x
4835.00	3562.00	0.25 fine	Well	Subrounded		x	x	x		xx	x
4836.000	3563.00	0.40 med	Well	Subrounded		x	xx	x	x	x	x
4837.00	3564.00	0.35 med	Well	Subrounded		x	x	xx		x	
4838.00	3565.00	0.30 med	Moderate	Subrounded		x	xx	xx		x	
4839.00	3567.10	0.50 med	Moderate	Subrounded		x	xx	x		x	
4840.10	3568.00	0.25 fine	Poorly	Subrounded		x	xx	x		xx	
4841.00	3569.00	0.25 fine	Moderate	Subrounded		x	xx	x		xx	

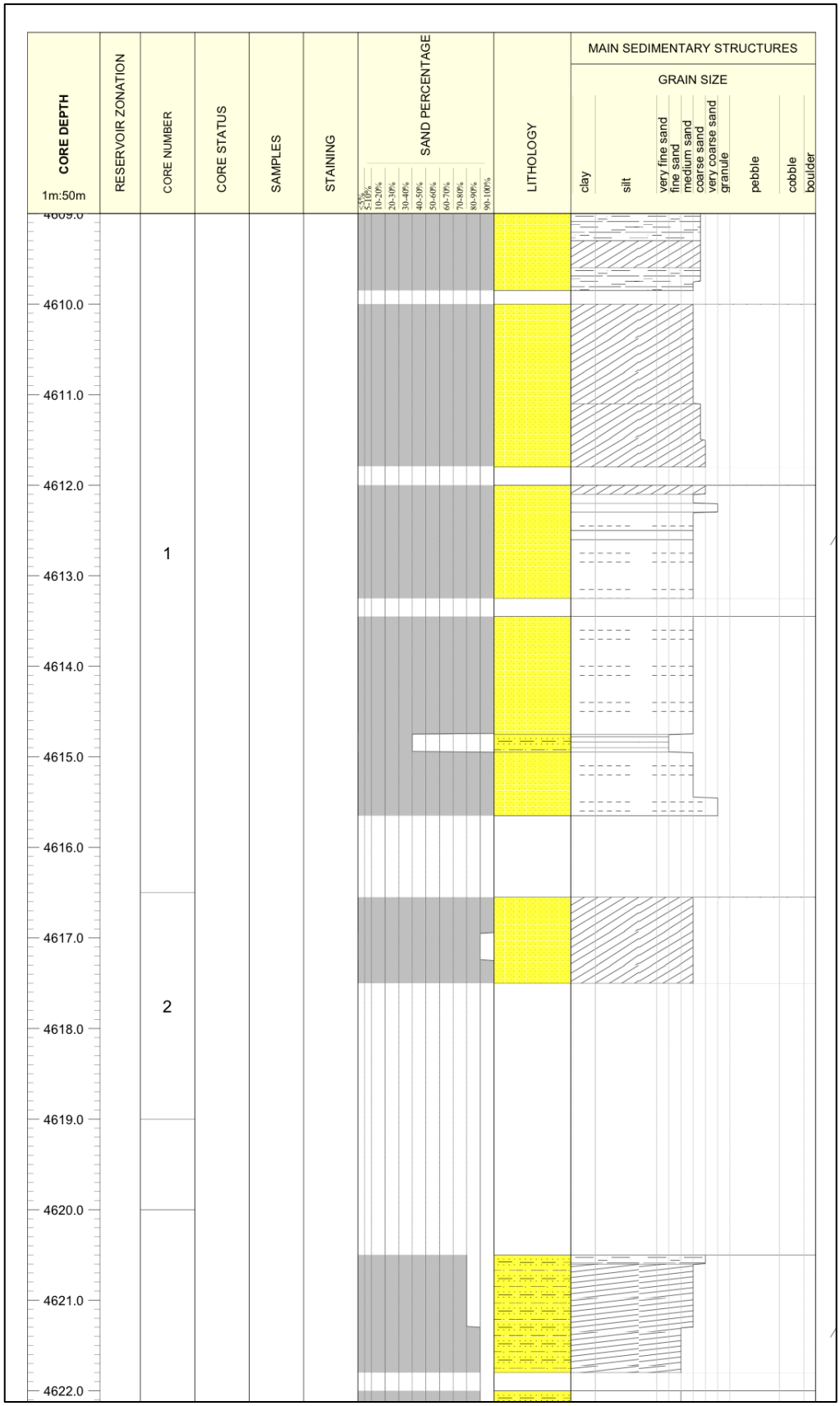

Figure B.1: Modified core description of well 15/3-7 provided by Statoil ASA.

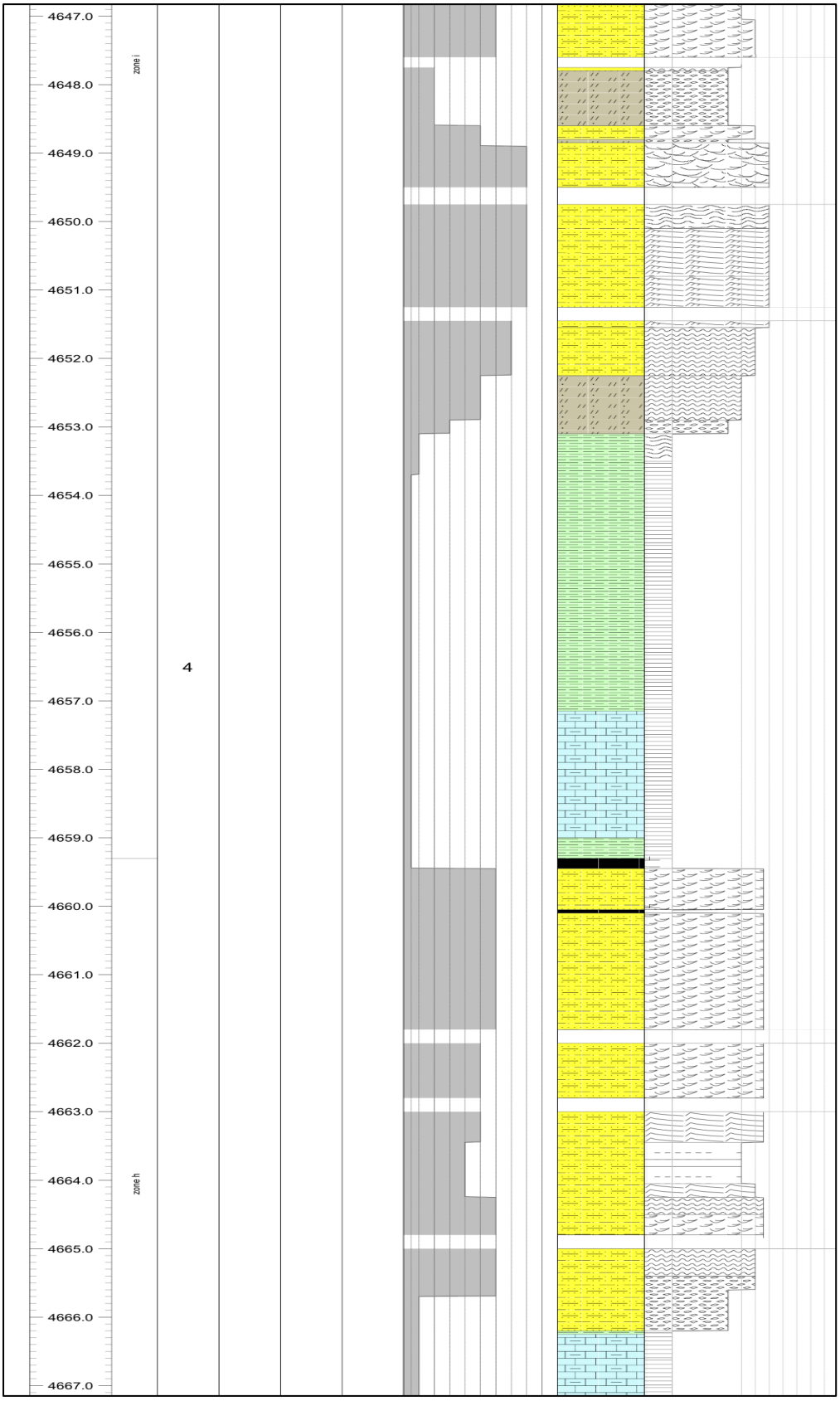

Figure B.2: Modified core description of well 15/3-7 provided by Statoil ASA.

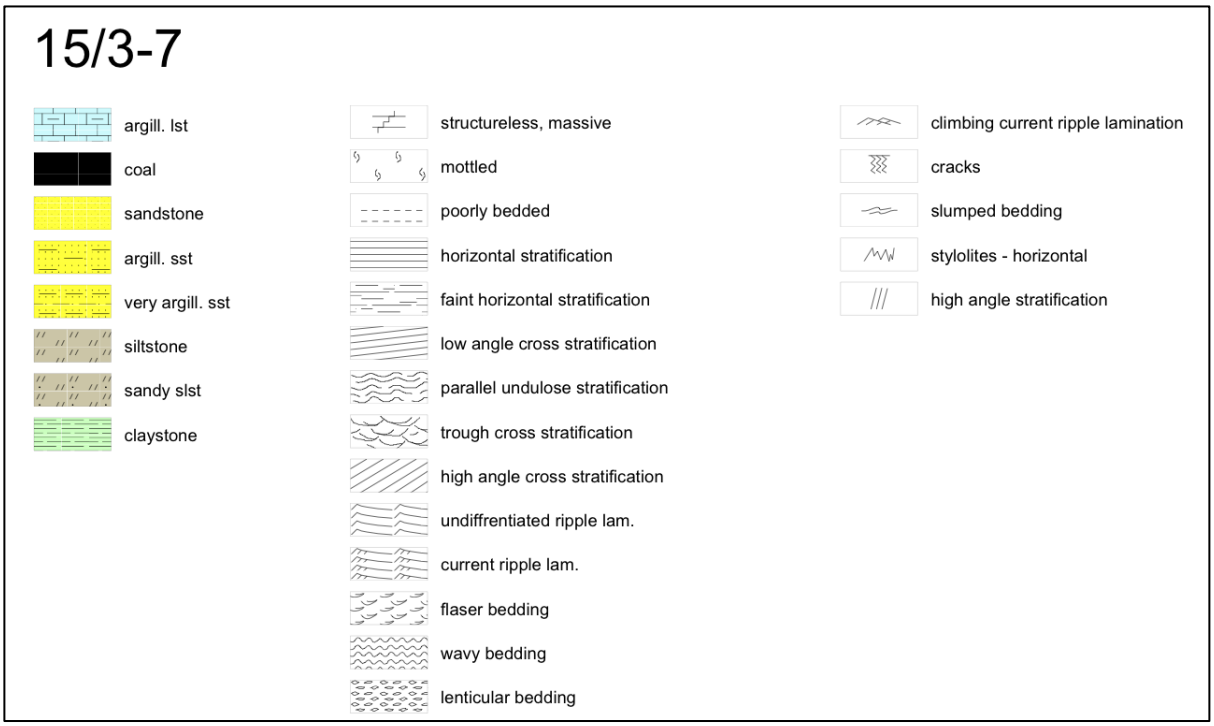

Figure C 1: Legend for core description well 15/3-7.